CHAPTER 1: Introduction

Chapter Summary: This chapter gives an overall introduction to the research theme of this thesis, states the principal aims and research objectives, and outlines the structure of the thesis.

1.1. Background

The Fourth Assessment Report (AR4) of the Intergovernmental Panel on Climate Change (IPCC) states that it is 'very likely' that the global warming trend since 1950 can be primarily attributed to increases in anthropogenic emissions of greenhouse gases (Trenberth *et al.*, 2007). Furthermore, human activities are believed to be responsible for a global surface temperature increase of around $0.13^{o}C \pm 0.03^{o}C$ (Trenberth *et al.,* 2007). In a study based on minimum and maximum air temperature data of 33 meteorological stations throughout Indonesia, it was found that both minimum and maximum temperature increases of about $0.047^{o}C$ and $0.017^{o}C$ per year respectively have occurred in each of the last 22 years (Boer *et al*., 2007). It is also possible that global warming has contributed to changes in rainfall patterns at the global, regional and local levels.

According to Trenberth *et al.* (2007), the intensity of heavy precipitation has increased, even over the areas where the total precipitation has decreased significantly, consistent with a warming climate. On the other hand, Manton *et al.* (2001) investigated rainfall changes in particular regions of the Asia-Pacific. Their study was based on the high quality data from 1961 to 1998 which were collected from 91 meteorological stations

in Southeast Asia and South Pacific. Their results showed an overall decrease number of rainy day with rain in Southeast Asia and South Pacific. In the local area, Aldrian & Djamil (2008) found that local rainfall in East Java has decreased at a statistically significant level over the last five decades. This finding was based on monthly rainfall data (1955-2005) obtained from 40 rainfall stations. Their results also showed that the number of extreme dry months has increased, particularly in the areas near the coasts.

There is a number of impacts of the climate trends such as those outlined above. El-Niño Southern Oscillation (ENSO) events, which are the extreme climatic condition, have dramatic impacts on the nature and human lives such as droughts and floods. For example, the economic cost of recent floods and droughts in Indonesia exceeds two billion dollars from data based on 1997/1998 El-Niño and La-Niña events (Kirono & Tapper, 1999). In addition, Boer *et al.* (2007) reported that ENSO events in Indonesia also impacted on agriculture, coral ecosystems, health, water reservoirs, and changes in levels of rainfall.

Several researchers have investigated rainfall variability and extreme climate in Indonesia. Kirono *et al.* (1999), Haylock & McBride (2001), McBride *et al.* (2003), Aldrian & Susanto (2003) and Hendon (2003) have demonstrated that rainfall in Indonesia is strongly related to inter-annual large-scale climatic phenomena such as the ENSO. The ENSO phenomenon affects the climate in many areas of the globe (Ropelewsky & Halpert, 1987; 1996), including Indonesia (Kirono *et al.,* 1999; Aldrian & Susanto, 2003). These physical ocean-atmosphere interactions are originated in the tropical Indo-Pacific regions, but the climatic impacts can be occurred worldwide (Allan *et al.*, 2001).

Recently, another important climate mode, called the Indian Ocean Dipole (IOD), has been proposed as another possible cause of floods and droughts in Indonesia (Saji *et*

al., 1999). Numerous studies have investigated if the IOD is independent of the ENSO, or if, somehow, these two sources of climate variability are interlinked (Saji *et al.*, 1999; Ashok *et al.,* 2003; Yamagata *et al.,* 2003; Behera *et al.,* 2000). Moreover, Annamalai *et al.* (2005) found that, since the 1970s, ENSO and IOD events frequently occurred simultaneously. Various research groups have studied the IOD influence on Indonesian rainfall variability. For more information, see Chapter 2.

Another climate mode that is potentially related to rainfall in Indonesia is the Interdecadal Pacific Oscillation (IPO) (Power *et al.*, 1999), due to the region's proximity to Pacific Ocean. This mode also has a major impact on the Australian climate (Power *et al.,* 1999) and has attracted much research (i.e. Salinger *et al.*, 2001; Speer *et al*., 2009). However, there is no particular study that has been conducted in relation to climatic impacts of the IPO on Indonesia. Only a limited number of systematic studies have been undertaken to quantify interdependencies between rainfall variability in Indonesia, large-scale climate drivers, and regional anomalies in Sea Surface Temperature (SST). See Chapter 2 for more details.

1.2. General Aims and Research Objectives

The aim of this thesis is to study the trends and variability in rainfall in the Indonesian region based on the available observational and re-analysis data. The research objectives are to:

1. Explore spatial differences in rainfall anomalies and rainfall trends within the Indonesian region.
2. Examine the relationship between Indonesian rainfall and large-scale climate drivers such as ENSO, IOD and IPO.
3. Investigate the relationship between rainfall and local SST.

1.3. Organisation of the Thesis

The thesis is organised as follows. In Chapter 2, a review of the relevant literature is presented. Chapter 3 outlines the data sources, analytical techniques and statistics used in this research. Chapter 4 presents the results, analysis and discussion of the research outcomes. Finally, a complete summary and conclusions, including recommendations for further research, are presented in Chapter 5.

CHAPTER 2: Literature Review

Chapter Summary: This chapter reviews literature of relevance to this thesis. This literature provides background information on the theories and methods employed in this study.

2.1 Geography of the Indonesian Region

Indonesia is located between Southeast Asian and Australian continent, and between Pacific and Indian Oceans, spanning the geographical area from 8^{o}S to 15^{o}N in latitude and 90^{o}E and 140^{o}E in longitude (**Figure 1**). The region encompasses more than 10,000 islands. The 5 major islands are: Sumatra, Kalimantan (Borneo), Java, Sulawesi (Celebes) and Papua. Additionally, the region is relatively mountainous, having a number of peaks of volcanic origin, ranging between 3,000 and 3,800 metres above sea level. The highest mountains are found in Sumatra, Java, and Papua, with the latter having the highest peak in Indonesia at 4,884 metres.

The seas of Indonesia have complicated coastal geographies, with several narrow straits and many small islands. Continental shelves with depths less than 200 metres surround a number of deeper ocean basins with depths of greater than 3000 metres. There are shallow seas in Indonesia; one of them is the Java Sea which lies on the Sunda Shelf with an average depth of about 40 metres. There also deep seas in Indonesia, especially in the eastern part. The Banda and Seram Seas, at more than 4500 metres in depth, are the deeper waters of this region, compared to the surrounding seas (Gordon *et al.*, 2003). Based on a bathymetric survey, Gordon *et al.* (2003) also pointed out that there are three

main deep sills within the sea off northern Indonesia: the Sangihe Ridge, the Halmahera Sea sill, and the Lifamatola Passage, which may act as barriers to throughflow transport.

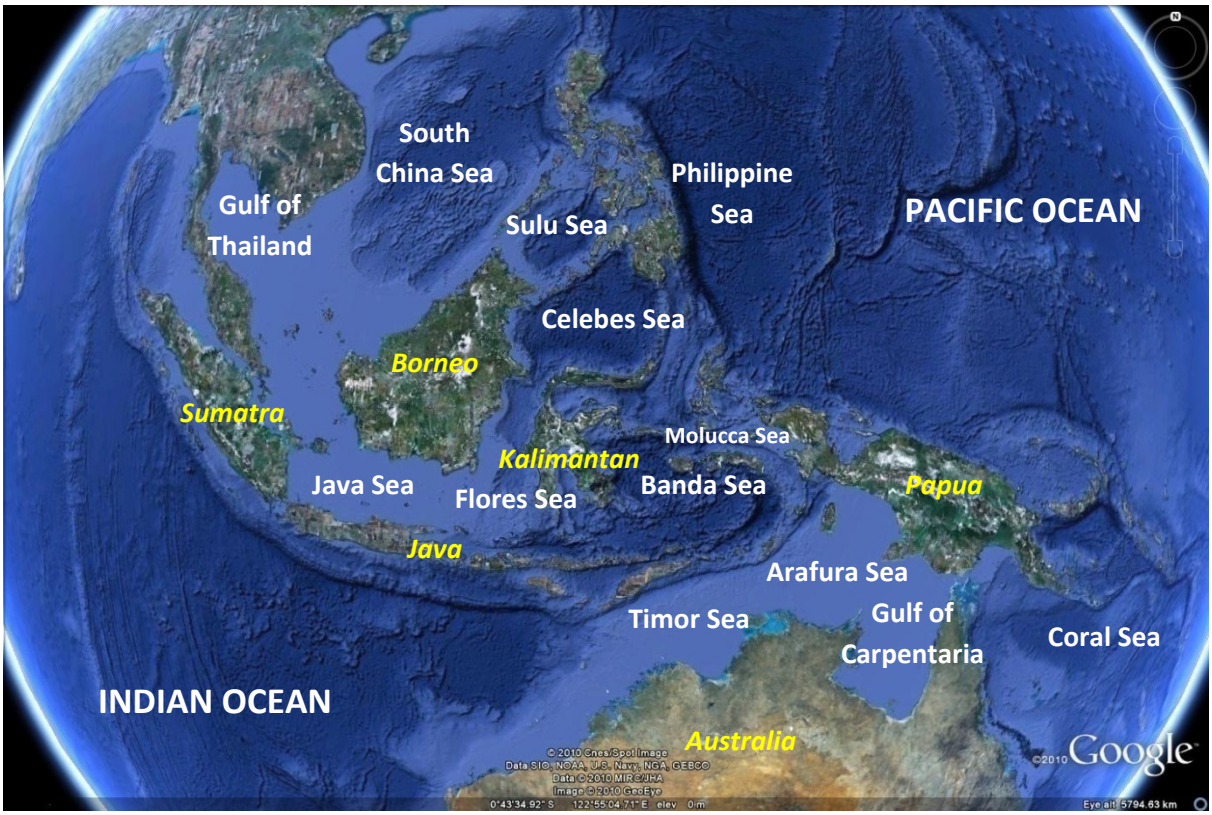

Figure 1. Map of Indonesian region as the study area. Source: Google Earth.

The ocean in the Indonesian region is known as the Indonesian Throughflow. Previous studies have indicated that, via the ENSO, variability in this region influences the volume transport of the Leeuwin current and, hence, oceanic heat movement influences climate in the south-eastern Indian Ocean (England *et al*., 2010 submitted). Moreover, the Indonesian Throughflow also affects the oceanic circulation and thermocline depth around Australia and the Indian Ocean (Schneider, 1997). The recent numerical modelling study of England *et al.* (2010 submitted) suggests that the Indonesian Throughflow plays an important role in total Indonesian rainfall.

2.2. Climate of the Study Area

Historically, the earliest climate research conducted on the Indonesian region was from the colonial era, when Braak (1929) published his climatic and meteorological research. He documented three main parameters: rainfall data, cloud levels and air temperature. Since then, a range of studies have been conducted in this area, exploring the potential impacts of these parameters on climate at the global level (i.e. Ramage, 1968; Neale & Slingo, 2003; Aldrian & Susanto, 2003; Chang *et al.,* 2004; Giannini *et al.*, 2007; Hidayat & Kizu, 2009).

The scientific community has recognised the Indonesian region as an important "hotspot" of global atmospheric circulation. Tapper (2002) pointed out that the Asian-Australian monsoon and the Walker circulation are the most significant features in this area. The Asian-Australian monsoon is related to the north-south tropical Hadley circulation, while the Walker circulation is related to the east-west atmospheric circulation. Furthermore, the location of the inter-tropical convergence zone (ITCZ) has a strong influence on both inter-annual and seasonal variations in climate (Tapper, 2002).

a. <u>The Inter-Tropical Convergence Zone (ITCZ)</u>

The ITCZ plays an important role in climate variability in the tropical region. It exists due to the convergence of trade winds in the low equatorial pressure zone where air from both hemispheres converges and moves upwards in the atmosphere (**Figure 2**) (Trenberth, 1991). In the northern hemisphere, the trade winds move in a south-westerly direction, while in the southern hemisphere they move north-westerly.

Due to the geographical position of Indonesia at the equator, the archipelago is influenced by changes in the position of the ITCZ. During the north-west monsoon, the position of the ITCZ is relatively close to Australia, while during the south-east monsoon,

it shifts far north of Indonesia into the northern part of the South China Sea (Wheeler & McBride, 2005). This shift modulates the seasonal rainfall cycle over Indonesia, with little rainfall during the south-east monsoon and heavy rainfall during the north-west monsoon (Wheeler & McBride, 2005). The south-east monsoon (dry season) is associated with easterly winds from Australia that carry warm and dry air over the region. Conversely, the north-west monsoon (wet season) is associated with westerly winds from the Asian continent that carry warm and moist air to the Indonesian region.

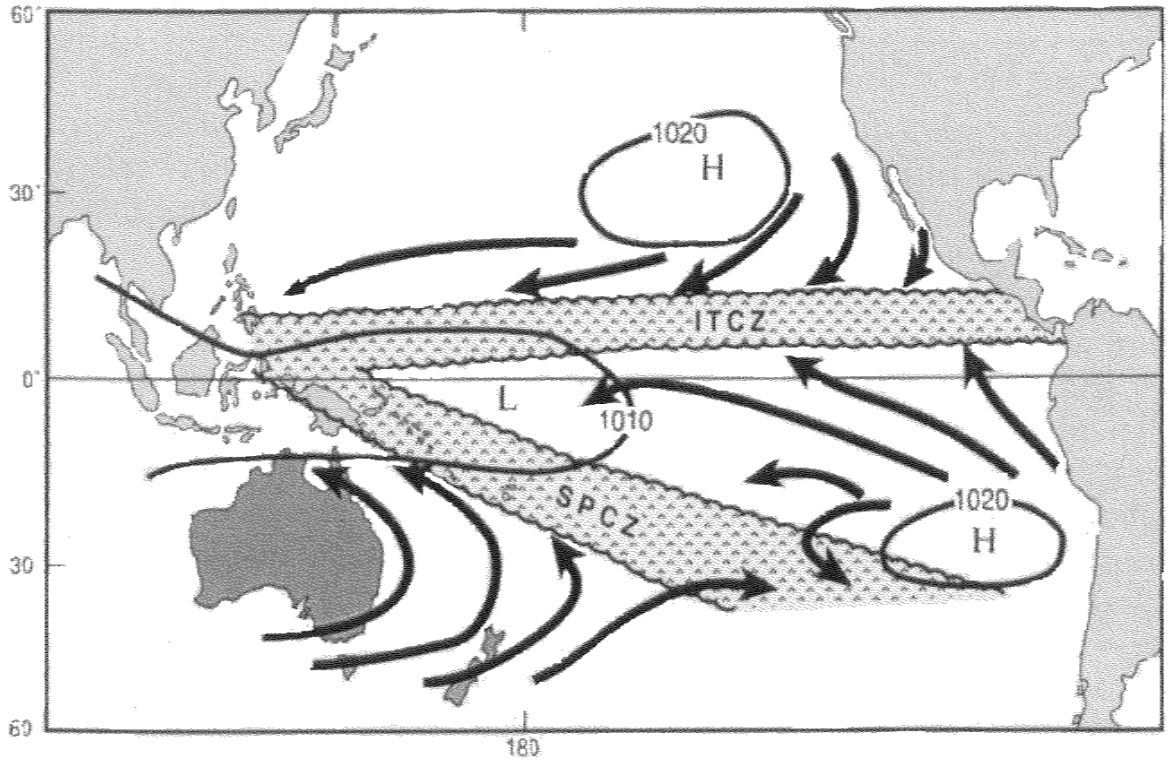

Figure 2: Location of the inter-tropical convergence zone (ITCZ) and the South Pacific convergence zone (SPCZ) in the South Pacific region. From Trenberth (1991).

The South Pacific Convergence Zone (SPCZ) contains convective cloud bands that influence the role of global atmospheric circulation and is characterised by cloudiness and precipitation (Vincent, 1994, Folland *et al*., 2002). It covers the area from the western Pacific warm pool south-eastward to about 30^{o}S, 120^{o}W (**Figure 2**). According to Folland *et al.,* 2002, however, this area moves north-east and south-west during El-Niño and La-Niña events respectively. Therefore, based on Salinger's (1995) study in the south-west

Pacific, these movements produced large precipitation anomalies on the mean area of the SPCZ (taking into account the average geographical position of the SPCZ). Only the eastern part of Indonesia is geographically aligned within both the ITCZ and the SPCZ.

b. Indonesian rainfall

There have been several studies on rainfall variability over Indonesia. The research has focused on the relationships between rainfall and diurnal variations (i.e. Qian, 2008; Hara *et al.*, 2009), annual changes, such as monsoonal seasons (Hamada *et al.,* 2002; Aldrian & Susanto, 2003; Chang *et al.*, 2005), and inter-annual large-scale climatic phenomena such as the ENSO (Kirono *et al.,* 1999; Haylock & McBride, 2001; McBride, *et al.,* 2003; Aldrian & Susanto, 2003; Hendon, 2003; Chang *et al.,* 2004).

In addition, it is also widely known that the Madden Julian Oscillation (MJO) is a dominant component of intra-seasonal (20-90 days) variability in the tropics, including Indonesia (Hidayat & Kizu, 2009). The findings of Hidayat & Kizu (2009) suggest that the MJO has an influence on Australian summer rainfall variability in Indonesia accounting for anomalies of amplitudes of 1–3 mm/day (10–30% of the climatological mean).

It has been long established that the seasonal pattern of rainfall over this region is significantly influenced by the local topography, consisting of many islands with high mountains in the marginal seas between Pacific and Indian oceans. Hamada *et al.* (2002) documented seasonal variations in rainfall at 46 meteorological stations during the period 1961–1990 and classified the stations objectively into five climatological regions. Another study, conducted by Aldrian & Susanto (2003), divided the Indonesian region into three climatological types; monsoon, equatorial, and local pattern (Figure 3). The latter division was based on a spatial correlation method termed ‘double correlation method’ (DCM) (see

Aldrian & Susanto (2003) for more information) using rainfall data for the period 1961–1993.

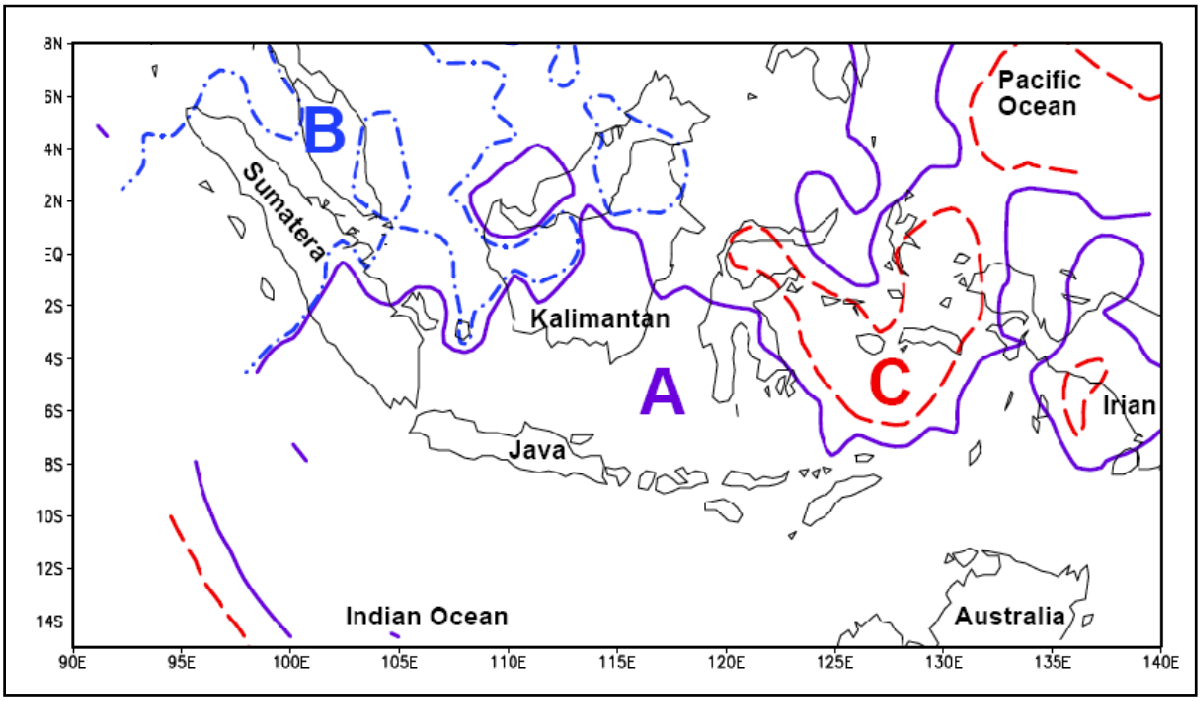

Figure 3. Rainfall classification in the Indonesian region. From Aldrian & Susanto (2003).

In general, the "monsoon pattern" (region A in Fig. 3) is characterised by a monthly rainfall distribution with maximum rainfall during the Australian summer months (December and January) (**Figure 4a**). This pattern covers a large portion of the Indonesian region including Java, parts of Sumatra, Sulawesi and Kalimantan. The "equatorial pattern" (region B in Fig. 3) characterises the intra-annual rainfall variability over northern Sumatra and northern Borneo. This pattern (**Figure 4b)** is bimodal with maxima occurring during November and March/April. In contrast, the "local pattern" (region C in Fig. 3) shows maximum rainfall during June/July (**Figure 4c)**. Only small parts of Indonesia have this pattern covering Molucca and the surrounding small islands.

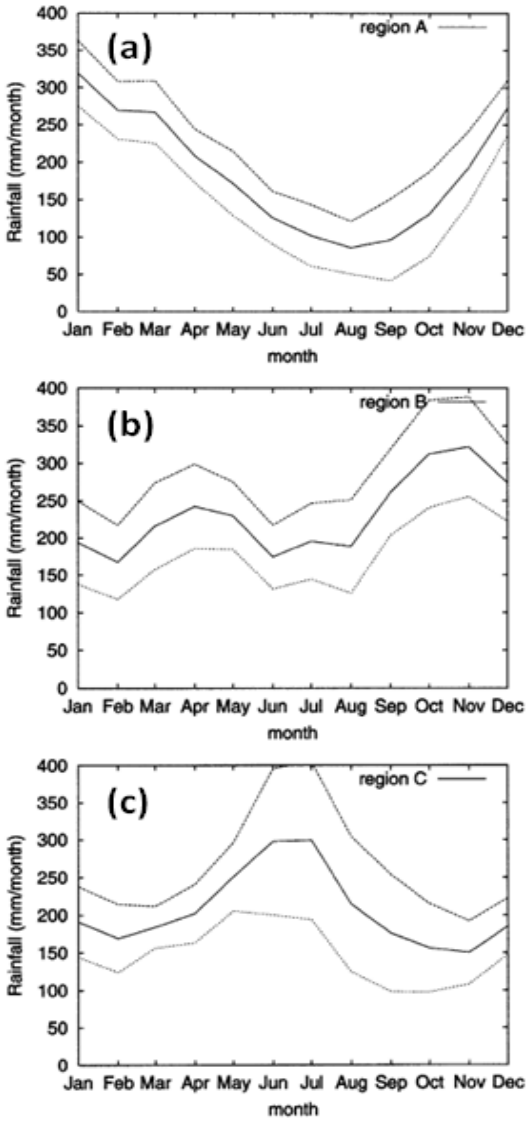

Figure 4. Climatological average monthly rainfall for regions A, B, and C. The dotted lines refer to one standard deviation from the mean. From Aldrian & Susanto (2003).

In terms of seasonal rainfall predictability, Haylock & McBride (2001) examined the coherency and predictability of seasonal rainfall anomalies in Indonesia. Their research was based on 63 rainfall stations across the region from 1950 to 1998. They found that there was only small part of this region (southern part of Sumatra, Borneo and Kalimantan), which was significantly coherent on inter-annual time scale. Another important finding is that dry season (JJA) is the most predictable season in Indonesia, and wet season (DJF) is the most unpredictable.

2.3 Indonesian sea surface temperature

One function of ocean is to stabilise the surface air temperature of the Earth. Research demonstrates that SST influences the ability of ocean to organize latent heat and to manage the distribution of atmospheric moisture (Tomczak & Godfrey, 2003; Marshall & Plumb, 2008). It can be surmised that SST plays a key role in modulating climate due to the processes of evaporation, precipitation and atmospheric heating.

SST across the Indonesian region is important to the process of atmospheric convection and to the distribution of precipitation. Convection is the dominant atmospheric process over the region. Warm SST around the islands is deemed to trigger substantial amounts of evaporation, generating high-energy convection over the area (Qu *et al.*, 2005). Based on the Global Circulation Model (GCM), Neale & Slingo (2003) highlighted the importance of SST in this area, which can modulate changes in precipitation across the Indo-Pacific region. These results emphasize the sensitivity of the relationship between SST and convective activity. Moreover, a strong correlation between SST and precipitation over the "Maritime Continent" (i.e. the Southeast Asian region) has been demonstrated in a recent study by Dayem *et al.* (2007). These authors found that high precipitation rates over the Maritime Continent are associated with high SST. Moreover, they also proposed a causal relationship between regional precipitation rates and the strength of the Walker Circulation. The Walker Circulation thus intensifies in response to the strengthening of easterly winds over the tropical Pacific Ocean, which occurs when precipitation rates increase (Dayem *et al.*, 2007).

The monsoon cycle influences the spatial and temporal scales of SST in this region, as described by Susanto *et al.* (2006) as shown in **Figure 5**. They found that this cycle affects the climatological monthly SST. Colder temperatures are found in the boreal winter months (December to March) in the South China Sea due to the north-west monsoon, and, south of the equator, from June to August, due to the south-east monsoon. Meanwhile, during the peaks of the south-east monsoon, from June to September, colder temperatures are observed in the Arafura and Banda Seas and in the region between southern Java and Timor Island. Strong south-easterly winds induce divergence along the coast of Java all the way to Timor and within the Banda Sea. This generates coastal upwelling reducing the SST on a regional scale. In addition, strong winds enhance vertical mixing on the ocean surface, also reducing the SST. Another evident of monsoon influence is also presented by Qu *et al*. (2005) as shown in **Figure 6**. The SST tends to warm up in the downstream direction of the wind and cool down in the upstream direction

In addition, according to Qu *et al.* (2005), the greatest variability of the seasonal SST cycle occurs in the Timor, Banda, Arafura and South China Seas. Based on peak-to-peak analyses, they found that SSTs in these areas vary by more than 4 ^{o}C (**Figure 7**). Another study of SST in the eastern Indonesia region, especially over the Banda Sea between 1982 and 2000, shows maximum SSTs in a range of 29^{o}C to 30^{o}C from late November to May, then decreasing to 26.5^{o}C in August (Gordon & Susanto, 2001). SST variability also related to thermocline depth changes, which vary with the monsoon and the ENSO events (Gordon & Susanto, 2001). A recent study by Iskandar (2010), focusing on the Banda Sea, confirms the significant influence of ENSO and IOD events on inter-annual SST variations.

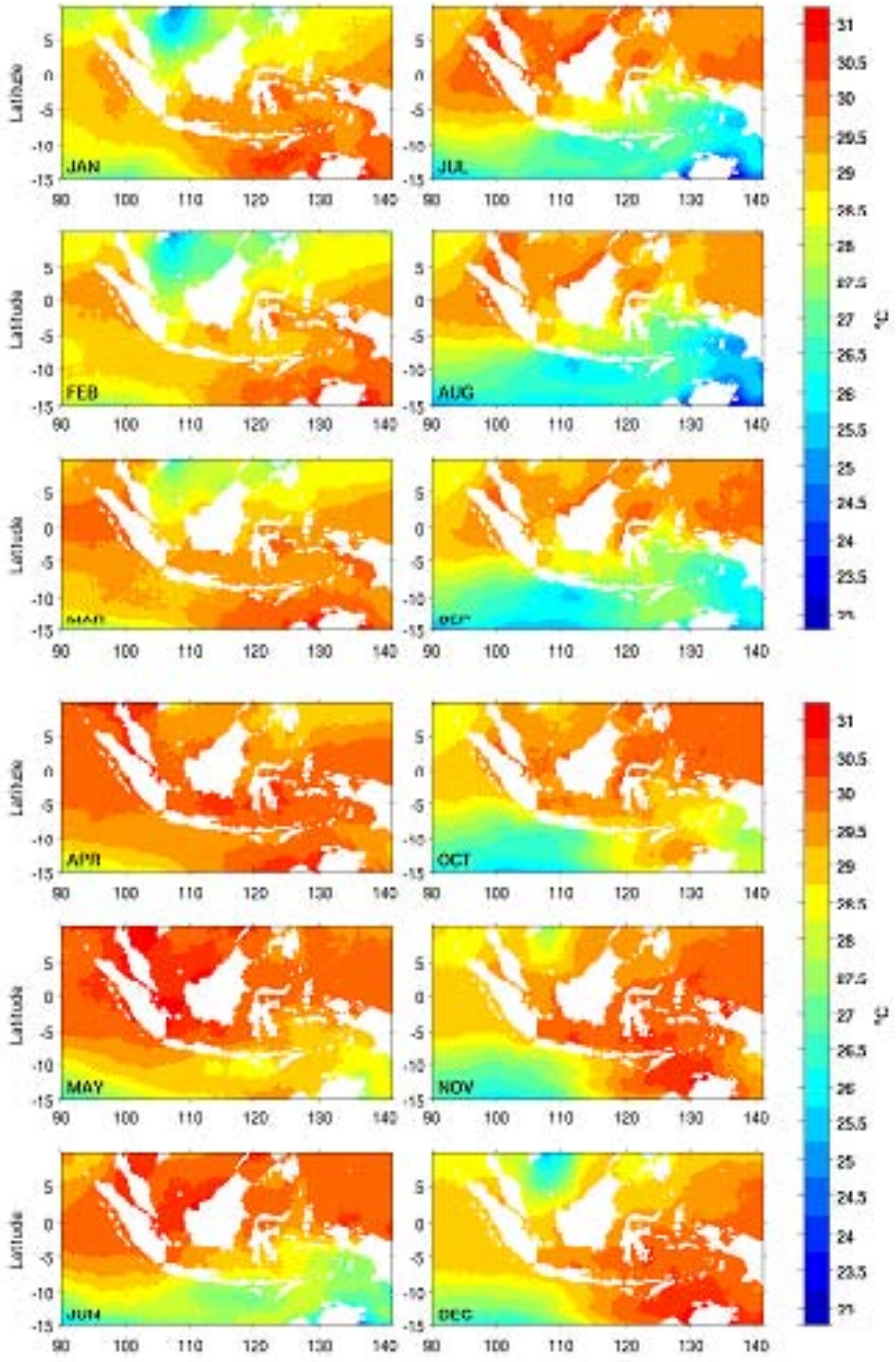

Figure 5. Monthly climatological mean of SST derived from NOAA-AVHRR based on monthly mean data from January 1998 to December 2003. From: Susanto *et al.*, (2006).

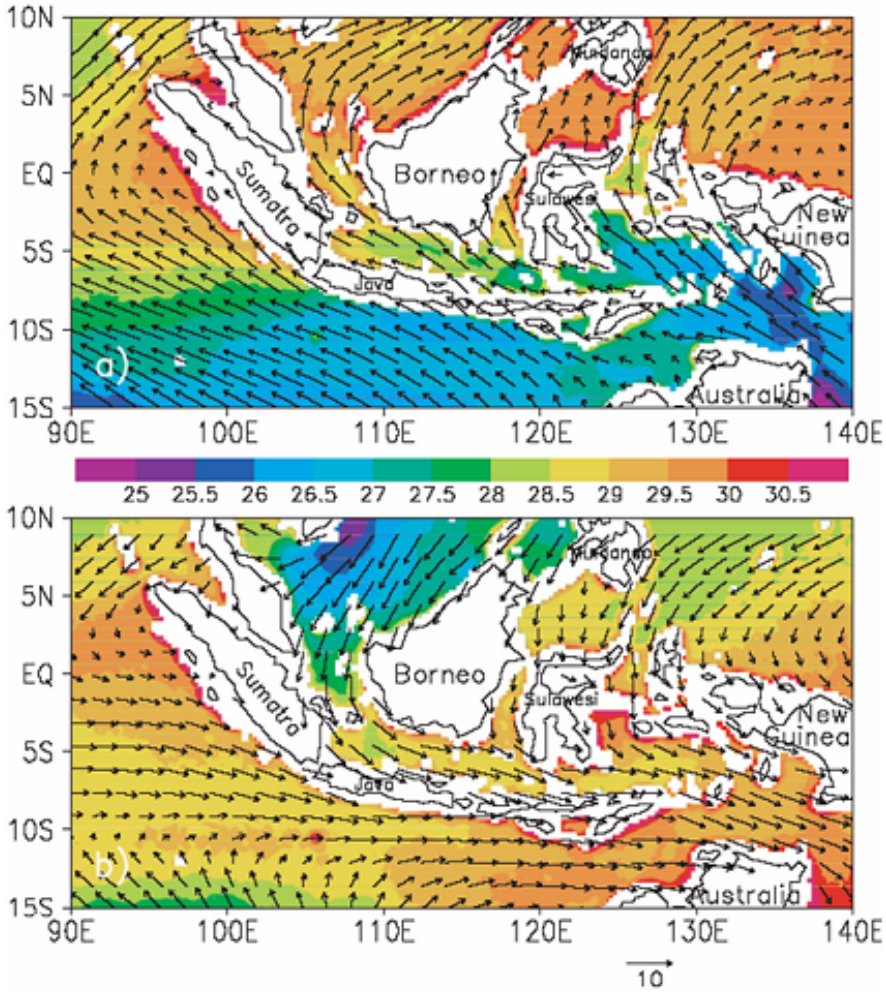

Figure 6. Monthly mean TRMM sea surface temperature (°C) superimposed with Quick Scatterometer (QuikSCAT) wind (m/s) in (a) August and (b) February. Data are averaged from December 1997 to June 2004 and from July 1999 to January 2005, respectively. From: Qu *et al.* (2005).

Meanwhile, the lowest overall wind speeds/stress appears in April, which clearly represents the month of transition between the north-west (NW) monsoon and the south-east (SE) monsoon. The SE monsoon begins in May, with winds in the Arafuru Sea and the eastern Indian Ocean indicating first. The zone of maximum wind moves northwest in the Indian Ocean along the Nusa Tenggara Island chain from Java to Sumatra. Easterly winds spread and intensify through June reaching their maximum in July and August, and then they begin to subside. A band of very low wind speed brackets a zone slightly north of the equator During the NW monsoon (rainy season), the precipitation is higher than the evaporation, so that the sea surface salinity and SST become lower. On the other hand,

during SE monsoon (dry season), the evaporation is higher than the precipitation. Hence, sea surface salinity and SST are increased (Susanto *et al*., 2006).

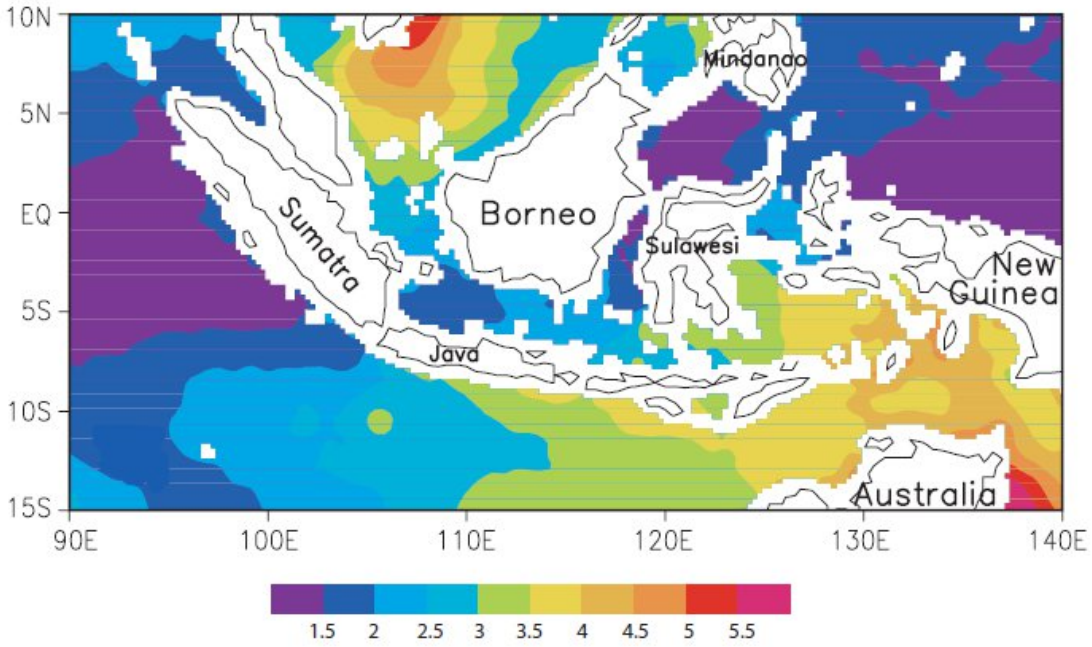

Figure 7. Peak-to-peak SST variability in Indonesian seas. From Qu *et al.* (2005).

SST anomalies associated with the ENSO are recognised as the most dominant factors for short-term global climate prediction (Nicholls, 1984; Trenberth 1997; Annamalai *et al*., 2005). For instance, Nicholls (1989) found a pattern of SST anomaly that was strongly related to the SOI and correlated closely with rainfall anomalies in southern Australia. This pattern had a dipole shape, with one pole in the middle of the Indian Ocean and the other in the seas around Indonesia. Allan & Haylock (1993) found that SST changes in the Indian Ocean were affected by the Indonesian Throughflow.

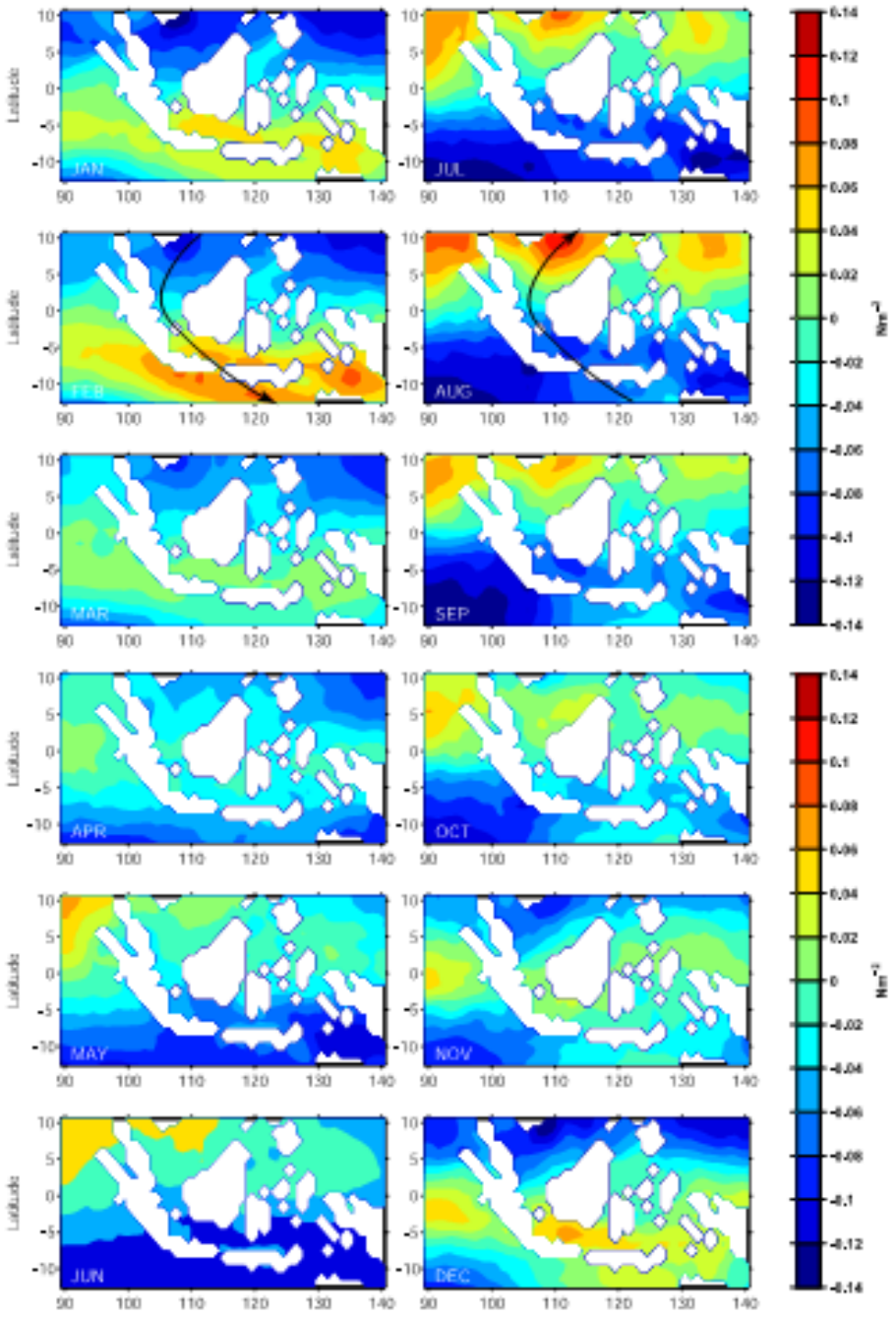

Figure 8. Monthly climatological mean of zonal wind stress derived from ERS1/2, NSCAT, and QSCAT scatterometers based on monthly mean data from January 1998 to December 2003. Seasonal monsoon winds are clearly seen. Stronger eastward zonal winds from the Australian continent affect the southern part of Indonesia during the SE monsoon (April–October). Conditions are reversed during the NW monsoon (October–April). Solid arrows in the months of February and August represent the general pattern of wind directions during the NW monsoon and SE monsoon, respectively. From : Susanto *et al.* (2006).

The Indonesian Throughflow plays an important part in distributing water heat content from the Pacific to the Indian Ocean, influencing global and tropical climates (Schneider, 1997). Recent research conducted by England *et al*. (2010, submitted) concurs with these previous results. These authors employed a coupled climate model with open and closed Indonesian Throughflow experiments. In contrast to the closed case, the open case leads to changes in atmospheric circulation patterns contributing to reduced rainfall in Africa and increased rainfall over Australia and southern Asia.

The Indonesian Throughflow transfers warm, low salinity waters from the western Pacific into the Indian Ocean (Gordon, 1995; Gordon, 2005). Gordon describes two main Indonesian Troughflow pathways in the Indonesian seas; the western and eastern route. In addition, the source of water in the western route is mostly from the northern Pacific (Gordon, 1995). It flows through the Makassar Strait, the Flores Sea and the Banda Sea before exiting into the Indian Ocean (Gordon, 2005) (**Figure 9**). Waters in the eastern route originate primarily from the South Pacific and flow through the Halmahera and Seram Seas into the Banda and the Timor Seas (Gordon, 2005).

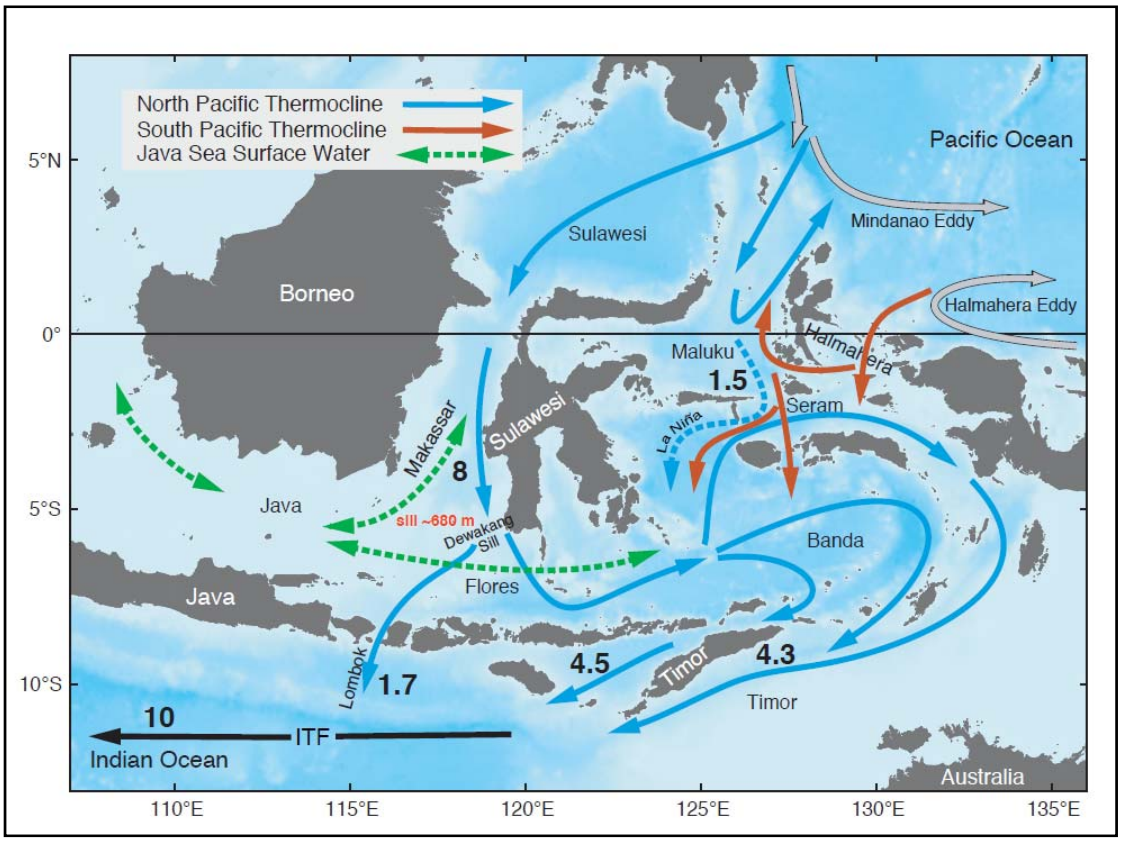

Figure 9. Indonesian Throughflow pathways and estimates of total volume transport (in Sv = 10^6 m^3/s). From Gordon (2005).

2.5. Modes of Climate Variability

Large-scale climatic processes modify the stability of the atmosphere through the exchange of mass and energy from the ocean to the atmosphere and from the equator to the poles (Holton, 2004). In addition, the rotation of the Earth develops these exchanges into complex systems of variability which not only govern the climate and weather patterns, but also generate extreme climatic events (Holton, 2004). Indonesia is influenced by a range of large-scale climatic phenomena due to its relative location to the Pacific and Indian Oceans, and its significance for global climate dynamics.

The understanding of large scale climatic modes and their influence on each other, and the regional climate of Indonesia, are of value to weather forecasting and climate

research. Having a better understanding of how these large-scale processes influence Indonesian rainfall should assist the management of climatic impacts in this region. There are several modes that may possibly relate to Indonesian rainfall on inter-annual to inter-decadal time-scales, which are being the ENSO, the IOD and the IPO.

A. <u>El-Niño Southern Oscillation (ENSO)</u>

Although there is still much debate concerning an international scientific definition of ENSO (Trenberth, 1997; Hanley, 2003; Meyers *et al.,* 2007), basically the phenomenon consists of two main components: oceanic and atmospheric. Their interactions are essential during the ENSO period (Philander, 1983). The oceanic component is known as El Niño manifesting itself as a) transient weakening of equatorial upwelling due to the propagation of equatorial Kelvin waves eastward and b) disappearance of coastal upwelling of cold and nutrient-rich water along the Peruvian coast (Tomczak & Godfrey, 2003). The atmospheric component of ENSO is called the Southern Oscillation. This oscillation is observed as a global phenomenon which involves variations in the atmospheric pressure difference at the ocean surface between the Indonesia-Australia region and the southeast Pacific (Drosdowsky & Williams, 1991). Therefore, the ENSO is a set of interacting parts of a global system of coupled ocean-atmosphere climate fluctuations.

ENSO is a source of inter-annual variability in weather and climate at the global level. ENSO events start in the western Pacific Ocean as a regional instability of the tropical Pacific ocean-atmosphere system (Philander, 1985). The onset of this event typically occurs during the transition between the wet and dry southern hemisphere monsoon seasons (Giannini *et al*., 2007). Generally, there are two phases of the ENSO; the warm (El-Niño) and cold (La-Niña) phases (**Figure 10**). The "normal phase" refers to the long-term average situation, comprising the east-west Walker Circulation (Marshall &

Plumb, 2008) in the atmosphere; relatively warmer water in the western Pacific (Marshall & Plumb, 2008), called the Pacific Warm pool; and upwelling in the ocean along the coasts of Peru and California in the eastern Pacific (Trenberth, 1997; Tomczak & Godfrey, 2003). The central mechanism that powers the Walker Circulation are the Trade Winds that take up moisture and heat along their pathway to the west, triggering convective cloud formation and intensified rainfall in the western Pacific.

The Walker Circulation weakens during El-Niño conditions, leading to an overall weakening of the Trade Winds, or even a reversal in the western Pacific accompanied or initiated by a tropical cyclone (Tomczak & Godfrey, 2003). In addition, wind anomalies in the western Pacific trigger equatorial Kelvin Waves that, transiently, weaken equatorial upwelling (leading to positive SST anomalies along their path) and, in conjunction with modified winds, substantially weaken the intensity of coastal upwelling in the eastern Pacific. In this situation, most of the equatorial Pacific Ocean is anomalously warm, and the SST anomalies in the central and eastern tropical Pacific can be more than 5^{o}C warmer than the long-term average (Marshall & Plumb, 2008). As a consequence of this warming, the centre of atmospheric convection, clouds and precipitation is shifted from the usual western Pacific into the central Pacific (Marshall & Plumb, 2008).

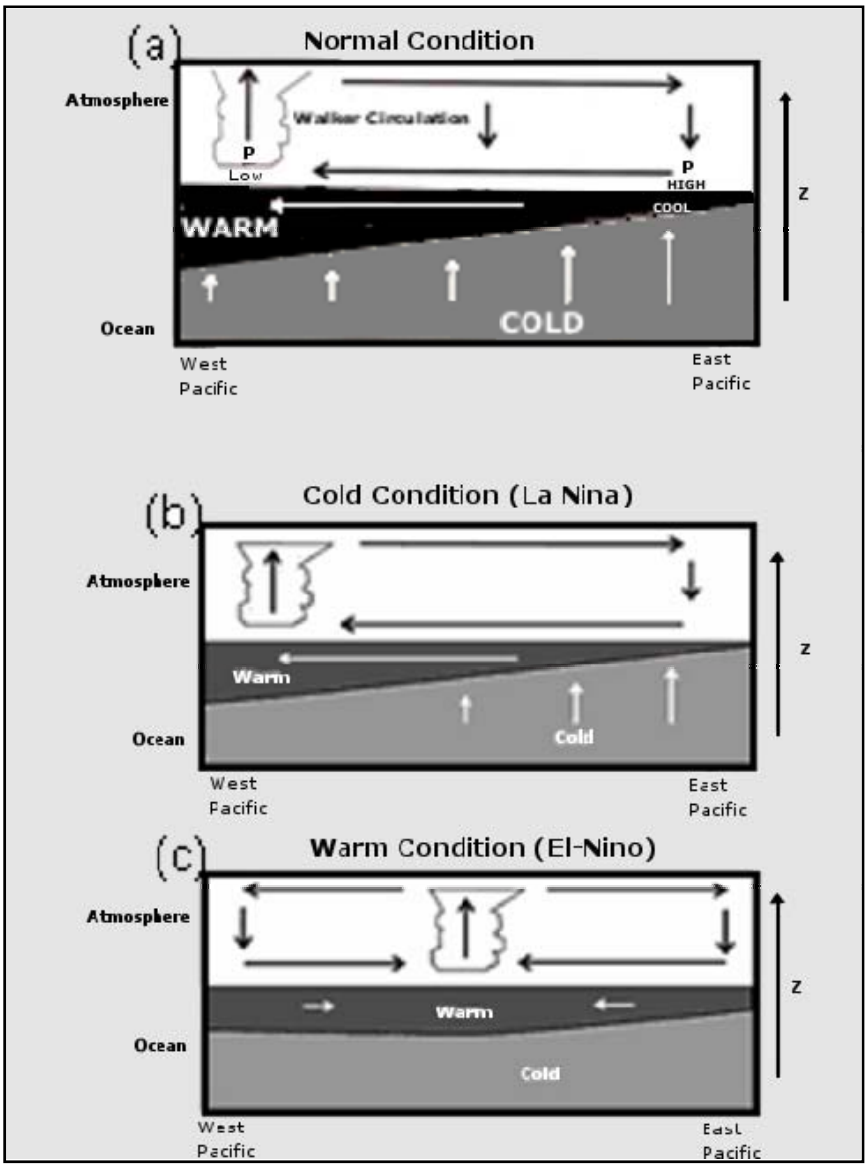

Figure 10: ENSO conditions. From Marshall & Plumb (2008).

La Niña is the phase opposite to the El Niño and it is characterised by cooler than normal ocean temperatures in the central and eastern Pacific (Philander, 1985; Trenberth, 1997; Marshall & Plumb, 2008). Moreover, this phase is accompanied by intensified Trade Winds in the tropical Pacific and enhanced coastal upwelling in the eastern Pacific (Hanley *et al*., 2003; Philander & Fedorov, 2003). As is well known, warm El-Niño phases of the ENSO are associated with marked declines in rainfall and increased air temperatures in the

western tropical Pacific, whereas the cool La-Niña events are often associated with enhanced rainfall and cooler air temperatures (Philander, 1985; Hanley *et al*., 2003).

ENSO events are monitored and archived using measurements of certain oceanic and atmospheric parameters. Several indices have been developed in the past to characterise different phases of ENSO events. The most commonly used indices are the Southern Oscillation Index (SOI) (Troup, 1965) and the temperature based index which is defined by area-averaged surface sea temperature average in various equatorial Pacific regions such as the NINO 1+2, NINO 3, NINO 3.4, and NINO 4 (**Figure 11**) (Trenberth, 1997; Hanley *et al*., 2003). A recent study proposes a new index called "El-Niño Modoki Index" (EMI) (Ashok *et al*., 2007). This latest ENSO index is calculated based on the second Empirical Orthogonal Function (EOF2) of SST anomaly in the central Pacific Ocean. Nevertheless, according to Hanley *et al.* (2003), there is currently no international agreement within the scientific community as to which index best characterises ENSO events.

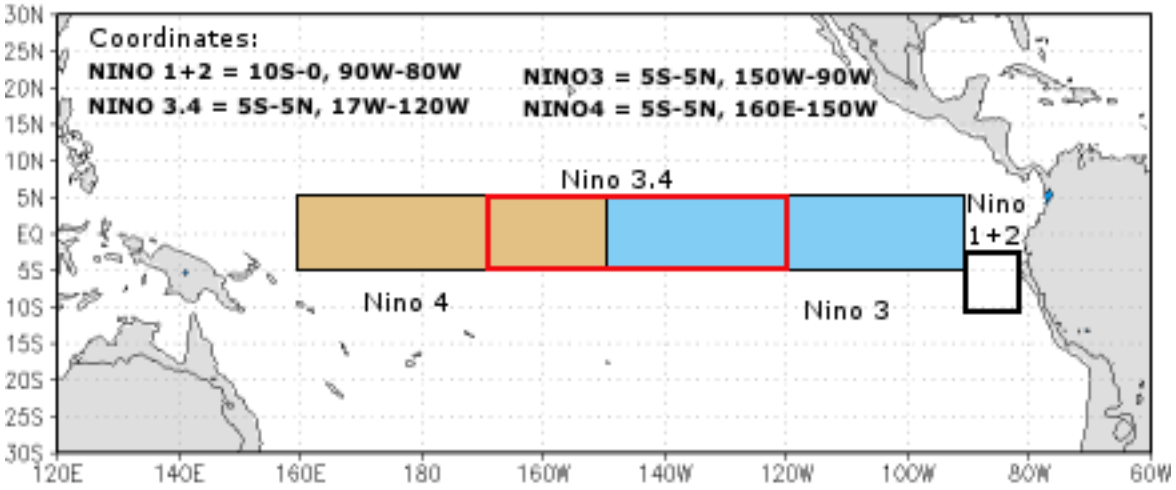

Figure 11. The regions of Nino indices in Pacific Ocean.

The SOI is a direct measure of the strength of the Walker Circulation. It is defined as the sea-level pressure difference between Tahiti (17.6^{o}S, 149.6^{o}W) in the central Pacific and Darwin, Australia (12.4^{o}S, 130.9^{o}E) in the western Pacific (Troup, 1965; BoM, 2002). The SOI fluctuates between a positive and a negative phase; the positive phase of the SOI corresponds to La-Niña events while the negative phase often indicates El-Niño events (BoM, 2002) (**Figure 12a**). In terms of seasonal cycle (**Figure 12b**), this index shows coherent negative index from 1990 to 1995 and from 2002 to 2006 for all seasons. Meanwhile, the highest negative index occurred in June-August 1997, during which the devastating ENSO events happened. Based on data from 33 rainfall stations, Kirono & Tapper (1999) found a highly significant positive correlation between rainfall in Indonesia and the SOI during June to November, especially in southern Indonesia. Therefore, they proposed to employ June to August SOI data in order to predict September to November rainfall anomalies in Indonesia.

On the other hand, according to Barnston *et al.* (1997), the stronger correlation between SST anomalies in the Pacific Ocean and the SOI was found in the Nino 3.4 region. Therefore, based on this region, the Nino 3.4 has been developed as a climate index and has been extensively used by researchers since April 1996 (Trenberth, 1997). Based on a 1997–1998 ENSO study, Barnston *et al*. (1999) found this index has better performance in statistical and dynamic modelling than the other indices. Seasonal Nino 3.4 index (**Figure 12c**), as an example, shows dramatic positive value during September-October 1997 and December-January 1998, during which extreme ENSO events occurred. Meanwhile, the latest index shows highly negative in December-February in early 2008 as shown in **Figure 12c**. This seasonal index will assist recognising ENSO events in terms of season.

a)

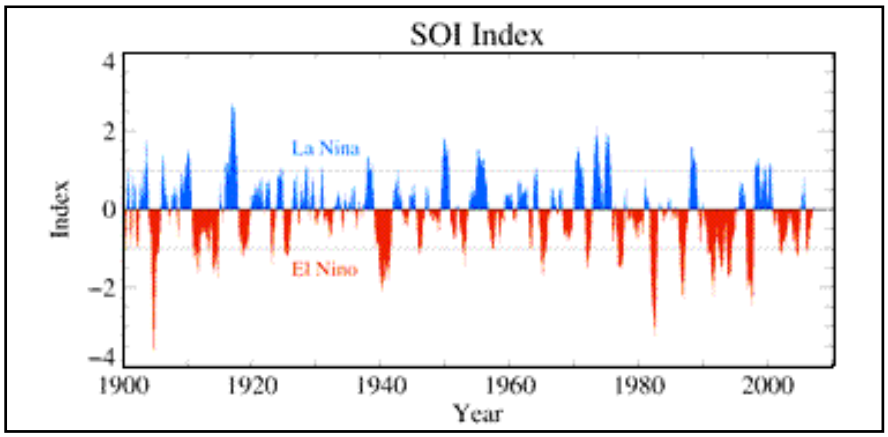

b)

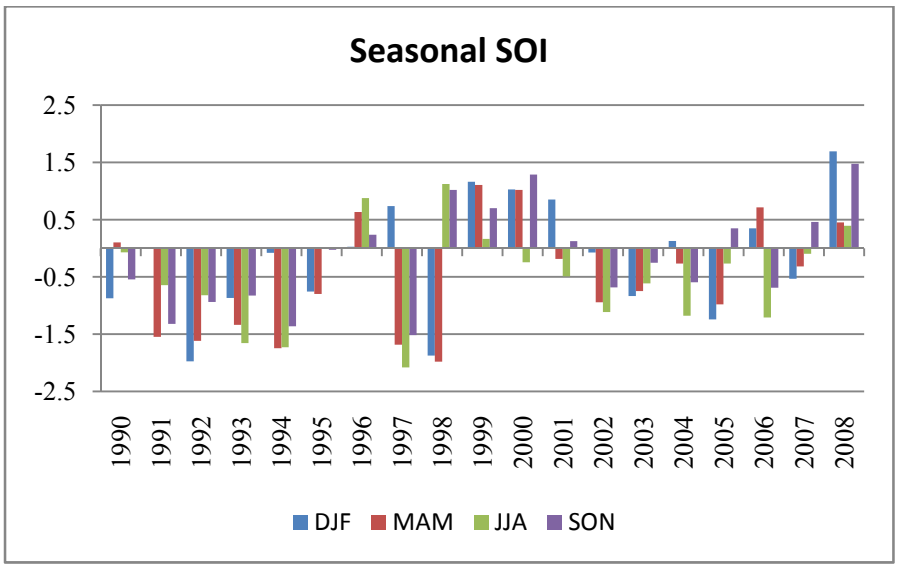

c)

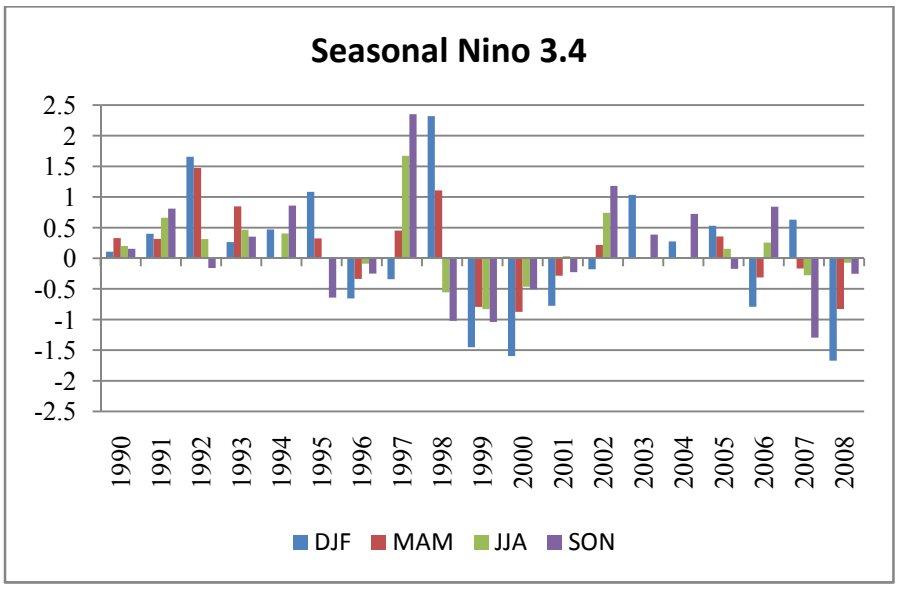

Figure 12. a) Time series of SOI. From : www.mfe.govt.nz. b) Seasonal SOI from 1990-2008 derived from BoM (2002). c) Seasonal NINO 3.4 from 1990-2008 obtained from HadISST 1.1 data.

B. Indian Ocean Dipole (IOD)

The Indian Ocean Dipole (IOD) is a coupled ocean-atmosphere phenomenon in the Indian Ocean being characterised by anomalous cooling of the SST in the south-eastern equatorial Indian Ocean and anomalous warming of the SST in the western equatorial Indian Ocean (Saji *et al.*, 1999) (**Figure 13**). The mode accounts for about 12% of the SST variability in the Indian Ocean. Saji *et al.* (1999) suggests that IOD anomalies are responsible for droughts in Indonesia and above-average rainfall in eastern Africa.

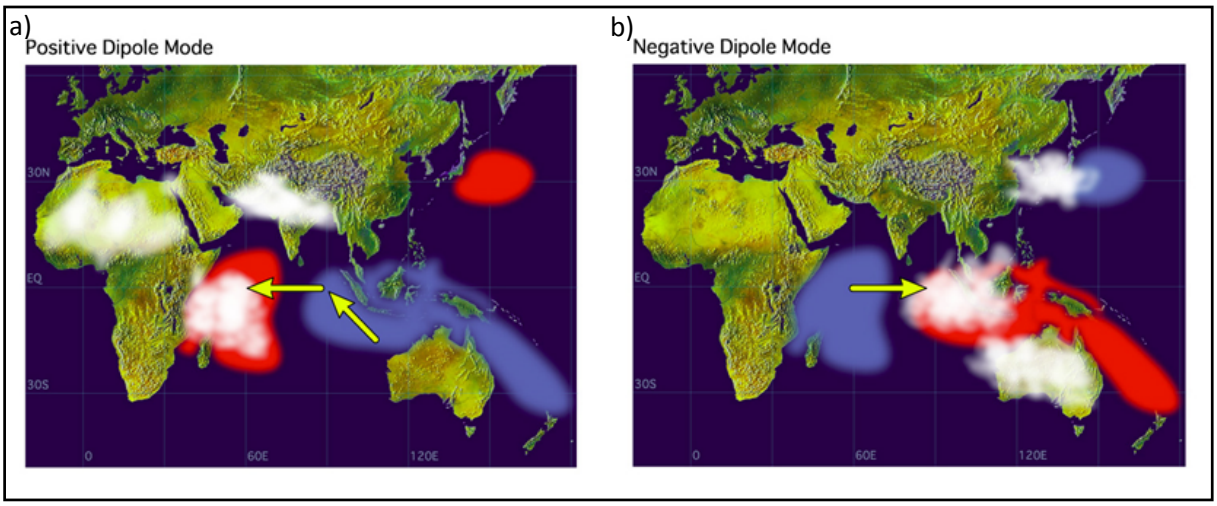

Figure 13. Positive (a) and negative phase (b) of the IOD. Adopted from http://www.jamstec.go.jp/frsgc/research/d1/iod/

The IOD is an important influence on global climate (Saji *et al.*, 1999; Saji & Yamagata, 2003) and it has been intensively studied in recent times. An index to quantify the IOD has been defined (Saji *et al.*, 1999) as the SST difference between the tropical western Indian Ocean (50°–70°E, 10°S–10°N) and the tropical south-eastern Indian Ocean (90°–110°E, 10°S–equator), called the Dipole Mode Index (DMI). When the DMI is positive (negative), the phenomenon is referred to as the positive (negative) IOD. For example, the positive IOD can initiate drought conditions over the western Indonesian region and heavy rains over eastern Africa, while a negative index indicates heavy rain

over the western Indonesian region and drought conditions over eastern Africa (Saji *et al.*, 1999). **Figure 14a** displays a time series of the DMI and **Figure 14b** shows seasonal index of DMI from 1990-2008. The extreme index can be clearly seen for the most interesting ENSO events, during which 1997/1998 periods. September-November were the highest index, which occurred in 1997; Then followed by December-February in 1998, which peaked at 0.8 normalised anomaly.

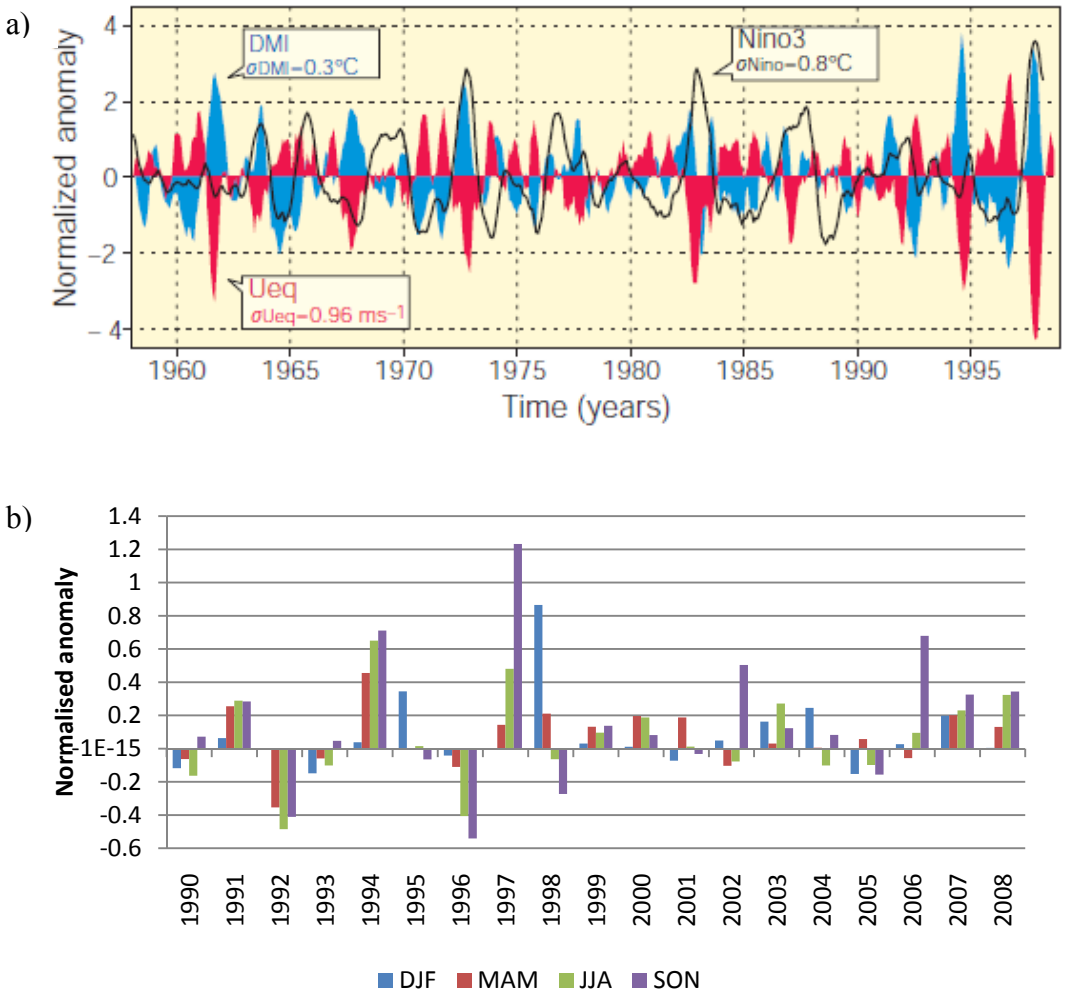

Figure 14. a) Time series of DMI from 1958–1998. From Saji *et al.* (1999). b) Seasonal DMI from 1990-2008 derived from HadISST 1.1 data

The IOD influences both regional climate patterns (Ashok *et al.*, 2001) and the global climate (Saji & Yamagata, 2003). In terms of regional effect, the Indian summer

monsoon rainfall is clearly modulated by the IOD (Ashok *et al*., 2001). Meanwhile, at the global level, IOD, with a positive DMI, is related to reduced rainfall and warm land surface anomalies in several regions such as Europe, North and South America, South Africa and north-east Asia. In addition, a recent finding by D'Arrigo *et al.* (2008) demonstrated that, over the past two centuries, rainfall over Java was strongly related to the IOD. Other evidence indicates stronger and more regular IOD events during the twentieth century (Abram *et al*., 2008). This intensification has had effects not only on climate variability, but also on marine ecosystems such as coral reefs (Abram *et al*., 2008) and land crops, especially potatoes in Pangalengan, West Java, Indonesia (Boer & Wahab, 2007).

C. Inter-decadal Pacific Oscillation

The Inter-decadal Pacific Oscillation (IPO) was first proposed by Power *et al.* (1999). The IPO is defined as the coherent pattern of SST variability occurring on inter-decadal time scales in the Pacific Ocean (Power *et al.,* 1999). This anomalous warming and cooling of the extra-tropical Pacific is characterised by changes in persistent large-scale SST anomalies that occurred in 1921, 1944 and 1973 (Power *et al.,* 1999). Moreover, they also documented an association in inter-decadal variability between the SOI and year-to-year changes in the overall Australian averages of rainfall, maximum surface temperature, and the wheat crop yield. Their results demonstrated the possible influence of the IPO on the Australian climate.

The IPO has been identified as part of a continuous spectrum of low frequency modulations of the ENSO (Folland *et al.*, 2002), and is characterised using the time series of the EOF3 of 13 years low pass filtered global SST (Folland *et al*., 1999; Power *et al*., 1999). A number of studies have shown that the IPO influences both the strength and the nature of the ENSO cycle (Power *et al*., 1999; Verdon *et al*., 2004). A recent study by Power *et al.* (2006) demonstrated that ENSO events and their impact on Australian rainfall are correlated to the IPO. A study by Folland *et al.* (2002) also demonstrated the significant affect of the IPO on the movement of the South Pacific Convergence Zone (SPCZ), independent of the ENSO. The influence of the IPO on rainfall in tropical regions is documented (i.e. Manton, 2001; Meinke *et al.,* 2005), but there has been little focus so far on the Indonesian region.

Different techniques are used to produce the IPO index. Whereas Power *et al.* (1999) used a spectral filter with a 13 year cut-off, Folland *et al.* (1999) applied a low-pass filter to global SST data. Both methods produce similar results. **Figure 15a** displays a time series of this index from 1900 to 2006. Seasonal IPO index are also presented in **Figure 15b,** which are consistent with the annual patterns of the IPO index.

2.5. Gaps in Knowledge

Although rainfall variability of the Indonesian region has been intensively investigated, the studies were conducted either more focused on regional scales (i.e. Aldrian & Djamil, 2008; Moron *et al.*, 2009) or more concentrated until the last 1990s (i.e. Haylock & McBride, 2001; Hendon, 2003; Aldrian & Susanto, 2003). As far as the author aware, there is only limited climate study in Indonesian, which incorporates recent climate data. It is important, therefore, to have the latest data or information in order to get further insight the climatic condition and the influence of global climate drivers in Indonesia.

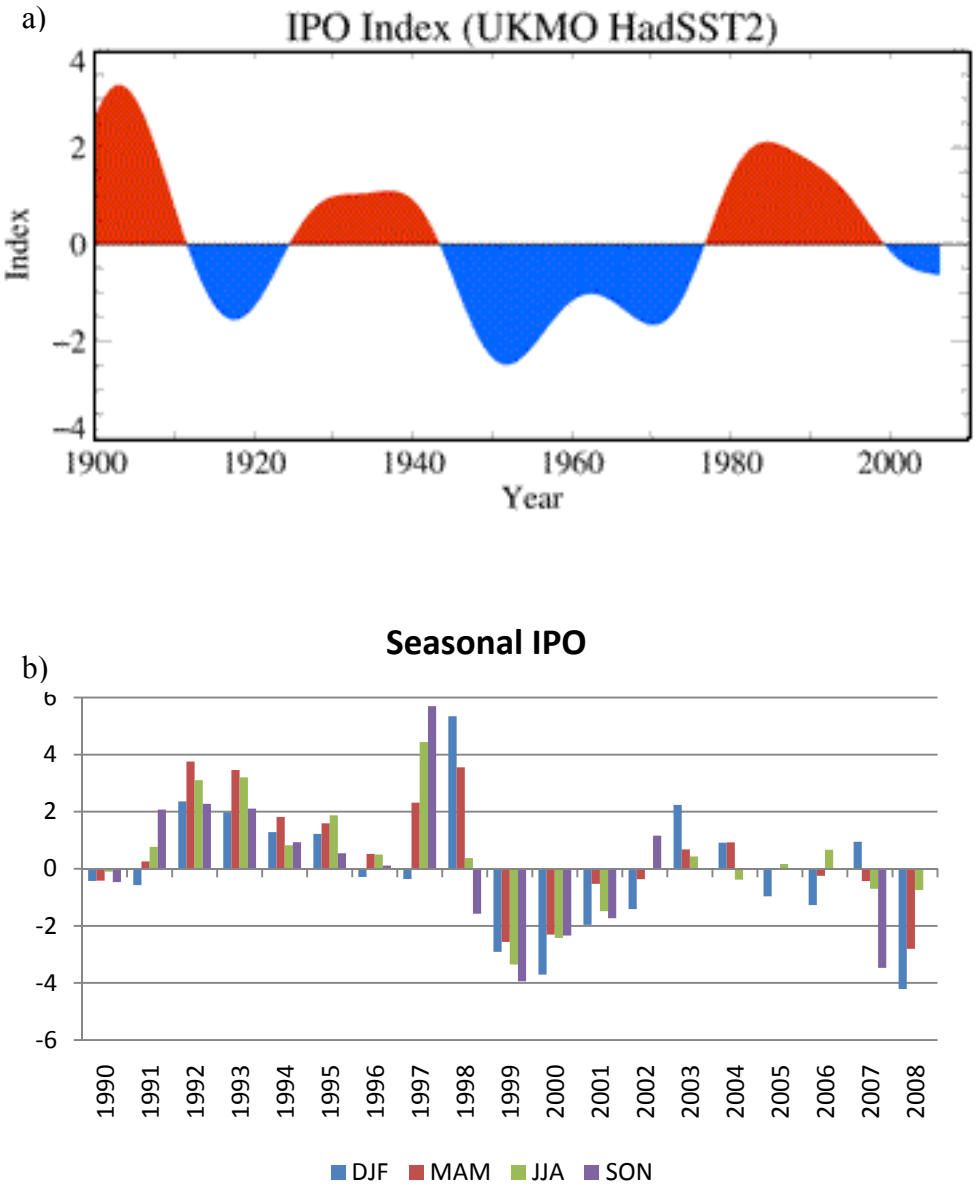

Figure 15. a) Time series of the IPO index. From : www.mfe.govt.nz. b) Seasonal IPO from 1990-2008 obtained from Parker (2007).

CHAPTER 3: Data and Methods

Chapter Summary: This chapter describes the data sets used and the methods employed in this study.

3.1. Data

A. Rainfall

The rainfall data used in this thesis are monthly terrestrial precipitation data set (version 2.01) for the period 1900-2008 developed by the University of Delaware. This gridded data is based on a 0.5-degree spatial resolution (Matsuura & Willmott, 2009). For Indonesia, the data sets are primarily based on station observations from the Global Historical Climate Network, version 2 (GHCN), station observations from the Global Surface Summary of the Day (GSOD) (Matsuura & Willmott, 2009) and including background climatology from the work of Legates & Willmott (1990).

The data set used in the study covers the area from 10^{o}S–10^{o}N and 90^{o}–140^{o}E, with a monthly resolution from January 1900 to December 2008. For a full explanation of the techniques used in the compilation, spatial interpolation and spatial cross-validation of this data set, the reader is referred to Matsuura & Willmott (2009). Vimont *et al*. (2010) have previously used this data set to investigate rainfall downscaling in the Indonesian region. Their results show that these data sets are reliable and appropriate for use in this region.

Spatial variation of rainfall over Indonesia is divided into three regions following Aldrian & Susanto (2003), based on the Double Correlation Method (see **Figure 3**). In this work, Indonesia is divided into four different rainfall regions. The first three regions;

region A, B, and C (the latter only to some extent) were adopted from Aldrian & Susanto's (2003) and Aldrian's (2007) findings. Region A covers the southern part of the country, region B covers the north-western part, and region C covers the Moluccan area (**Figure 16**). It should be mentioned that the Indonesian Bureau of Meteorology and Geophysics (BKMG) uses a different division of Indonesian climatic regions. This classification has been revised by Aldrian & Susanto (2003), even though the results are relatively similar (Aldrian, pers. comm., 2010). The last region, which is region D, lies over Papua. The rationale behind the separation of this region from the original region A used by Aldrian & Susanto (2003) is to verify whether rainfall trends in this subregion (located in close vicinity to the Pacific Warm Pool) differ from trends calculated in the other subregions.

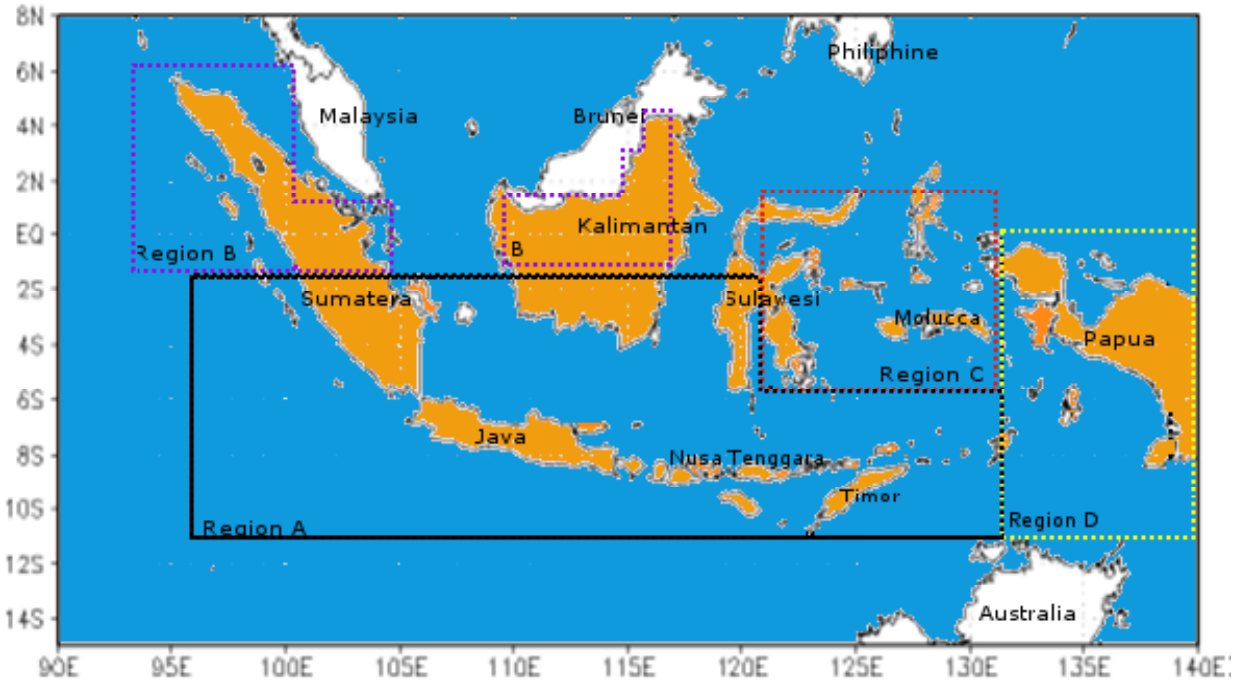

Figure 16. Definition of different rainfall regions used in this study.

B. Sea Surface Temperature

The relationship between rainfall variability over Indonesia and SST anomalies are diagnosed using SST data obtained from the Meteorology Office Hadley Centre for Climate Change, namely the HadISST data set (Version 1.1) (Rayner *et al.*, 2003). This data replaces the previous data set (GISST) by Smith *et al.* (1996). It is a combination of monthly globally-complete fields of SST and sea ice concentration on a 1 degree latitude by 1 degree longitude grid that are available from 1870 up to the present (Rayner *et al.*, 2003). This study only considers the period from 1900 to 2008. The SST data are taken from various sources such as the Meteorology Office Marine Data Bank (MDB) and the International Comprehensive Ocean-Atmosphere Data Set (ICOADS) as explained in detail, including the reconstruction processes, in Rayner *et al.* (2003). The HadISST1 data set is freely downloadable from http://hadobs.metoffice.com/hadisst/.

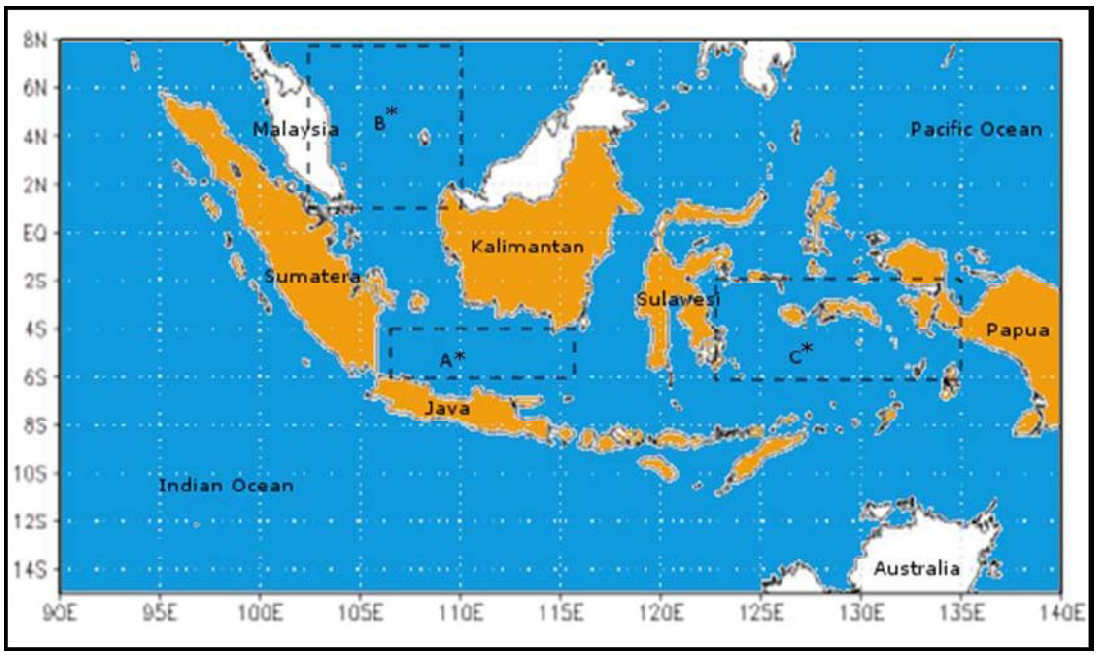

Figure 17. SST regions (A*, B* and C*) considered in this study (dashed boxes).

The monthly mean SST data set used in this study spans the period from 1900 to 2008 (the same period as the rainfall data). The local SST data has been acquired for the regions illustrated by the highlighted boxes in **Figure 17**. There are three local SST regions: A* (106°–112°E; 4°–6°S), B* (103°–110°E; 1°–8°N), and C* (123°–135°E; 2°–6°S). The choice of these regions is based on the pathways of Indonesian Throughflow and possible upwelling of cold water which has a local correlation to rainfall anomalies (Gordon, 2005). Moreover, there is a possible connection between local SST anomalies and climate events such as ENSO and IOD (Iskandar, 2010), especially in the eastern part of Indonesia, which together with the South China Sea, exhibit larger a seasonal variability compared with other regions (Qu *et al.*, 2005).

C. Climatic Indices: ENSO

Two ENSO-related indices were considered in this project; NINO 3.4 and the SOI. The first index is NINO 3.4, which is computed from monthly SST anomaly in the region 5°N–5°S, 120°–170°W based on HadISST1 data set. This index was used to compute the correlation between ENSO and rainfall variability in the Indonesian region in comparison with regional SST anomalies. Moreover, the SST variations in this region are associated with the convective anomalies that accompany the Southern Oscillation (Deser & Wallace, 1987). The second index is the SOI obtained from the Commonwealth Bureau of Meteorology (BoM) at **http://www.bom.gov.au/climate/current/soihtm1.shtml**. This archive comprises mean monthly data from 1876 up to the present computed using the Troup method (Troup, 1965). This method is a standardised anomaly given by the formula:

$$SOI = 10\frac{[Pdiff - Pdiffav]}{SD(Pdiff)}, \quad (1)$$

where *Pdiff* is the difference between monthly averages of Tahiti mean sea level pressure and that at Darwin (Autralia), *Pdiffav* is the long-term average of Pdiff for the month in question, and SD(*Pdiff*) is the long-term average of the standard deviation of *Pdiff* for the month in question.

D. Climate Indices: Inter-decadal Pacific Oscillation (IPO)

This study uses monthly time series based on Folland *et al.* (1999) and improved by Parker *et al.* (2007). Parker *et al*. (2007) reanalysed the data set using an updated HadSST2 data base.

E. Climate Indices: Dipole Mode Index

Monthly values of DMI are computed by taking the difference between the climatological mean and monthly mean SSTs of the western equatorial Indian Ocean (50^{o}–70^{o}E and 10^{o}S–10^{o}N) and the south-eastern equatorial Indian Ocean (90^{o}–110^{o}E and 10^{o}S–0^{o}N), as explained in detail by Saji *et al.* (1999). In order to obtain updated data of the DMI (Oldenborg, *pers.comm*., 2010), the data from the KNMI Climate Explorer (http://climexp.knmi.nl) were employed in this project.

3.2. Methods

A. Correlation Analysis

To establish the statistical connection between SST anomalies and anomalous Indonesian rainfall, Pearson's product-moment correlation coefficients between relevant SST anomalies and grid-point rainfall are computed.

Lagged correlation is the correlation between two times series, whereby one of the series is systematically shifted by certain time intervals with respect to the other time series. This is a standard method to determine potential temporal delays between the

values of two variables. To this end, the correlation coefficient as a function of the time lag is calculated from:

$$r(d) = \frac{\sum_i [(x(i)-mx)(y(i-d)-my]}{\sqrt{\sum_i (x(i)-mx)^2}\sqrt{\sum_i (y(i-d)-my)^2}} \quad (2)$$

where *mx* and *my* are the means of the corresponding time series *x* and *y* of *N* measurements, *i* is the time index, and *d* is the lag of either positive or negative value. This lag analysis is performed here on monthly mean data, but the display is grouped according to the seasons December–February (DJF), March–May (MAM), June–August (JJA), and September–October (SON). In addition to this, correlation coefficients are also calculated on the basis of a sliding window approach, being equivalent to the method of window-averaging. Uncertainly of correlation values is calculated at 95% confidence interval using Fisher's transformation (i.e. Plata, 2006.)

B. <u>Empirical Orthogonal Function (EOF)</u>

A number of different empirical techniques have been used to analyse rainfall variability. This project adopts the Empirical Orthogonal Function (EOF) technique. The EOF method by Lorenz (1956) is widely used in meteorological (i.e. Wilks, 2006; Hannacchi *et al.,* 2007) and oceanographic studies (i.e. Emery & Thompson, 1997). It is a statistical method used to reconstruct a multivariate dataset into its principal components (PCs). The purpose of the EOF analysis is to determine a small number of functions that describe the majority of the variance in the data, and to distinguish dominant modes from the remaining variance (Hannachi *et al.,* 2007). As applied in this research, the bulk of variance present in the rainfall data can be described by a small number of orthogonal

modes, making it easier to understand the major rainfall properties. However, even though EOFs offer the most efficient statistical means of data compression, the empirical modes derived do not necessary correspond to the true dynamical modes of physical behaviour. In some cases, a single physical process may be spread over more than one EOF mode, whereas in other situations, more than one process may contribute to the variance contained in a single EOF (Emery & Thomson, 1997).

The EOF analysis uses a set of orthogonal functions to represent a time series of spatial patterns, such that

$$T(x,t) = \sum_{n=1}^{N} \alpha_n(t).F_n(x), \quad (3)$$

where $T(x,t)$ is the original time series as a function of time (t) and space (x). $F_n(x)$ is a dimensional spatial pattern, and $\alpha_n(t)$ represents a non-dimensional principal component which describes how the amplitude of each spatial pattern varies with time. This project used the KNMI Climate Explorer of the Royal Netherlands Meteorological Institute, accessible via http://climexp.knmi.nl/, to determine the most important modes from the EOF analysis. According to Oldenborg (*pers. comm.*, 2010), this calculation is based on the covariance matrix approach from the anomaly data matrix *S*. In order to calculate the uncertainty of the eigenvalues and/or the eigenvectors of *S* and to obtain statistically significant levels, North's criterion was conducted in this study (North *et al.*, 1982). This test is widely used as a statistical significance test in meteorological and oceanographic settings (Emery & Thomson, 1997; Hannachi *et al.*, 2007).

C. Wavelet Analysis

In signal analysis, there are a number of different functions that one can perform on a particular signal in order to translate it into different forms that are more suitable for other applications. The most popular function is the Fast Fourier Transform (FFT) that converts a signal from time versus amplitude to frequency versus amplitude squared. This transformation is useful for many applications; however it is not based only on time, but also on non-stationary frequencies and amplitudes (McCowan, 2007). Wavelet transformation can be used to solve this issue. The aim of wavelet transformation is to estimate both the spectral content of the signal and its level of change over time. Therefore, wavelet transformation analysis provides information on both the amplitude of a periodic signal within a time series, and how this amplitude varies with time including trends, breakdown points and discontinuities (Torrence & Compo, 1998).

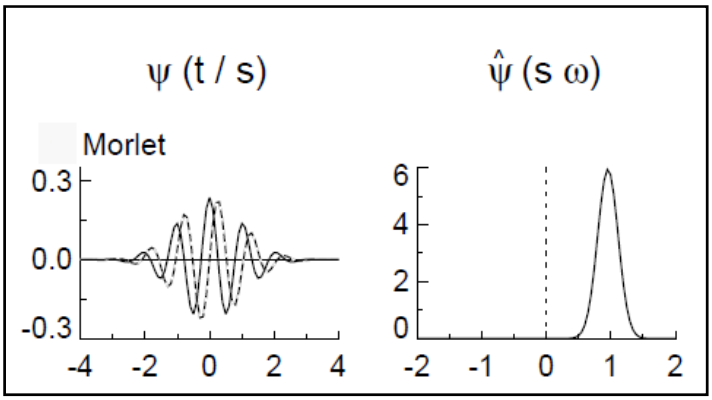

Figure 18. Morlet wavelet basis. The left plot shows the real part (solid) and imaginary part (dashed) for the wavelets in the time domain. The right plot shows the corresponding wavelets in the frequency domain. From Torrence & Compo (1998).

The wavelet analysis is calculated based on the Morlet function, which consists of a plane wave modulated by a Gaussian (4) for the power spectrum and global spectra. This function is used basically to refer to either orthogonal or non-orthogonal wavelets

(Torrence & Compo, 1998). The Morlet wavelet basis (**Figure 18**) refers to an orthogonal set of wavelet function given by:

$$\psi_0(\eta) = \pi^{-\frac{1}{4}} e^{i\omega_0\eta} e^{-\eta^2/2} \quad (4)$$

where η is a non-dimensional time parameter and ω_0 is the non-dimensional frequency. The transformation of the Morlet wavelet basis is performed in Fourier space using the method described in Torrence & Compo (1998). In order to test for non-stationary changes in variance, the Global Wavelet Spectrum (GWS) is performed, as also described in Torrence & Compo (1998). In this study, wavelet analysis was applied to rainfall data and time series of large-scale climate drivers.

3.3. Tools used for data analysis

Both the Matlab software suite (http://www.mathworks.com/products/matlab/) and the KNMI Climate Explorer (http://climexp.knmi.nl/) tools have been used in this project. All statistical analyses in this research have been performed at 95% confidence level.

CHAPTER 4: Results and Discussion

Chapter Summary: This chapter presents and discusses the results of this project. This includes statistical analyses of regional variability of Indonesian rainfall, lag correlations between rainfall anomalies and local SST anomalies, lag and sliding-window correlations between climate drivers and rainfall anomalies, and a detailed analysis of recent rainfall trends.

4.1. Annual Mean Rainfall and Recent Trends

The highest annual mean rainfall of ~30cm/month occurs on Borneo Island in the northern part of Indonesia and in the southern regions of Papua (**Figure 19a**). Other parts the country, including Sumatra and Celebes, experience medium levels of annual mean rainfall with values of ~20cm/month. The lowest rainfall values <15cm/month are found on regional scales (e.g. at the northern tip of Sumatra, and eastern Java). In contrast to this, the north-western parts of Australia experience much less precipitation of 5-10 cm/month. The standard deviation of rainfall amounts to 10-20% of the annual-mean value (**Figure 19b**).

The time series of annual mean rainfall from 1900 to 2008 in Indonesia (**Figure 20a**) reveals a sharp drop in rainfall exceeding 10% with reference to the long-term average (**Figure 20b**). This decline commences in the early 1990s with a series of years of anomalously low rainfall <15cm/month. A range in rainfall between 20 and 25cm/month was common before 1990 and the low-rainfall years after 1990 are unprecedented in the observational data set. Around the year 2000, annual-mean rainfall went back to a "normal" value of 25cm/month, but this was only a transient feature followed by low values of ~14cm/month in 2004. The lowest annual rainfall was found in 1997 dropping below 13cm/month.

This apparent shift in intra-decadal rainfall variability occurred in all Indonesian rainfall regions A – D (defined in **Figure 15**) (**Figure 18**). Annual mean rainfall dropped during the period from 1990 to 1997 in all regions, sharply increased in 2000, possibly related to ENSO activity, and decreased again to low values until 2004. However, annual mean rainfall increased again in all regions towards the end of the study period. After

1990, region C (comprising Molucca and the eastern parts of Sulawesi) experienced the highest intra-decadal rainfall decline of >15cm/month. The other regions displayed decline of ~10cm/month.

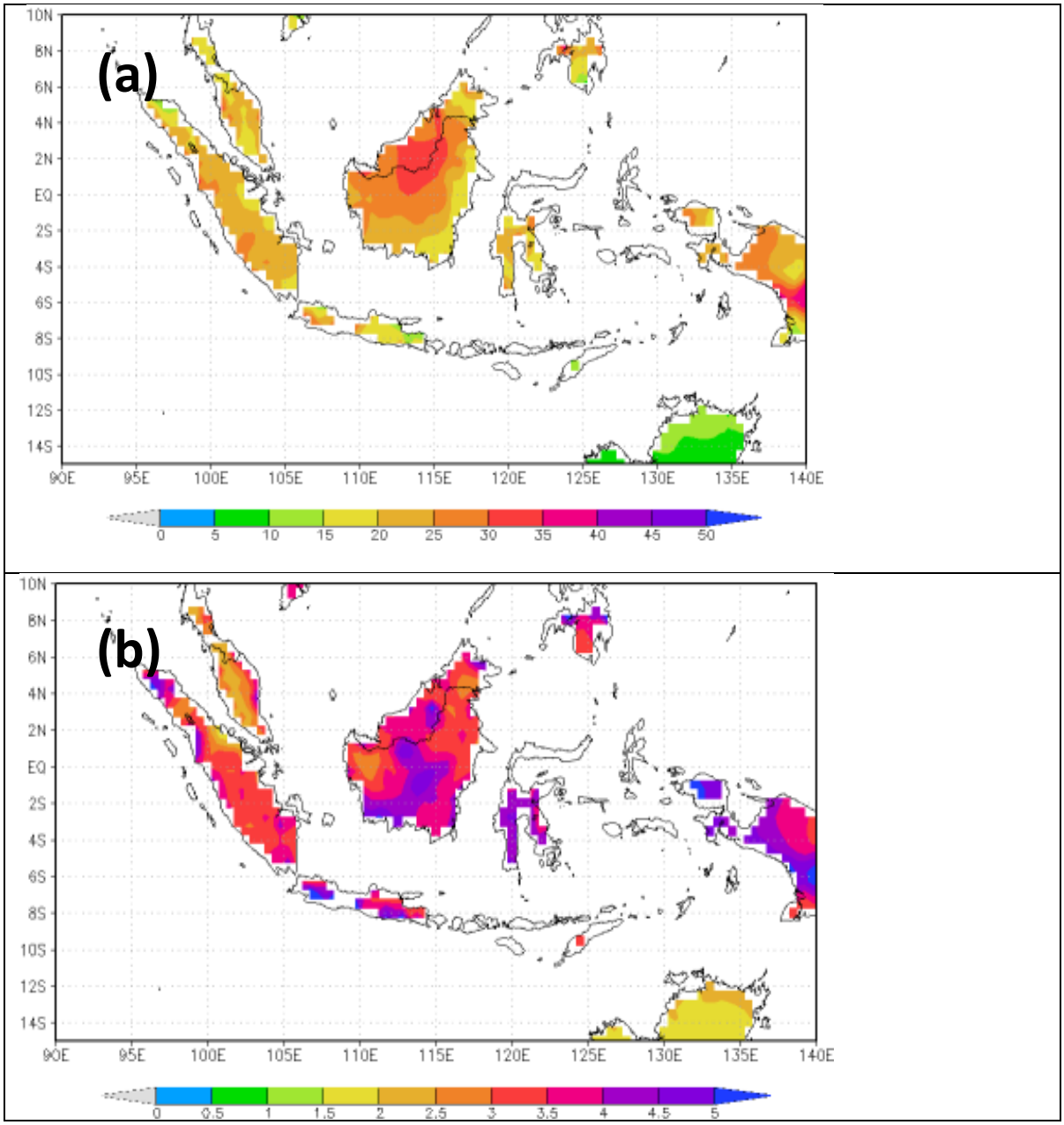

Figure 19. a) Annual mean rainfall (cm/month) in Indonesia, and b) standard deviation of annual-mean rainfall (cm/month) from 1900-2008.

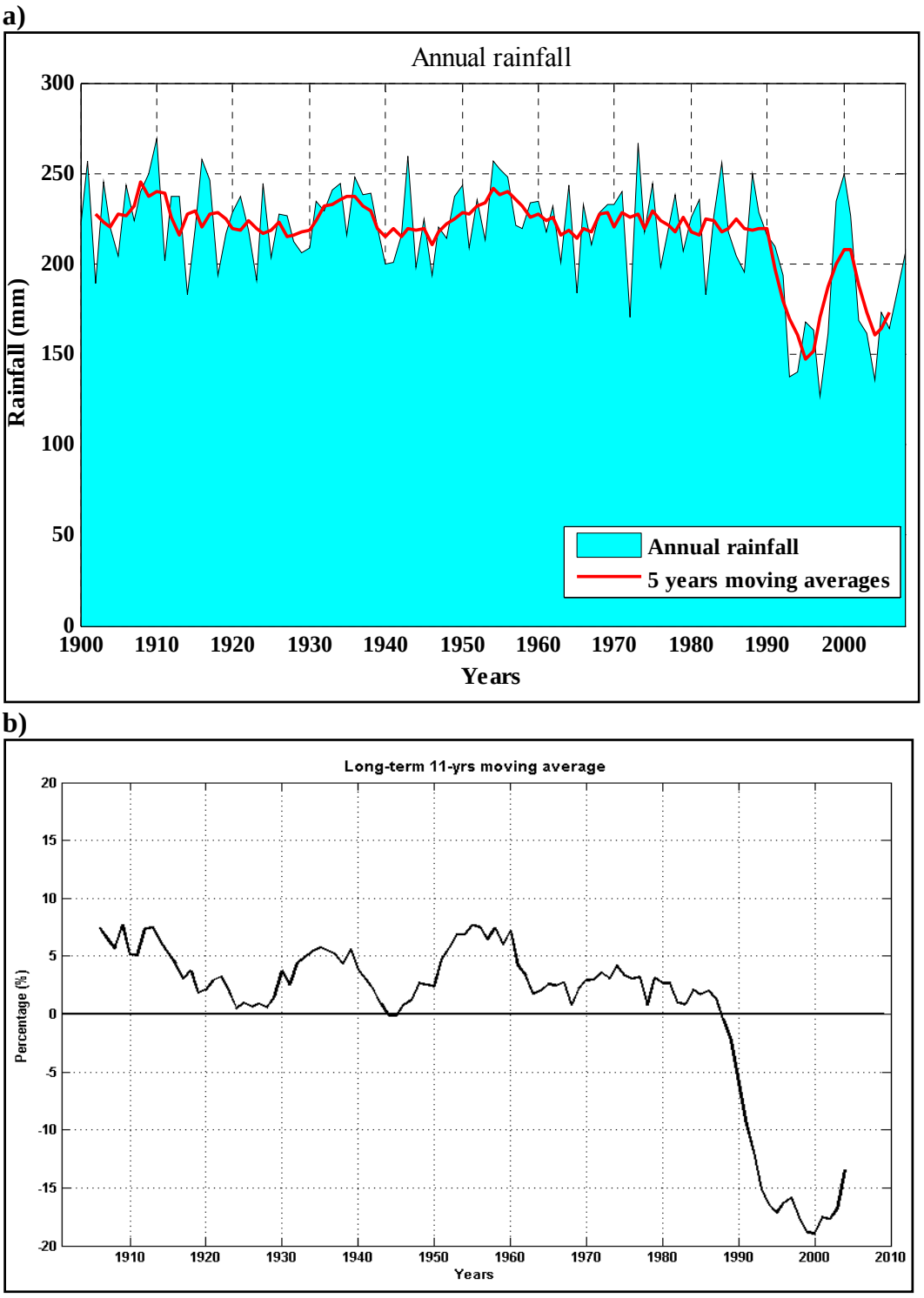

Figure 20. a) Annual-mean Indonesian rainfall from 1900 to 2008 (blue) with 5-year moving average (red line). b) Annual-mean percentages of rainfall values with reference to the long-term mean for the entire period. Shown is 11-year moving averages.

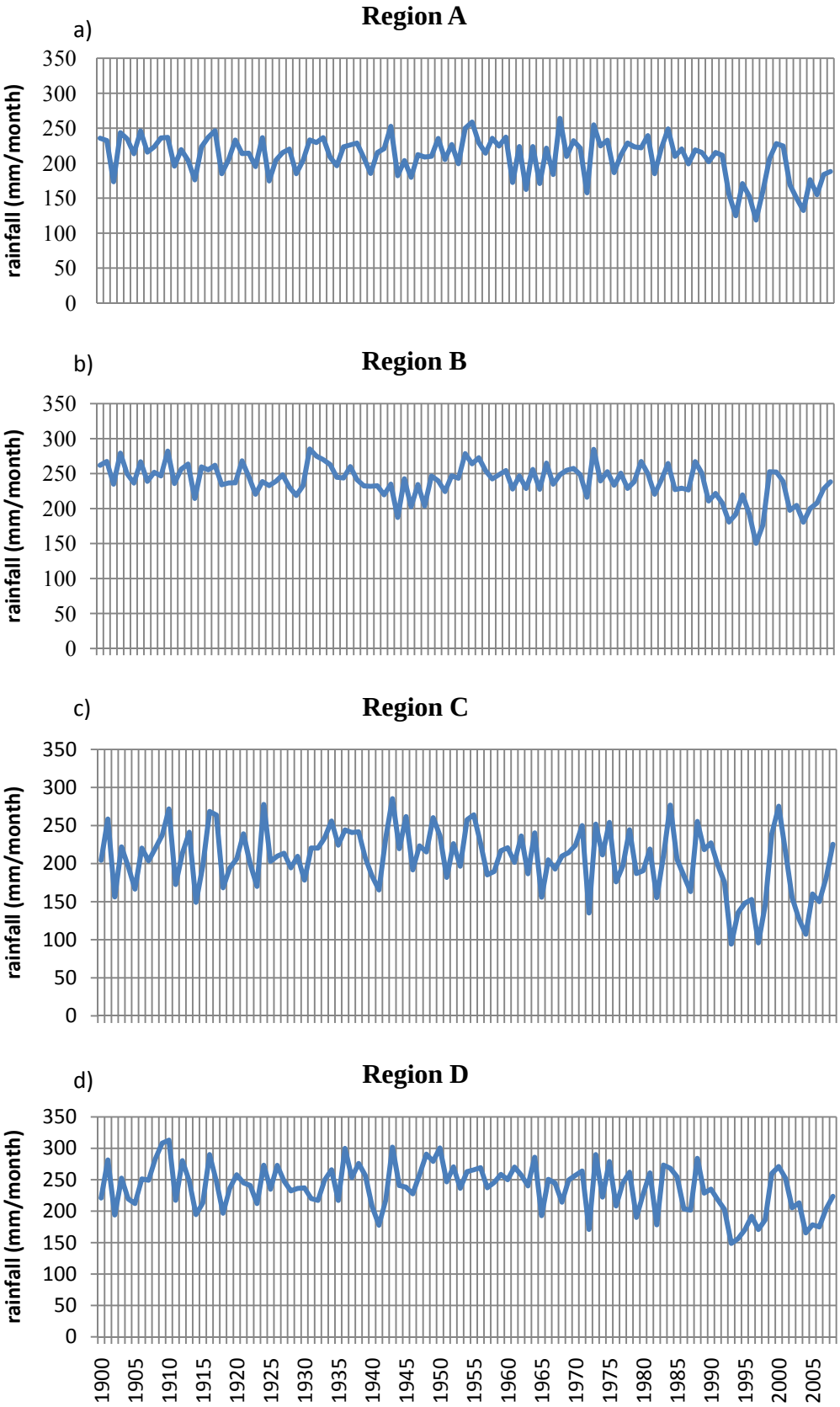

Figure 21. Annual-mean rainfall (mm/month) in regions A, B, C and D (see Fig. 16)

4.2. Intra-Annual Rainfall Patterns and Recent Trends

Figure 22 shows the mean annual rainfall cycles of each of the regions including their standard deviations. Each region has its own characteristics. Region A has a precipitation peak (~30cm/month) in January, whereas minimum rainfall (~5cm/month) usually occurs in the period September – November, in agreement with previous findings by Aldrian & Susanto (2003) (see **Figure 4**). This feature is mainly related to monsoonal activity; that is, the wet northwest monsoon occurring from November to March and the dry southeast monsoon coming into play from May to September (Aldrian *et al.,* 2007). In contrast, Region B has two precipitation peaks; one in the period March – May (~25cm/month) and the other one in the period October – November (~30cm/month). This feature is related to the southward and northward movement of the ITCZ (Aldrian & Susanto, 2003). Region C experiences maximal precipitation in the period May – June (~27cm/month) with another seasonal rainfall peak occurring in January (~22cm/month). This region has the lowest rainfall in the period September – November (~13cm/month), which is 2 months later than in Region A. Region D experiences relatively steady rainfall over the seasons with maximal rainfall (~30cm/month) occurred around March, and minimum rainfall of ~20cm/month occurred from May to November.

Aldrian & Susanto (2003) included Region D as part of their Region A in their rainfall analysis. The treatment of Region D as a separate rainfall regime, as done in this thesis, reveals the existence of more pronounced seasonal rainfall variations in Sumatra, Java and southern parts of Kalimantan and Sulawesi than apparent in Aldrian & Susanto's work (2003). Minimum monthly rainfall in Region A, according to Aldrian & Susanto (2003), amounts to ~100cm/month (see Figure 4a), whereas the minimum monthly rainfall in this work's modified Region A (without Region D) is only ~50cm/month (see Figure 19). This marked difference justifies the separate treatment of Region D in this study.

To reveal climatic shifts in annual rainfall cycles in Indonesia, **Figure 23** displays the same as Figure 18, but exclusively for the last 15 years of data (1994–2008), a period that was not covered in the previous study by Aldrian & Susanto (2003). Interestingly, during this period, rainfall in Region A during the period July – September has declined to extremely small levels with minimum values of <5cm/month in August. Such low rainfall did not occur prior to the 1990s.

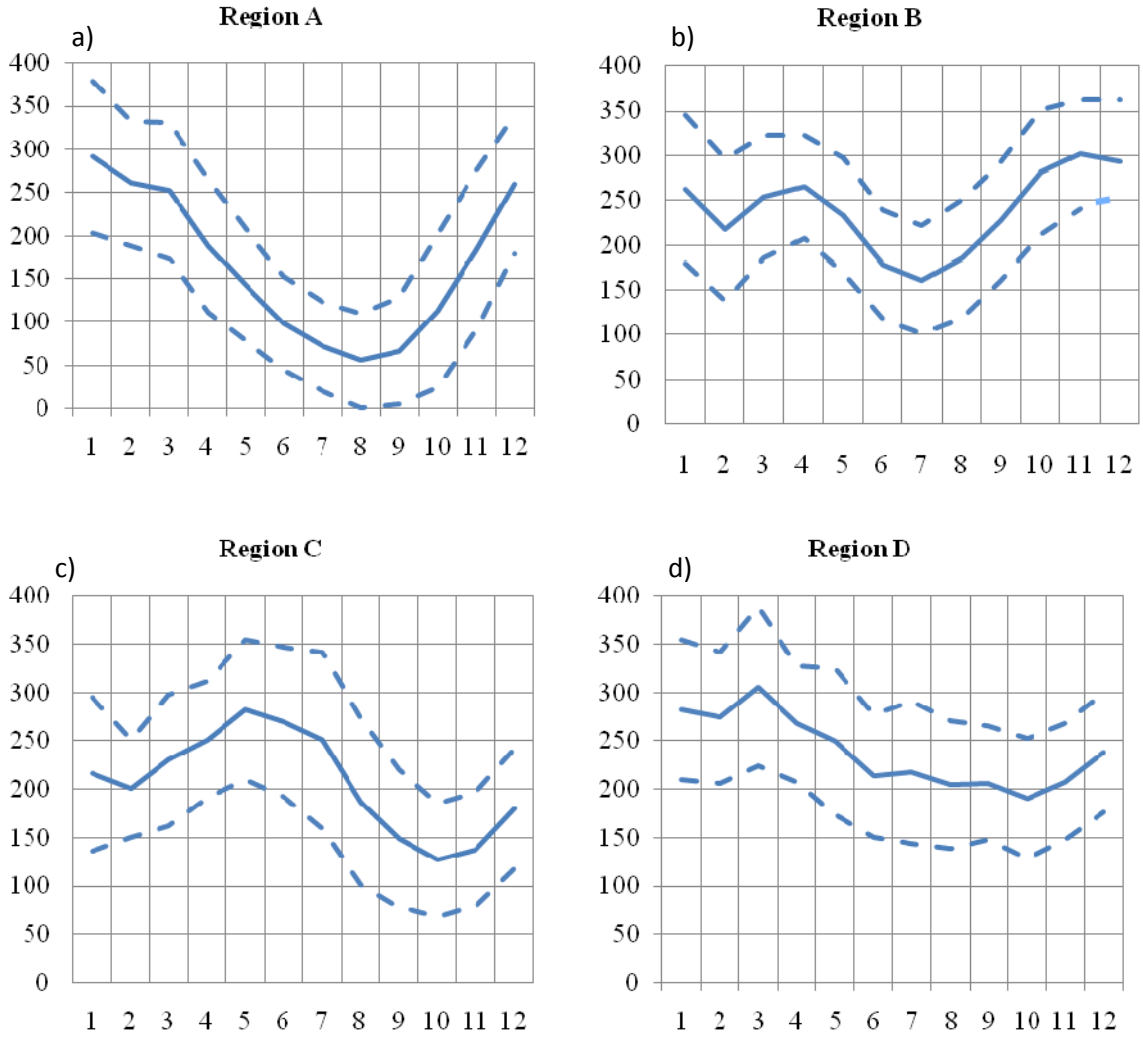

Figure 22. Climatological monthly mean precipitation (mm/month) in a) region A, b) region B, c) region C, and d) region D from 1900–2008 (solid lines). Dashed lines denote the mean value ±1 standard deviation. The horizontal axis represents month while the vertical axis represents rainfall (mm/month).

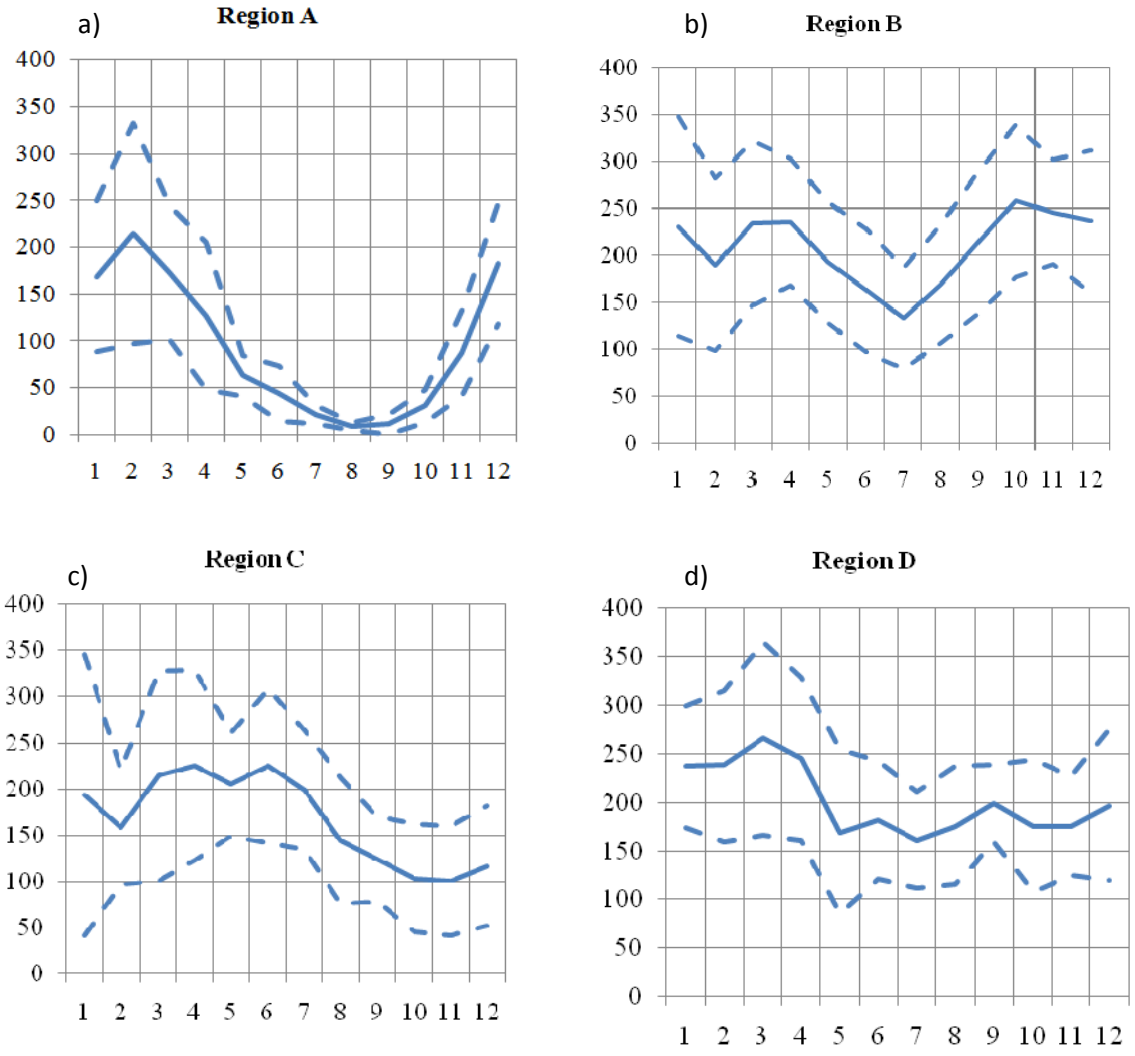

Figure 23. Climatological monthly mean precipitation (mm/month) in a) regions A, b) region B, c) region C and d) region D from 1994–2008 (solid lines). Dashed lines denote values ±1 standard deviation. The horizontal axis represents month and the vertical axis represents rainfall (mm/month).

Differences in monthly mean rainfall patterns between the period 1994-2008 and the entire time period from 1900 to 2008 reveal more details (**Figure 24)**. These differences show that rainfall has decreased throughout Indonesia and, with few exceptions, during every month of the year. Rainfall declines over the months in Region A are more coherent than in other regions except for increased differences in January. Conversely, Region B experiences the smallest overall monthly rainfall declines, especially in August and September. In Regions C and D, the greatest rainfall decline occurred during May.

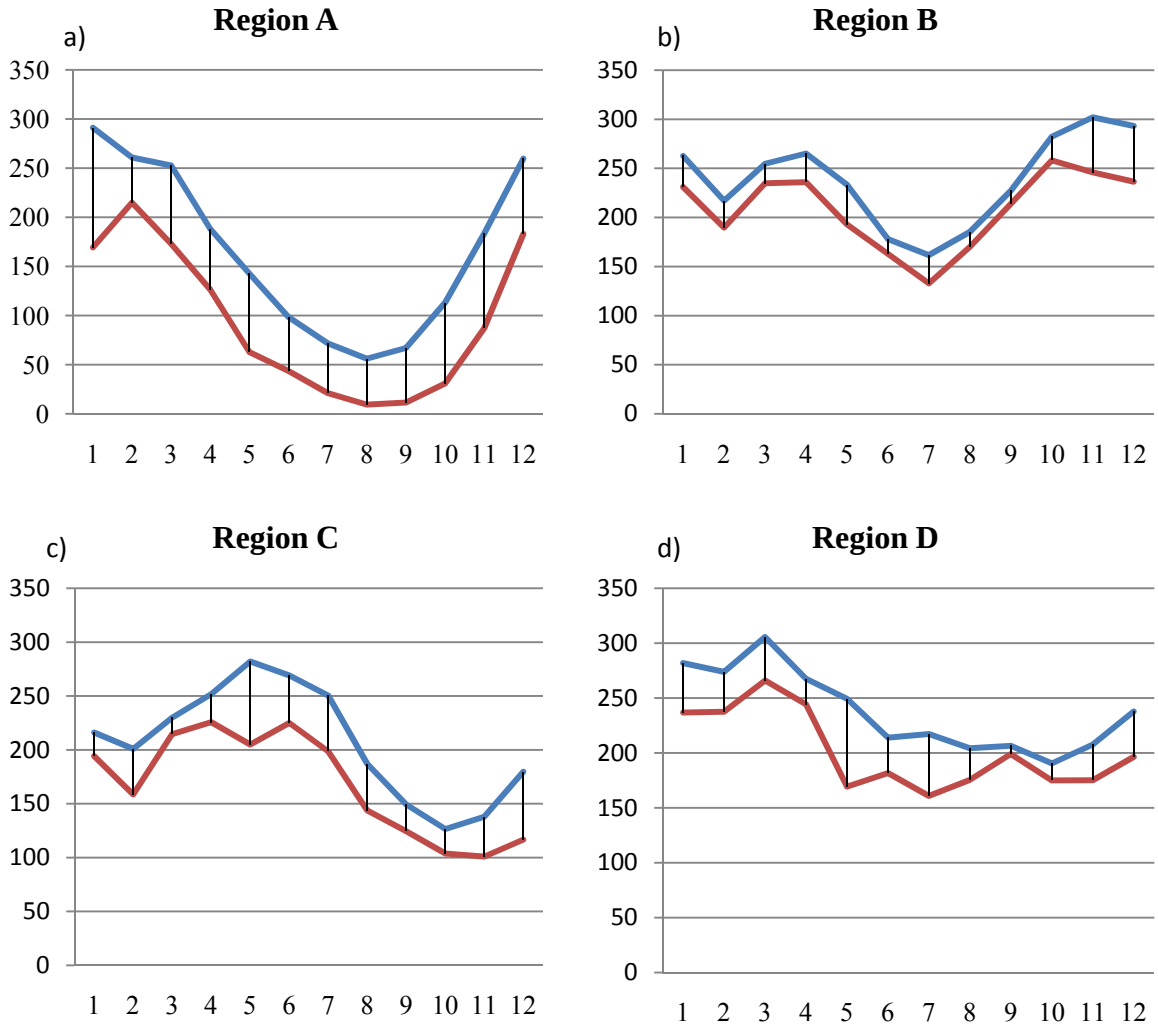

Figure 24. Differences in climatological monthly mean precipitation values in a) region A, b) region B, c) region C, and d) region D between 1900–2008 (blue) and 1994–2008 (red). The horizontal axis represents month (January – December) and the vertical axis represents rainfall (mm/month).

Figure 25 summarises the monthly decline in Indonesian rainfall for the four regions used in this study. The average decline in rainfall is ~ 4.4cm/month in all regions. Long-term average Indonesian rainfall for the period 1900–2008 is ~20.7cm/month. Hence, the observed rainfall decline of 21% during the period 1994–2008 compared with the long-term mean is significant. Rainfall in Region A displayed more intra-annual variability than the other regions. The rainfall decline in January is ~12cm/month, only ~4.5cm/month in February, and ~8cm/month in March. The main reason for this variability could be a 1-month shift in the occurrence of the rainfall maximum. August shows the lowest rainfall decline in Region A of ~4.7cm/month. On average, the rainfall decline in Region B is only half that in Region A with the greatest decline of ~7.6cm/month in December and the lowest decline of 1.3cm/month in September. Rainfall declines in Region C are >4cm/month in February, the period from May to August, and in December, peaking at ~8cm/month in May. Rainfall declines in Region D follow a pattern similar to that in Region C. The rainfall decline in Region D has a maximum of ~8cm/month in May and a minimum of <1cm/month in September.

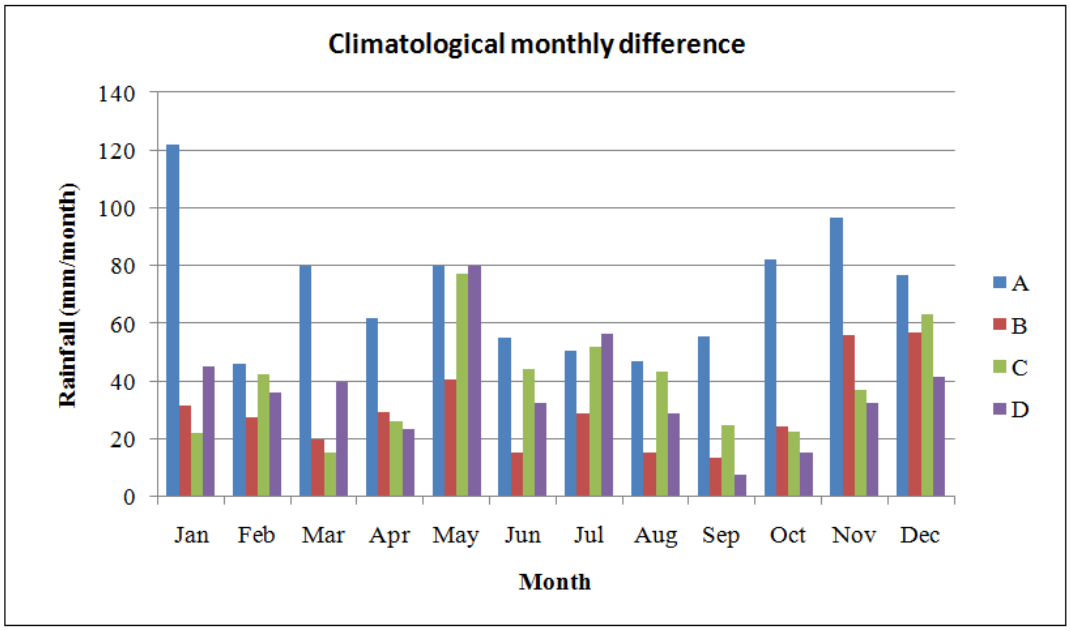

Figure 25. Average monthly rainfall declines in regions A, B, C and D in the period 1994–2008 with reference to the long-term average for 1900–2008.

4.3. Spatial Characteristics (EOF) Analysis

In order to gain further insight into dominant spatial and temporal variability of Indonesian rainfall and its relation to various climate modes, an EOF analysis has been applied to the gridded annual mean precipitation data. Based on North's criteria, only the first two EOFs were considered in this analysis (see Appendix A).

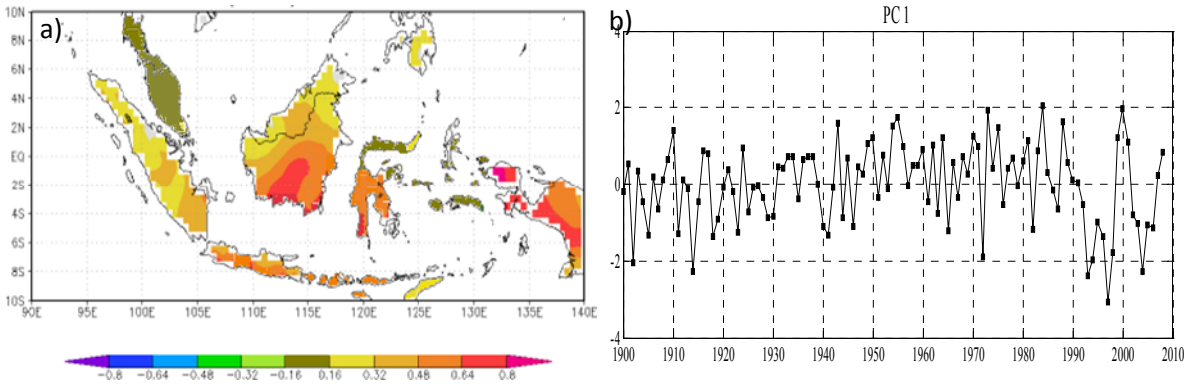

Figure 26. The first EOF for a) spatial loading and b) PC of Indonesian rainfall for 1900–2008 accounting for 38% of the observed variability.

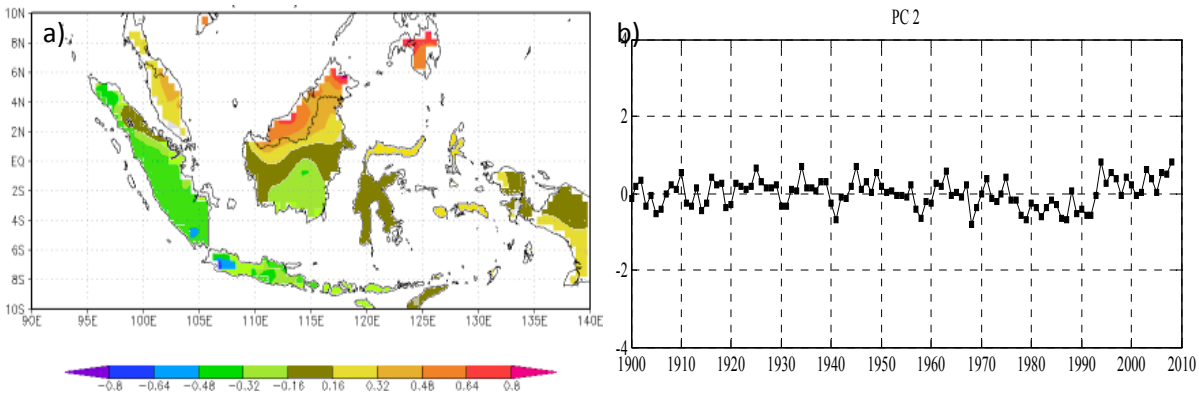

Figure 27. The second EOF for a) spatial loading and b) PC of Indonesian rainfall for 1900–2008 accounting for 9% of the observed variability.

The first two EOFs (**Figure 26** and **Figure 27**) together explain approximately 47% of the total rainfall variability over Indonesia. The dominant mode (EOF1) of the rainfall data accounts for 38% of the variability. This mode shows a spatial loading that agrees with the variability inferred from the standard deviation of the annual mean rainfall pattern (see **Figure 18b**). The principle component (PC) time series of EOF1 is very similar to the original precipitation time series (see **Figure 20**), capturing the sudden change in temporal variability starting in the early 1990s. The lack of negative spatial-loading values implies that the entire Indonesian region follows *in unison* the variability characterised by the PC time series of this mode.

The second EOF represents 9% of the total variability. The spatial loading consists of a dipole pattern with one pole centred over Sumatra and the other pole centred over the northern part of Kalimantan. The associated PC time series reveals an interesting shift from negative to positive values in the early 1990s indicating a relative rainfall shift from the Sumatra region to northern Kalimantan. This spatial shift, however, is negligibly small compared with rainfall variability associated with the first EOF mode.

4.4. Periodicity of rainfall variations

The wavelet power spectra for the four rainfall regions are shown in **Figure 28 – 31** respectively. In each figure, panel a) represents monthly rainfall, panel b) represents the wavelet spectrum, panel c) represents GWS, which highlights the power or strength of the periodicity with respect to the total power/strength within the time period, and panel d) displays the average variance for 0.5- to 1-year periodicity. The analysis focuses on intra-annual and inter-annual periodicities, noting that intra-decadal periodicities are not statistically resolved here by the Wavelet method.

a. Intra-annual periodicity

The four rainfall regions display relatively high intra-annual variability in their wavelet spectra for periods < 1 year (**Figures 28-31)**. Region A has the highest intra-annual variability followed by Regions C, B and D. Note that this intra-annual variability is statistically significant at 95% confidence interval. Unlike Regions A, C, and D, intra-annual rainfall variability in Region B also shows a dominant ~6-month periodicity associated with the occurrence of two rainfall maxima during the year (see Figure 22).

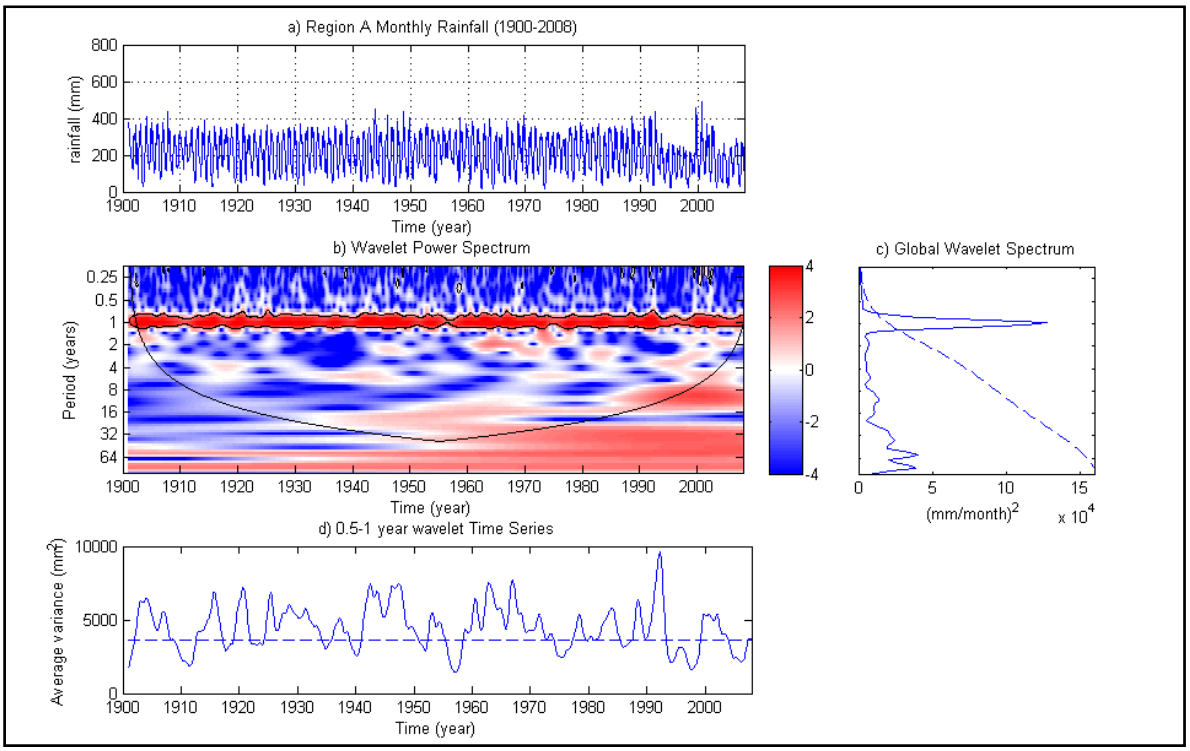

Figure 28. Wavelet analysis of rainfall in region A for 1900 – 2008. a) Monthly-mean rainfall (mm/month), b) wavelet power spectrum (line shows cone of influence; i.e. data points below this line are statistically insignificant), c) global wavelet spectrum (dashed line denotes the 95% significance level), and d) wavelet time series for the 0.5-1 year periodicity range.

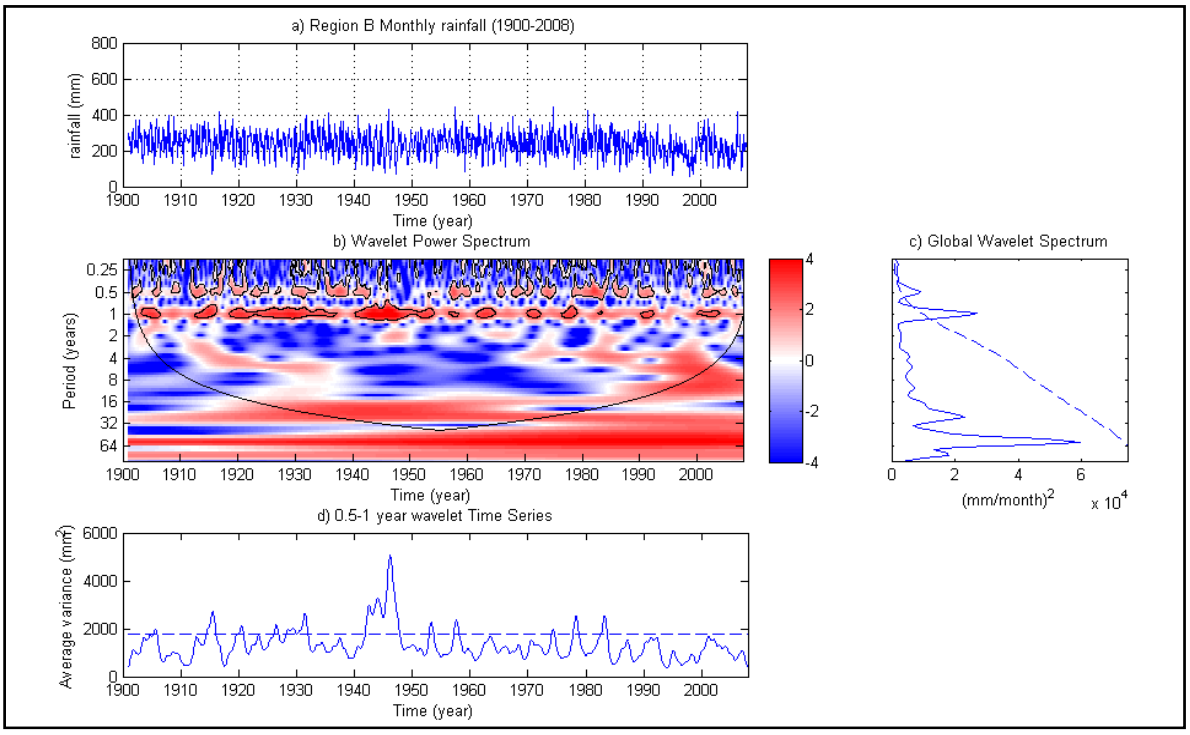

Figure 29. Wavelet analysis. Same as Figure 28, but for region B.

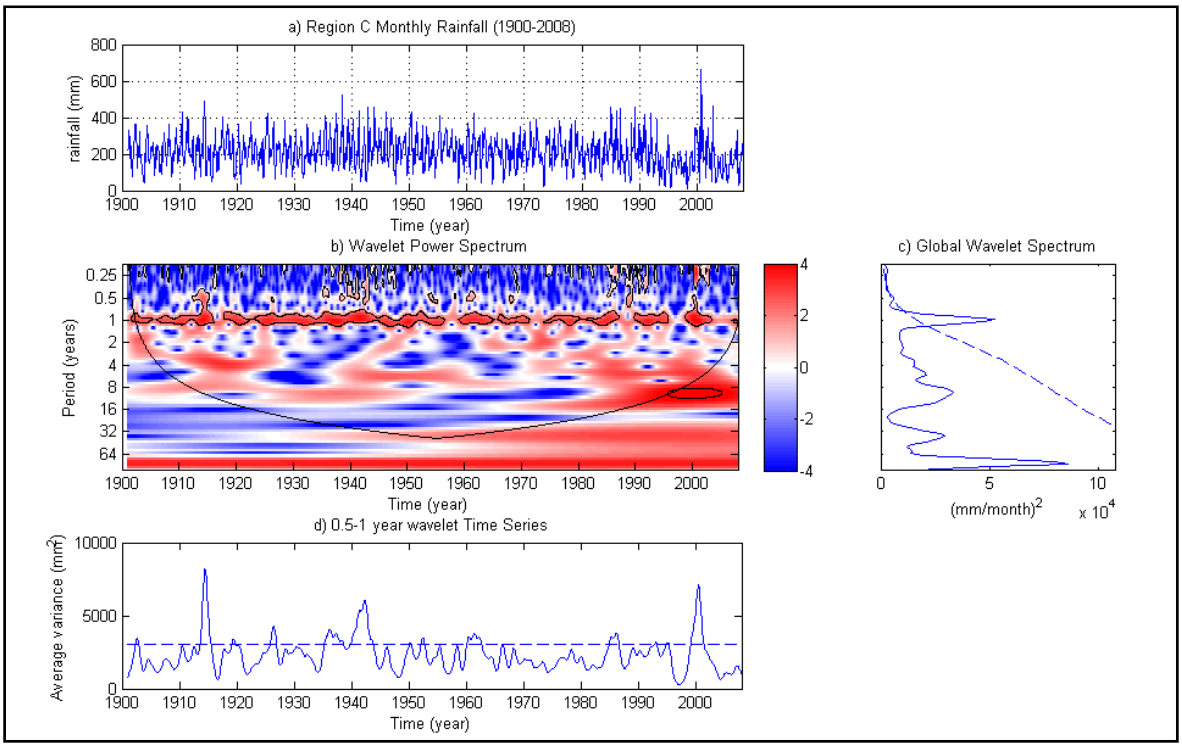

Figure 30. Wavelet analysis. Same as Figure 28, but for region C.

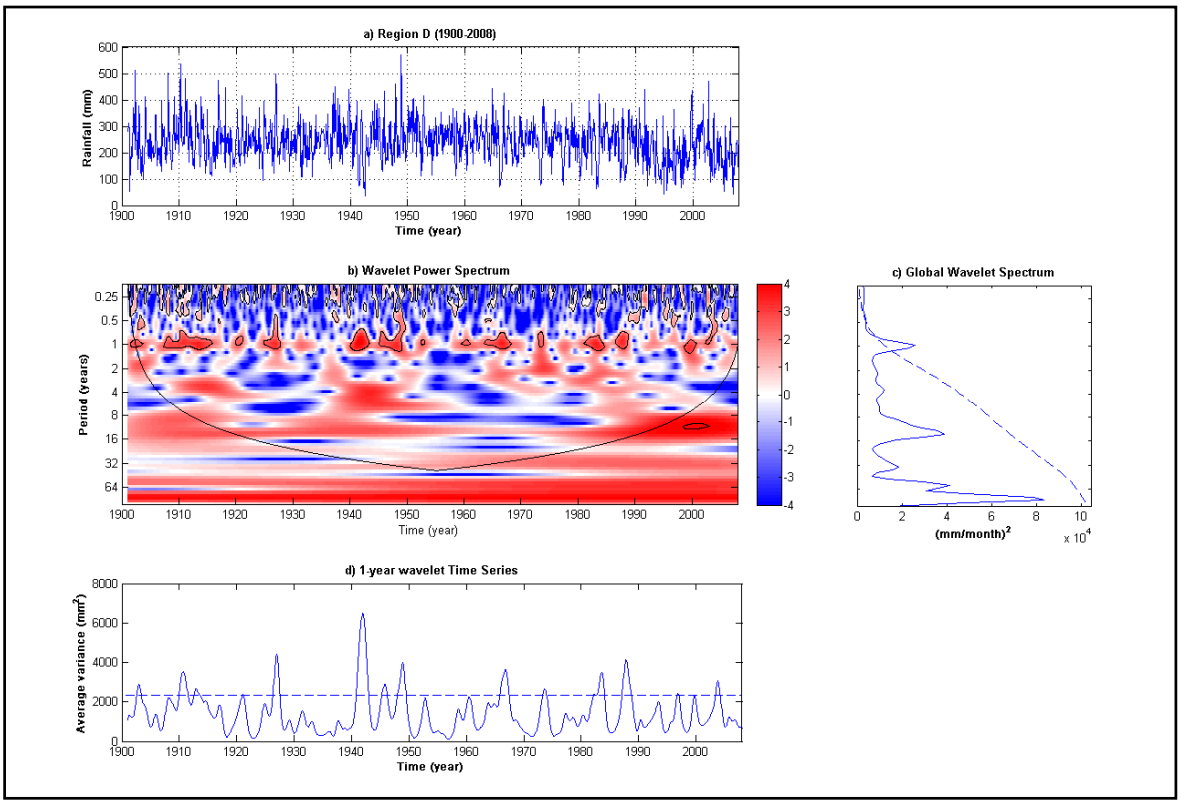

Figure 31. Wavelet analysis. Same as Figure 28, but for region D.

The 0.5-1 year wavelet time series describes temporal changes in the intra-annual rainfall variability. This variability becomes smaller either by a reduction of the rainfall maximum and/or an increase of the rainfall minimum in a region. For instance, the apparent reduction in peak rainfall in Region A for the months of December and January starting in the early 1990s (see **Figure 28a**) corresponds to a reduced variability in the wavelet time series (see **Figure 28d**). In contrast to this, in other time periods, such as 1957–1959, lower rainfall variability in Region A is rather caused by an increase in rainfall during the low-rainfall season (July – September). The wavelet analysis cannot distinguish between these different cases.

Note that the highest intra-annual rainfall variability in Regions B and D appeared during the 1940–1950 period. As far as the author is aware, the reason for this transient increase in rainfall variability is unknown.

b. Inter-annual periodicity

Inter-annual variability derived from the wavelet analysis is not statistically significant at 95% confidence level. Nevertheless, this analysis indicates rainfall variability at longer periods >4 years. For instance, the wavelet analysis indicates rainfall periodicity of 8-12 years in Regions C and D. Whether this variability reflects the true variability of the system cannot be quantified with the required statistical confidence.

4.5. Influence of Large-Scale Climate Drivers

Long-term annual-mean SST anomalies in regional areas in Indonesia (A*,B*, C*) follow the global SST trend as shown in **Figure C1**. These patterns are important as a clue of their relation to rainfall variability in Indonesia and also their links to large scale climate drivers.

a. Entire Indonesian region

The following section presents a lag correlation analysis between rainfall anomalies in both the entire Indonesian region and each of the four rainfall regions with several indices (Niño 3.4, IOD and IPO) and regional SST anomalies in the regions A*, B* and C* (see **Figure 32**). This analysis is based on monthly-mean data, but the display is grouped into rainfall seasons DJF (December – February), MAM (March – May), JJA (June – August), and SON (September – November). Lags are multiples of a month and

the maximum lag considered is ±1 year. A positive lag means that the index (or SST) anomaly precedes the rainfall anomaly, whereas a negative lag means that the rainfall anomaly leads the index anomaly. Note that standard deviations are generally less than ±0.2.

Rainfall anomalies in the entire Indonesian region have a zero lag correlation with respect to the Niño 3.4 index (**Figure 32a**). The period June – November shows a stronger correlation (between -0.7 and -0.65) than the December – May period during which the correlation coefficient decreases in magnitude to values around -0.4. This is in accordance with previous studies (i.e. Aldrian & Susanto, 2003) suggesting ENSO effects on Indonesian rainfall anomalies are pronounced during June – November. This seasonally pronounced rainfall variability reflects the ENSO-related variations of the Walker circulation.

Similar to the Niño 3.4 dependency, rainfall anomalies in the Indonesian region also show stronger (negative) correlations with the other two climate indices, DMI and IPO, during the period June – November (**Figure 32b-c**). The IPO dependency, characterised by relatively strong correlations of -0.6 during this period, is not surprising because this index includes the low-pass filtered oceanic response to ENSO events as a dominant signal. Nevertheless, the more independent DMI shows similarly strong correlations of -0.6 for the June – November period with weaker negative correlations a values around -0.4 in other months of the year. Hence, rainfall variability in the Indonesian region is strongly controlled by two major influences: 1) ENSO events in the equatorial Pacific Ocean, and 2) SST anomalies associated with the Indian Ocean Dipole. These influences, however, appear seasonally more pronounced during the June – November period (when the lag-correlation is applied to the entire time series) and, apparently, they cannot explain rainfall variability of the other months of the year.

It should be noted that overall there is a slightly negative offset correlation of around -0.2 between Indonesian rainfall and temperature anomalies. While statistically insignificant, this feature is a signature of a correlation between SST increases in the Indonesian region (**Figure 33**), presumably due to global warming, and the observed decline in Indonesian rainfall commencing in the late 1980s. This has been confirmed by running the lag correlation analysis over a reduced period 1900–1980 which eliminates this correlation offset.

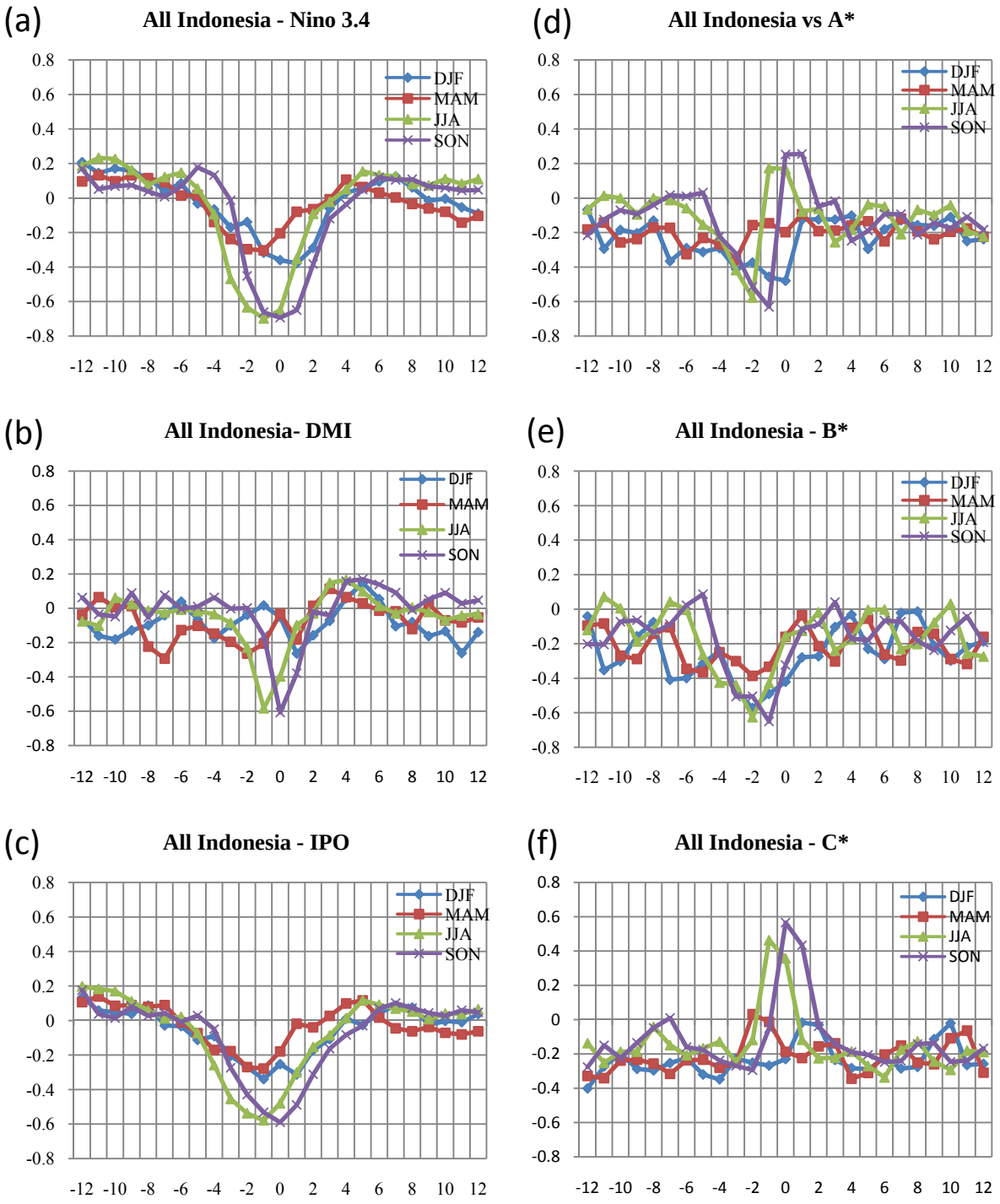

Figure 32. Lag correlations between rainfall in the entire Indonesia region and climate indices (Niño 3.4, DMI, IPO), and SST anomalies in regions A*, B* and C*. X-axis represents lag (months), and y-axis gives the correlation coefficient. Note: lag positive, climate indices and SST anomalies leading index.

Lag correlations between rainfall anomalies and regional temperature anomalies (which include both larger-scale and regional-scale effects) are more puzzling (**Figure 32d-f**). Exclusively Region C* (located in close proximity to the Pacific Warm Pool) shows a positive zero-lag correlation in a range of 0.5 – 0.6 during the period June – November (**Figure 32f**). This response of reduced rainfall over the Indonesian region and lower SSTs in the Pacific Warm Pool is anticipated after the onset of El-Niño events.

In contrast to this, the correlation between SST anomalies in the other regions A* and B* with rainfall anomalies is more complex. In Region A*, for instance, while there is an indication of a weak (~0.2) positive zero-lag correlation with Indonesian rainfall, this region shows a strong negative rainfall-SST correlation during the period June – November of -0.6 whereby the rainfall anomaly leads the SST anomaly by 1-2 months (**Figure 32d**). This implies that events of less (more) rainfall than usual are followed by warmer (colder) surface water in the following couple of months. This negative correlation extends to the period December – February when it displays a zero lag.

Region B* shows a similar behaviour to Region A*, but in contrast to the latter, this region lacks any positive correlation peak between rainfall and SST anomalies (**Figure 32e**).

b. <u>Regional differences</u>

Lag correlations between rainfall anomaly with climate drivers and with regional SST anomalies in the rainfall regions A – D are similar to those for the entire Indonesian region (**Figures 33-36**, compare with **Figure 32**). However, there are a few noteworthy differences being outlined in the following.

Rainfall variability in Region A attains, by far, the strongest negative zero-lag correlation with the DMI during the period June – November in comparison with the other regions. Here, the correlation attains values between -0.7 and -0.6 (**Figure 33b**) whereas the other regions show weaker correlations in a range between -0.5 and -0.3 (**Figures 34b, 35b, 36b**). On the other hand, the Niño 3.4 influence on rainfall anomalies during the period June – November is most pronounced in region C where the zero-lag correlation peaks at values around -0.7 (**Figure 35a**).

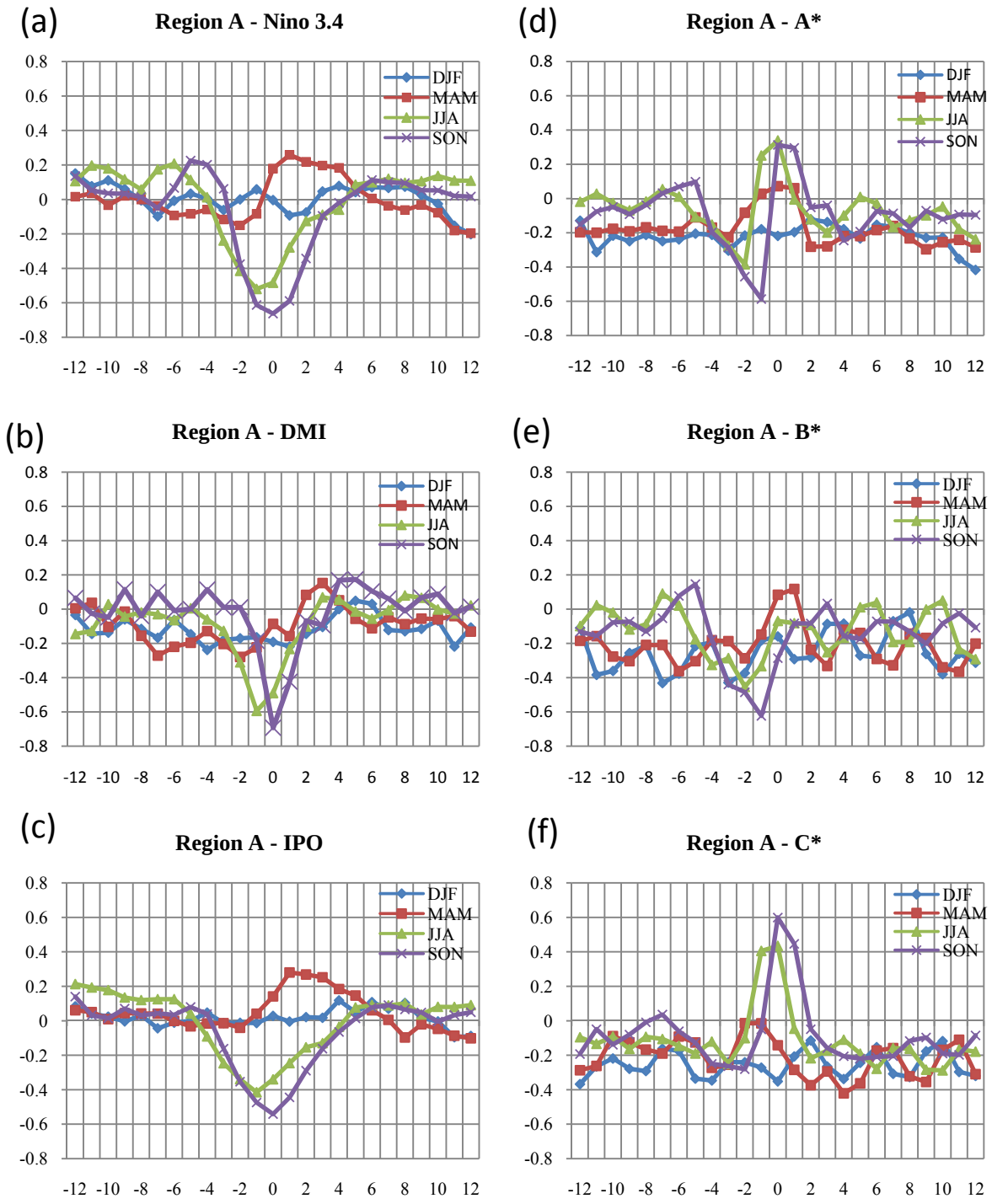

Figure 33. Same as **Figure 32**, but for rainfall anomalies in region A.

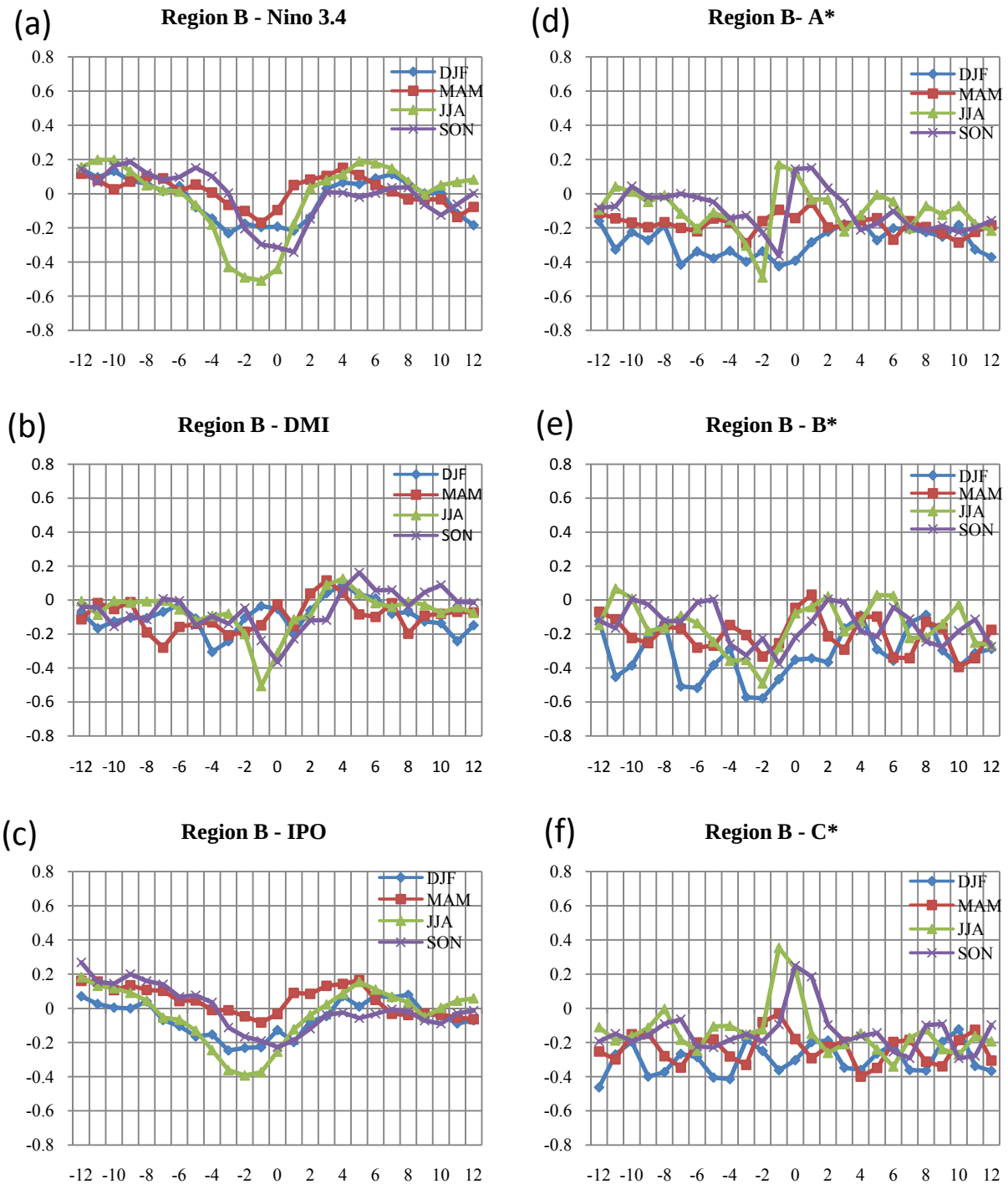

Figure 34. Same as **Fig. 32**, but for rainfall anomalies in region B.

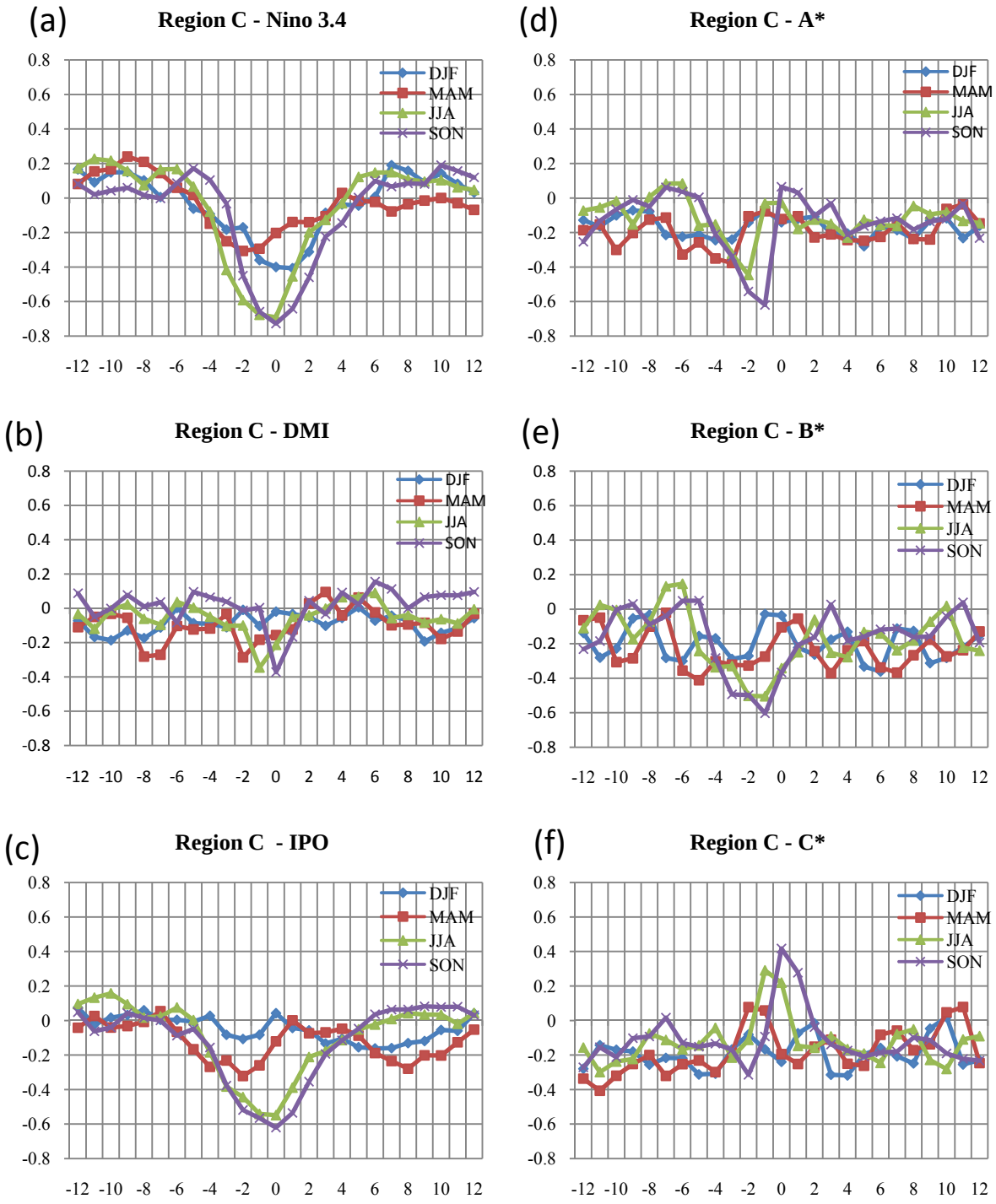

Figure 35. Same as **Fig. 32**, but for rainfall anomalies in region C.

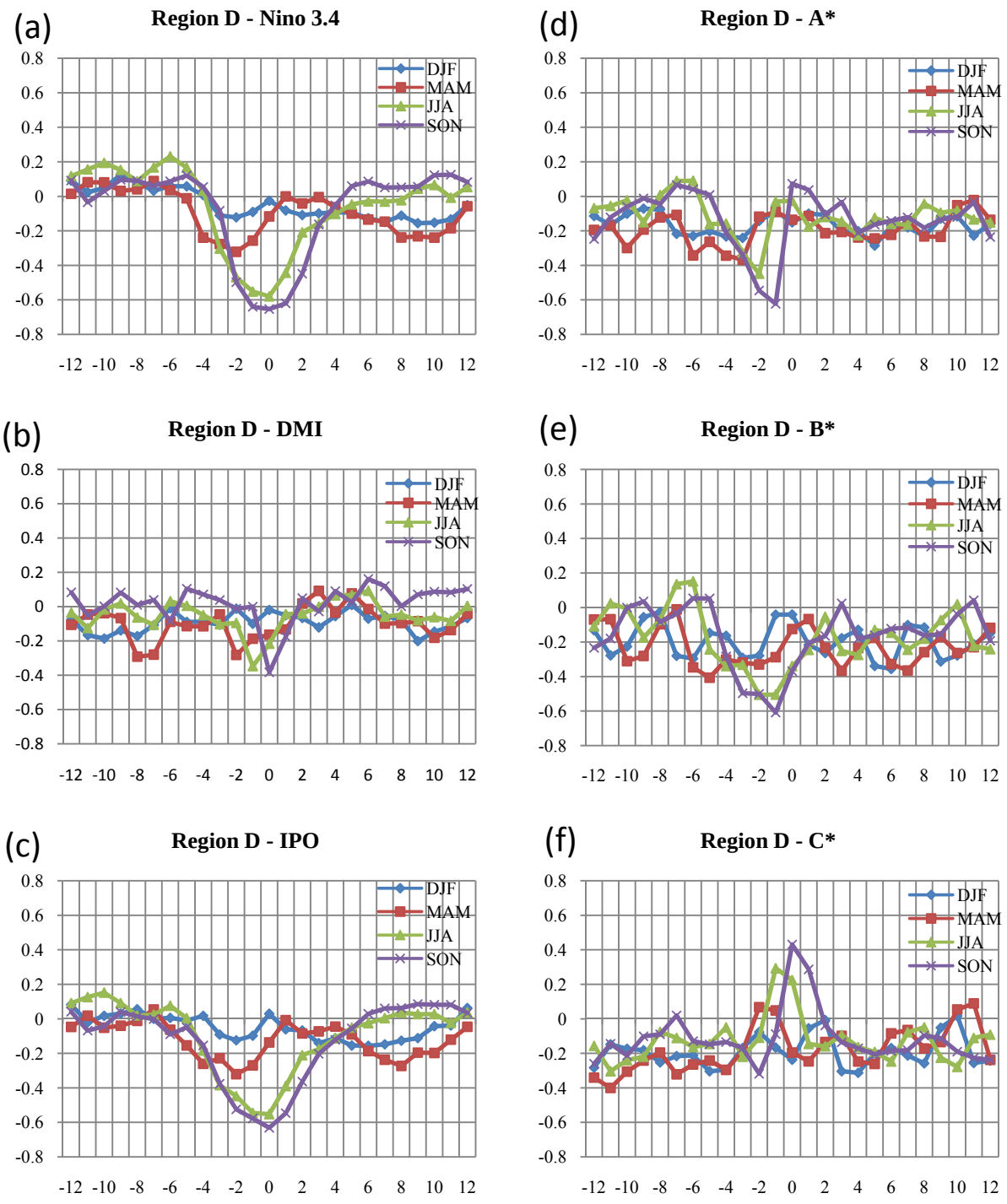

Figure 36. Same as **Fig. 32**, but for rainfall anomalies in region D.

In region A, this influence is stronger at -0.7 during September – November than during June – August when the correlation is reduced to -0.5 (**Figure 33a**). In region B, this influence is stronger during June – August, with a correlation of -0.5, than during September – November when the correlation is markedly reduced to values of -0.35 (**Figure 34a**). Region D experiences a relatively strong negative correlation of values of -0.6 during the entire June – November period (**Figure 37a**).

Rainfall anomalies in region B are far less correlated with climate drivers as compared with the other regions. For instance, the rainfall-Niño 3.4 zero-lag correlation weakens to a value of -0.5 during June – August and to -0.35 during September – November (**Figure 34a)**. Similarly, the DMI influence is reduced to a zero-lag correlation of -0.5 during June – August and -0.4 during September – November (**Figure 34b)**.

Meanwhile, SST anomalies in region A* in the period June – November have a stronger positive zero-lag correlation of ~0.35 with rainfall anomalies in region A (**Figure 33d**) and ~0.2 in region B (**Figure 35d**). In contrast to this, there is almost no zero-lag correlation between SST anomalies in region A* with rainfall anomalies in regions C (**Figure 35d**) and D (**Figure 36d**).

SST anomalies in region C* attain the strongest positive zero-lag correlations with rainfall anomalies when compared to regions A* and B*. In Region A, this correlation peaks with a value of 0.6 during September – October and 0.4 during June – August (**Figure 33f)**. In the other regions, this positive correlation is slightly smaller at 0.4 during September – October and at 0.3 during June – August (**Figures 34f, 35f, 36f**).

c. <u>Relationship between local SST anomalies and climate indices</u>

As revealed in the previous section, with a few exceptions such as region C*, regional SST anomalies and rainfall anomalies are generally characterised by negative correlations of a negative lag of 1-2 months (rainfall anomalies lead SST anomalies). In order to understand this unusual relationship, this section describes the correlation between local SST anomalies with the climate drivers (Niño 3.4, DMI and IPO) considered in this study. **Figure 37** presents lag correlations for the regions A*, B* and C*.

The regional SST correlation with the Niño 3.4 index varies between the regions (**Figure 37a)**. Region C* displays the anticipated response of a negative zero-lag

correlation with maximum values between -0.7 and -0.5 for the period June – November and little correlation during other months of the year, in accordance with the findings of Hendon (2003). This reflects the expected response of regional cooling of surface waters in the western equatorial Pacific Ocean after the onset of El-Niño events. In alignment with this is a positive correlation between rainfall anomalies and temperature anomalies in region C*, as shown in **Figure 32f**. This pattern indicates the pathway of the Indonesian Throughflow that transfers water mass from the western Pacific to the Indian Ocean mainly through this C* region, which covers the Banda Sea (Qu *et al*., 2005; Iskandar, 2010).

In contrast to region C*, regions A* and B* show a positive correlation between SST anomalies with variations of the Niño 3.4 index. SST anomalies follow Niño 3.4 anomalies with a lag of 1-3 months with the shortest lag being given for the December – February period (when the correlation is highest at 0.7) and the longest delay occurring during the period June – August (when the correlation is reduced to 0.2-0.4). This interesting finding indicates that regions A* and B* experience a warming after the onset of El-Niño events, which also explains the unexpected negative correlations between SST anomalies in regions A* and B* and rainfall anomalies (the latter leading the former) shown in **Figs. 32-36**. As far as the author is aware, this feedback mechanism has not been previously reported.

The lag correlation for the DMI (**Figure 37b)** is similar to that for the Niño 3.4 index, except that positive correlation peaks are slightly weaker and that region A* also exhibits a peak of zero-lag negative correlation with regional SST anomalies of values between -0.5 and -0.4 for the period June – November. This influence is consistent with the positive zero-lag correlation peak between Indonesian rainfall and SST anomalies in region A*, shown in **Fig. 32**. Another difference between DMI and Niño 3.4 events appears in region C* where, next to a zero-lag negative correlation peak, DMI anomalies trigger a positively correlated SST response (correlation is 0.4) with a delay of 2-4 months (depending on the season). This feature, however, disappears during December – February. Apart from these details, the influence of DMI events on regional SST anomalies is very similar to that of El-Niño events. The correlation patterns for the IPO index (**Figure 37c**) are very similar to those for the Niño 3.4 index.

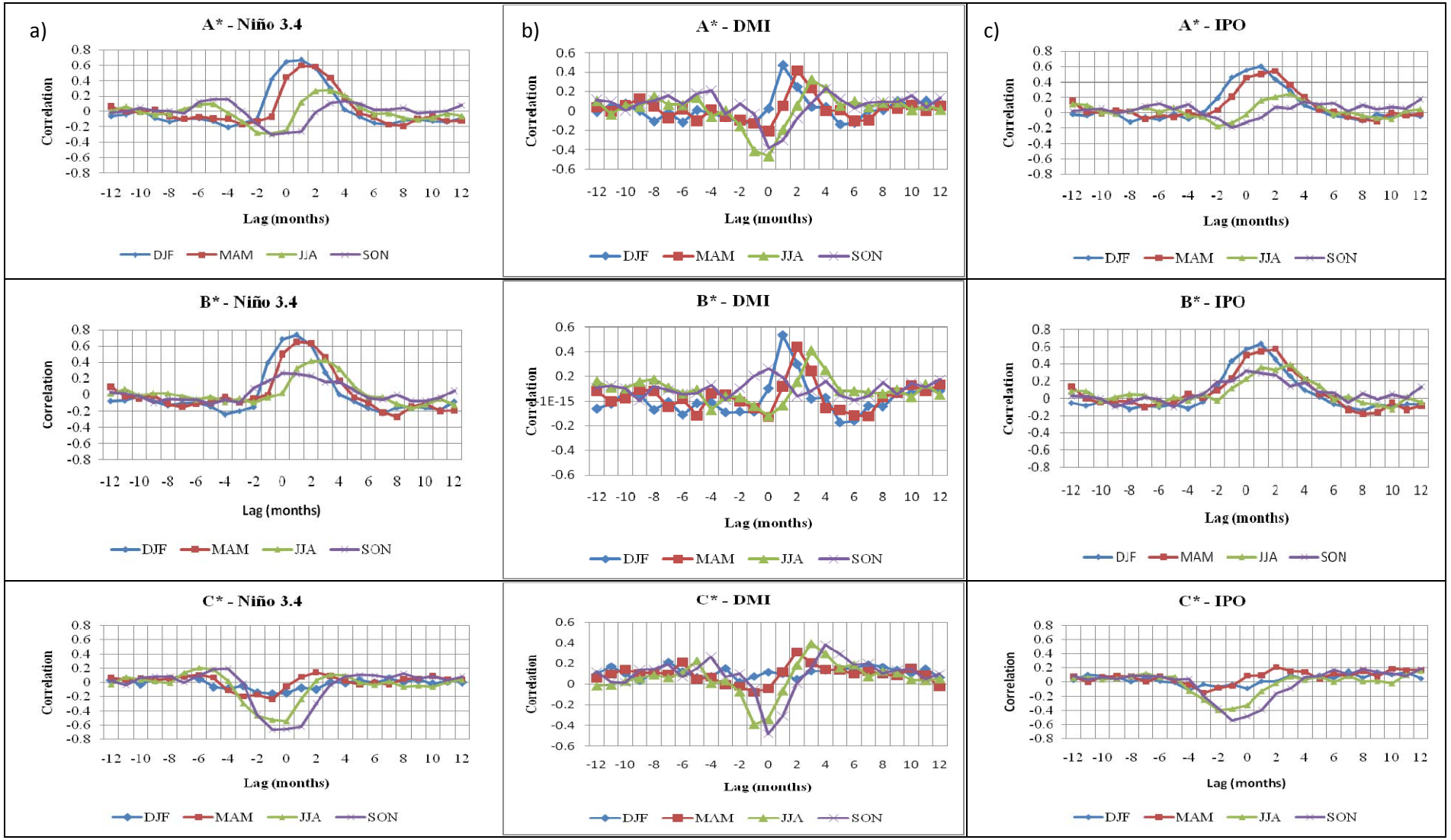

Figure 37. Lag correlations between SST anomalies in regions A*, B* and C* and climate indices (Niño 3.4, DMI and IPO).

4.6. Further analysis of recent rainfall trends

Annual and seasonal based rainfall anomalies are presented in **Figure 38**. The lag correlation analysis (see **Section 4.5**) indicates that ENSO influences are more dominant in the JJA and SON periods, in agreement with Haylock & McBride (2001) and Hendon (2003). **Figure 38** indicates that maximum/minimum rainfall anomalies are often found during these months.

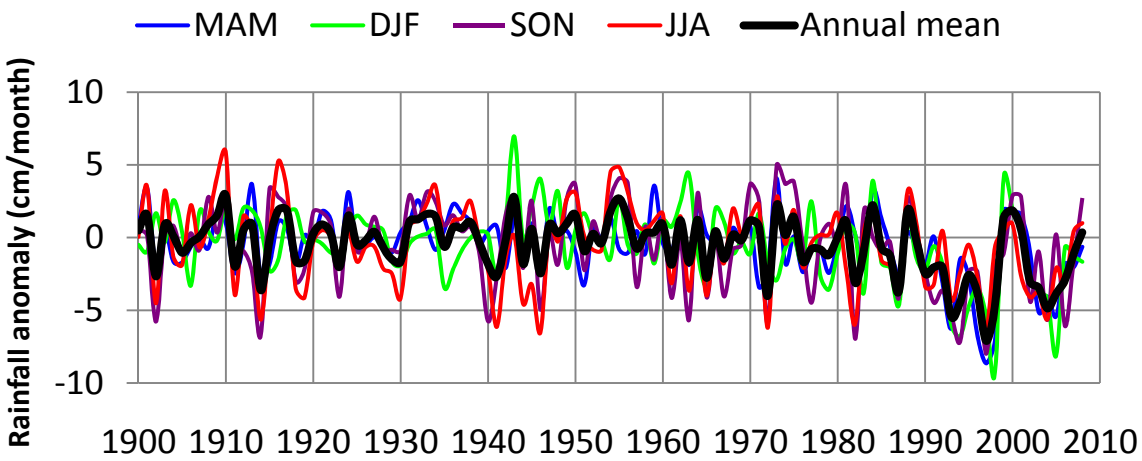

Figure 38. Indonesian rainfall anomalies (cm/month) during 1900-2008. Shown are averages for DJF, MAM, JJA, SON, and the annual mean. Anomalies refer to the long-term mean value for the 1900-1979 period of 22.5 cm/month.

Until the mid 1980s, the annual-mean value of rainfall anomaly seems to be controlled by these seasonal anomalies, which serves as a hypothesis for the following considerations. The schematic in **Figure 39** illustrates this seasonal control of JJA ENSO events on annual-mean rainfall anomalies. If this assumption holds, then it should be possible to reconstruct the time series of annual-mean rainfall anomalies based on JJA and/or SON values of Nino 3.4, noting possible IOD influences. In the following, this hypothesis is tested via correlations of rainfall anomalies with seasonal averages of Nino 3.4 and the DMI. The latter is included here to specify IOD influences. Each time series is hereby normalised by their standard deviation.

Figure 40a displays normalised annual-mean rainfall anomalies together with normalised JJA values of Nino 3.4 for a selected period of 1900-1969. Here we can clearly recognise the influence of JJA ENSO events on annual-mean rainfall anomalies. To give one example, during 1954, the Nino 3.4 index reached -1.5 units, conversely annual rainfall

anomaly reached 1.8 units, which indicates a negative correlation. **Figure 40b** shows the same as **Figure 40a**, but with JJA values of the DMI. There are some signals that are negatively correlated with each other, but some periods (e.g. 1940s) show a positive correlation. Further analysis is needed to investigate these relationships.

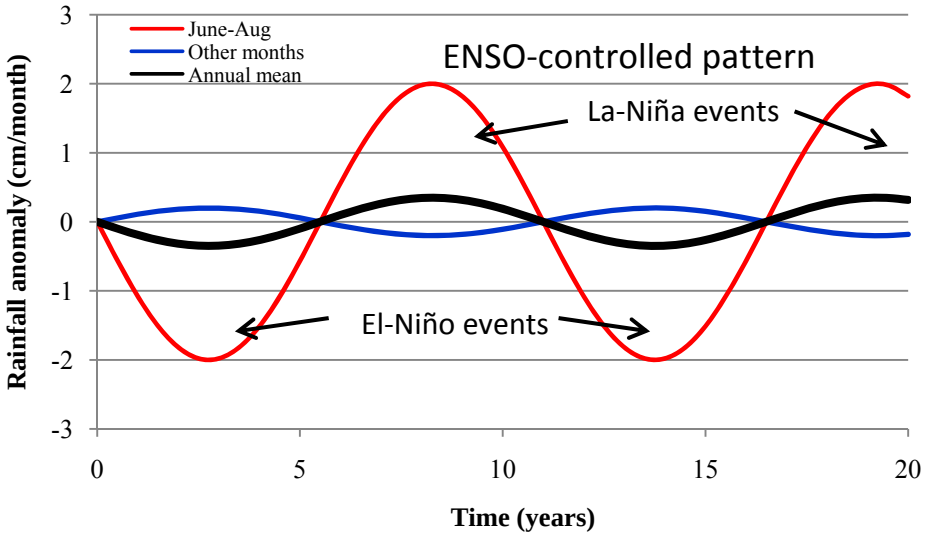

Figure 39. Schematic of seasonally ENSO-controlled annual-mean rainfall patterns.

In order to test the relative influence of seasonal ENSO and IOD events on annual-mean rainfall anomalies, a combined index is defined as:

$$\kappa(\mathrm{NINO\,3.4}, \mathrm{DMI}) = (1-\varepsilon)\frac{\mathrm{NINO\,3.4}}{std(\mathrm{NINO\,3.4})} + \varepsilon\frac{\mathrm{DMI}}{std(\mathrm{DMI})}\,, \qquad (5)$$

where ε is a weighting factor and *std.()* denotes the standard deviation. Note that $\varepsilon = 0$ represents a full correlation with Nino 3.4, $\varepsilon = 0.5$ implies equal weight between both indices, and $\varepsilon = 1$ denotes full correlation with DMI.

The calibration of ε follows implicitly from a series of correlations of (5) with normalised annual-mean rainfall anomalies. In order to reveal changes in rainfall dynamics in the past decades, this calibration and standard deviations are exclusively calculated from values for the period 1900-1979. Once the best value of ε is found, annual-mean rainfall anomalies over the entire period (1900-2008) can be reconstructed via:

$$\text{Reconstructed rainfall anomalies} = -std(\text{rainfall anomalies}) \cdot \kappa(\text{NINO3.4}, \text{DMI}) \qquad (6)$$

whereby the standard deviation of rainfall anomalies is a constant derived from 1900-1979 values.

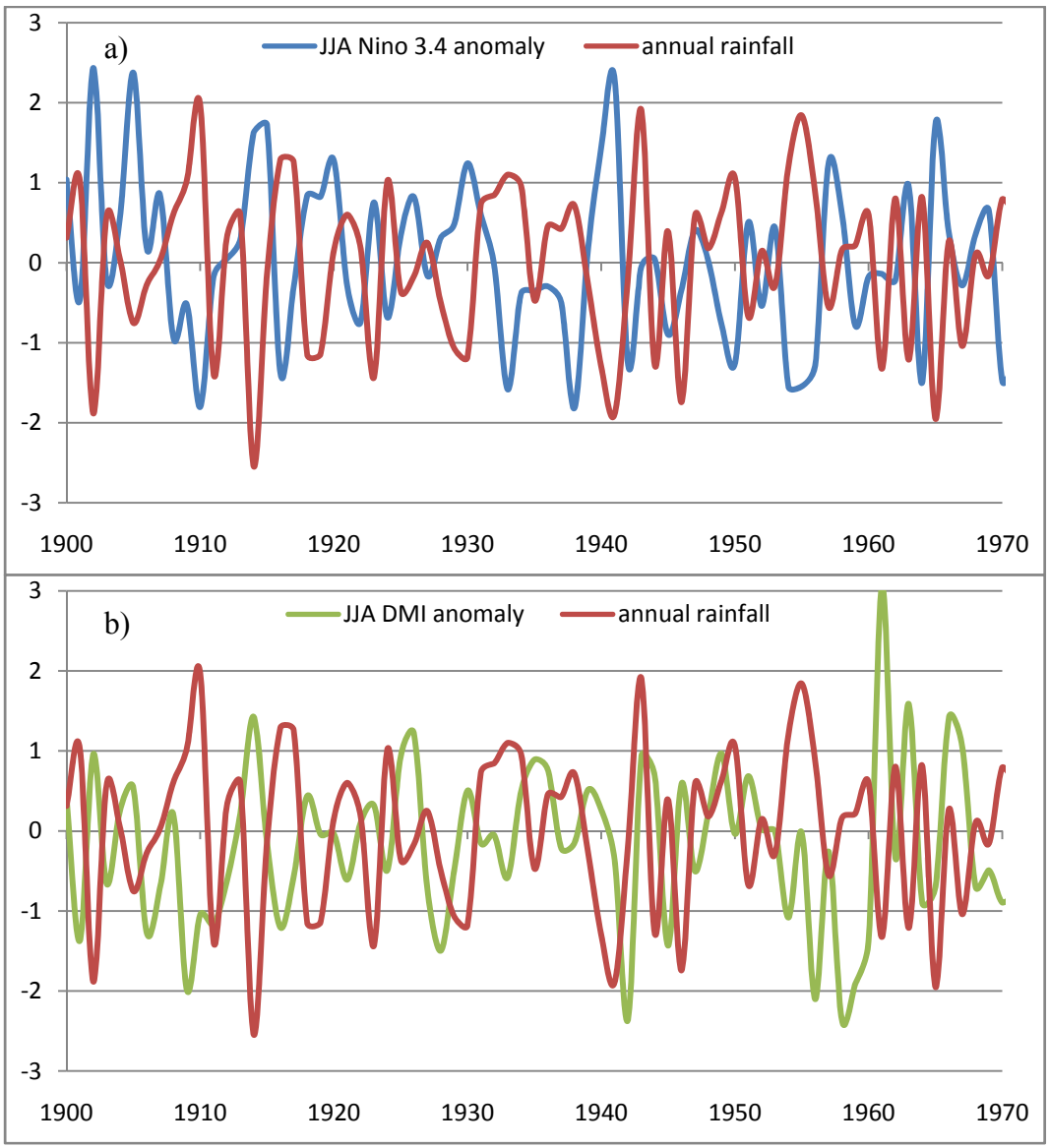

Figure 40. Time series (1900-1969) of rainfall anomalies (annual mean) and JJA values of a) Niño 3.4 and b) DMI. The data are normalised by one standard deviation (units on the y-axis). The standard deviations for rainfall, Niño 3.4, and DMI anomalies are 1 cm/month, 0. ^{o}C, and 0.2 ^{o}C respectively.

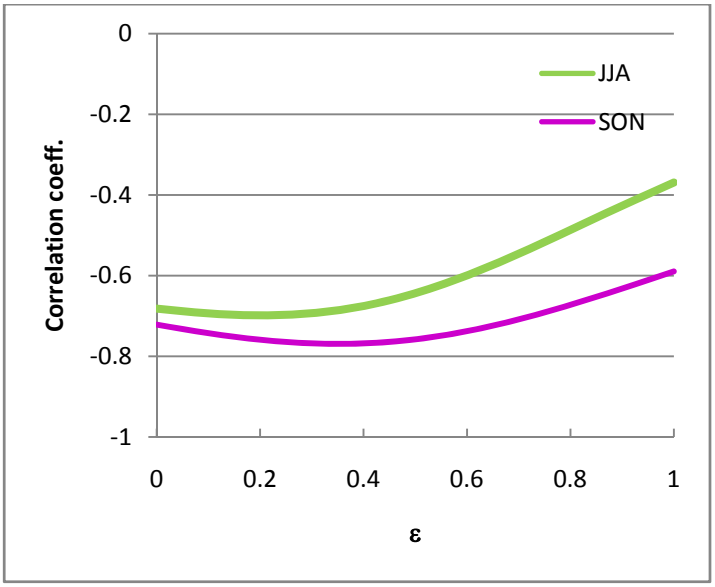

Figure 41. Correlation value of the correlation between the combined index (5) and annual-mean rainfall anomalies. The best correlation of -0.77 is given for SON values of climatic indices and ε = 0.3.

Correlation between the combined index with SON anomalies of the climate indices together with ε = 0.3 gave the best correlation of a value of -0.77 (**Figure 41)**. At 95% confidence level, the correlation value lies in a range between -0.87 to -0.70 when using Fisher's transformation (Plata, 2006). This indicates that, compared with ENSO effects, the Indian Ocean Dipole has a small but not dominant influence on annual-mean rainfall anomalies in the Indonesian region. Note that JJA values of climate indices give a slightly weaker correlation value of -0.73 for ε = 0.3 (See **Fig. 41**). These relatively high correlations for the period 1900-1979 can be taken as confirmation of the initial hypothesis. We can now use the combined index (4) with SON anomalies of climatic indices together with ε = 0.3 to explore rainfall variability of the entire time series.

Obviously, the reconstruction of annual-mean rainfall anomalies in the Indonesian region works well for the 1900-1979 period, but significant differences become apparent from the late 1980s onwards **(Figure 42**). Reasons for these differences, which might explain the observed rainfall decline in Indonesia in the past decades, are further explored in the following.

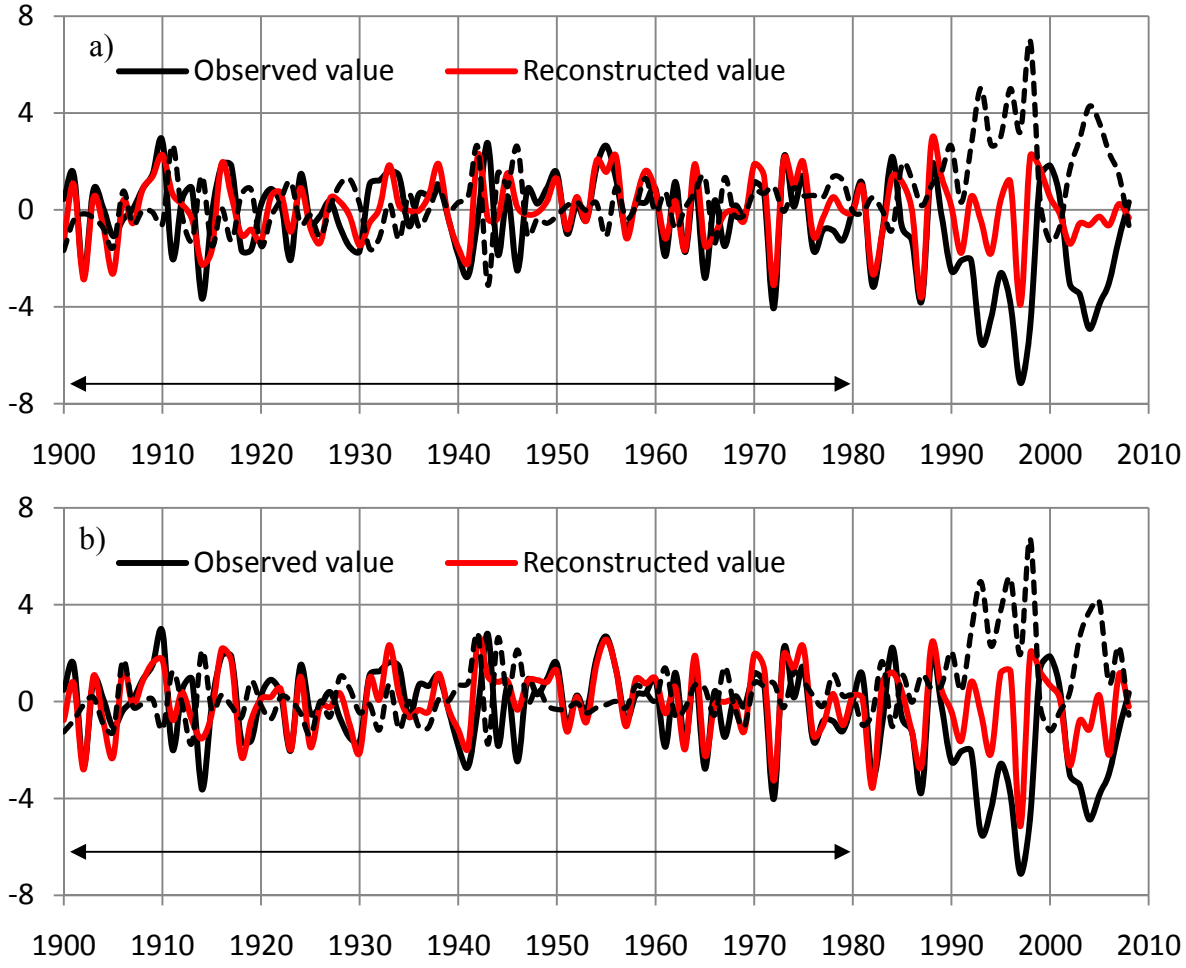

Figure 42. Observed and reconstructed annual-mean rainfall anomalies based on ε = 0.3. a) JJA values of climate indices. b) SON values of climate indices. Dashed lines show differences between reconstructed and observed values. Y-axis values are in cm/month. Arrows indicate the period of calibration (1900-1979). Anomalies refer to the long-term rainfall average over the calibration period.

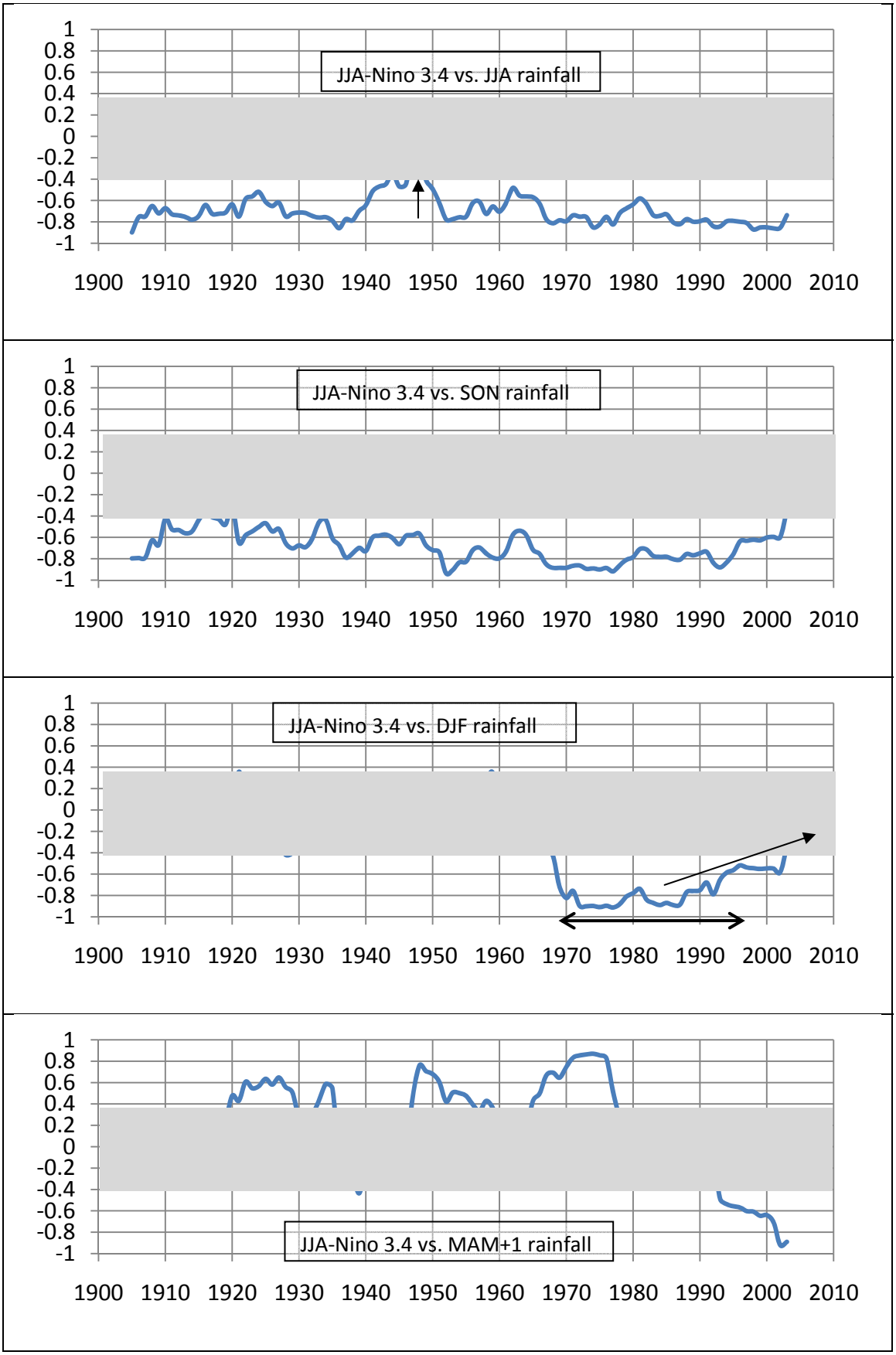

Figure 43. Sliding-window cross-correlation between JJA values of NINO 3.4 with seasonal rainfall anomalies in JJA, SON, DJF and MAM of the following year with visibility assistance in grey area.

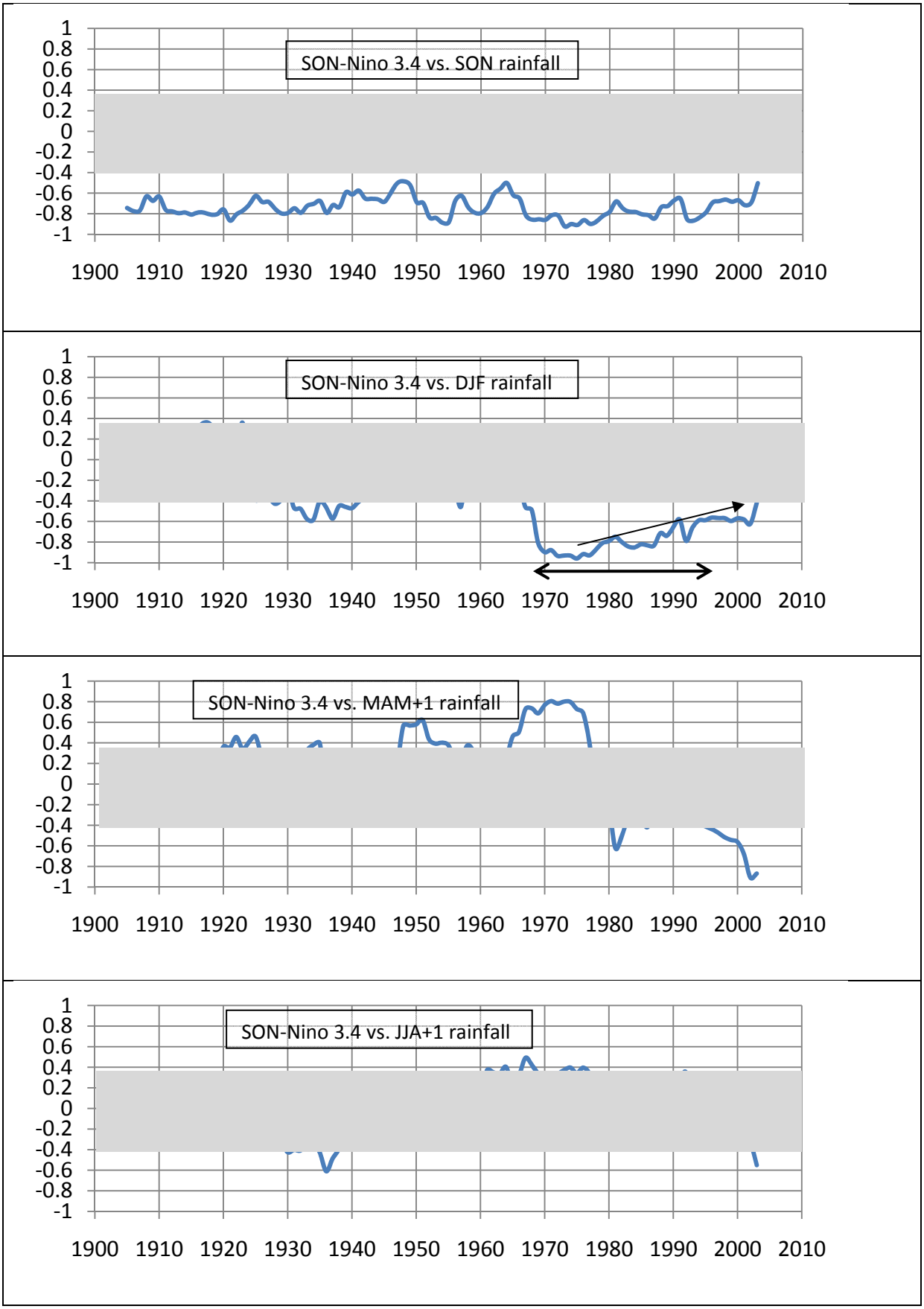

Figure 44. Sliding-window cross-correlation between SON values of NINO 3.4 with seasonal rainfall anomalies in SON and DJF, and MAM and JJA of the following year with visibility assistance in grey area.

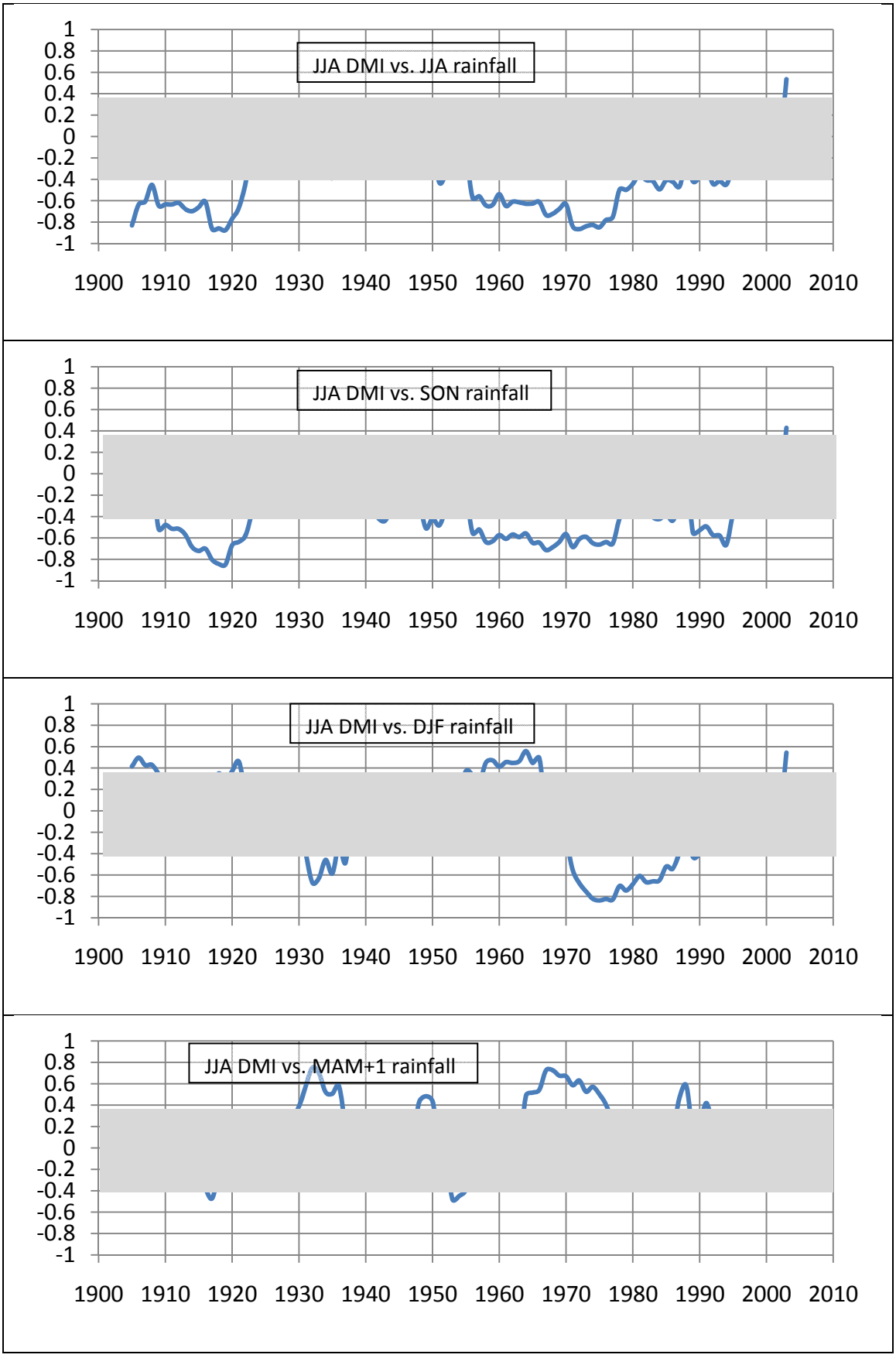

Figure 45. Same as **Fig. 43**, but using JJA values of DMI as a basis.

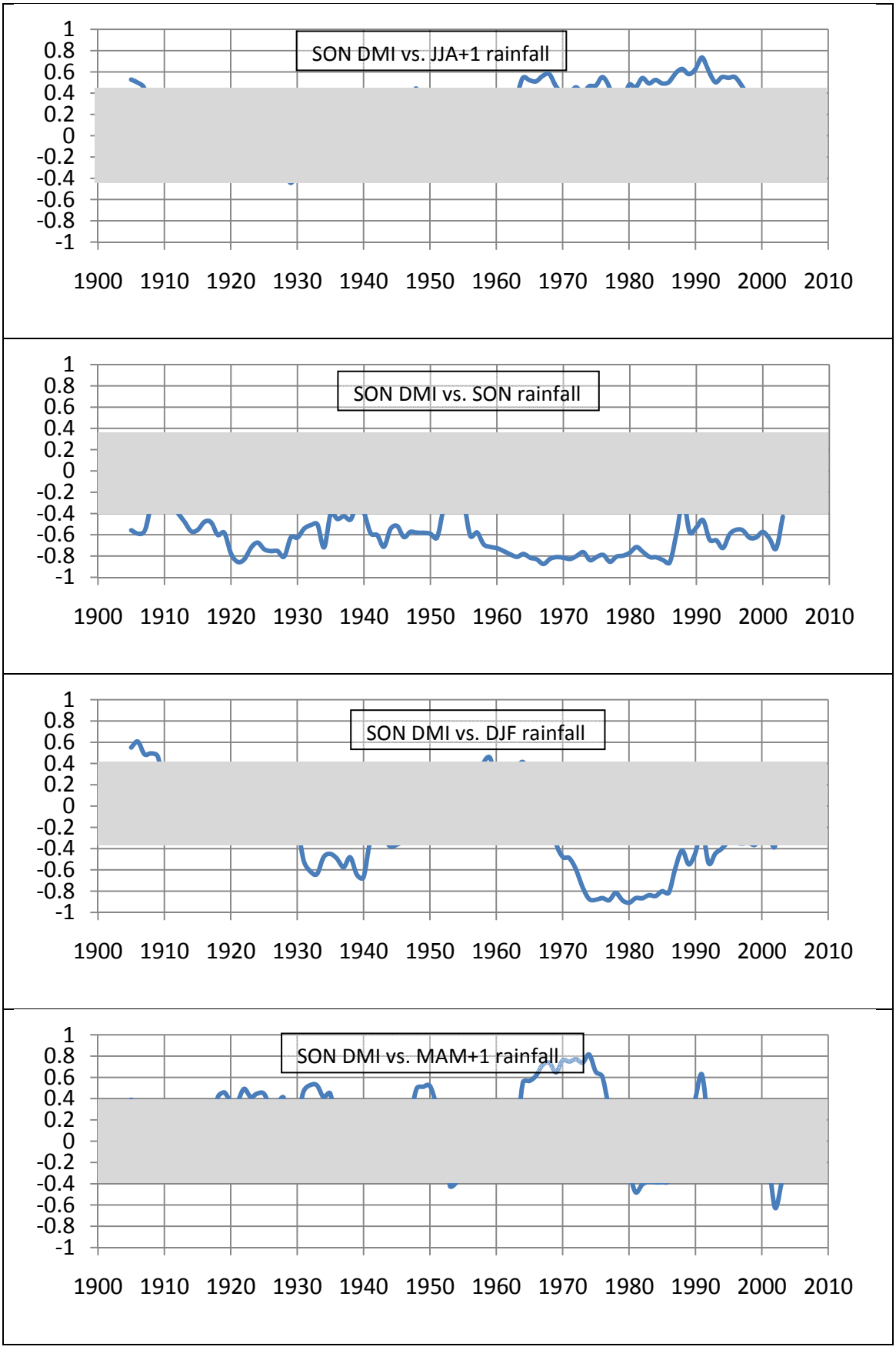

Figure 46. Same as **Fig. 44**, but using SON values of DMI as a basis.

In order to identify trends and shifts in Indonesian rainfall patterns, changes in correlation values are calculated on the basis of a sliding window of 11-yrs width. Although the accuracy of this approach is relatively low, this method can give first hints of shifts in the rainfall dynamics.

Figure 43 displays sliding-window correlations between JJA Nino 3.4 and seasonal rainfall anomalies over the following 12 months. Correlation between JJA Nino 3.4 and JJA rainfall anomalies shows a strong negative correlation except for the second half of the 1940s. The average value is -~0.7 for the entire period, in agreement with values shown in Fig. 38. Correlation between JJA Nino 3.4 and SON rainfall anomalies shows a similar result indicating that ENSO events in JJA control rainfall anomalies in the following SON period. On the other hand, JJA Nino 3.4 becomes suddenly strongly correlated with DJF rainfall anomalies from the early 1970s onwards. A direct correlation using JJA values of NINO 3.4 for the period 1971-1990 gives a correlation value of -0.89 and Fisher's transformation gives a value in the range of -0.96 and -0.74 at 95% confidence level. Notice that there seems to be a weakening trend in this correlation starting in the late 1980s, but this trend cannot be confirmed with any statistical confidence. Such unprecedented high correlations imply that ENSO events started to control rainfall anomalies outside the dry season from the early 1970s onwards. This effect is seen as a continuous pattern in DJF rainfall anomalies and as episodes in MAM rainfall anomalies. Note that there is no significant correlation between JJA Nino 3.4 values and rainfall anomalies in JJA a year later. Sliding-window correlations between SON values of Nino 3.4 and seasonal rainfall anomalies are similar to those using JJA values of Nino 3.4, except that the episodic influence on MAM rainfall anomalies after 1990 appears stronger (**Figure 44**).

Note that sliding-window correlations using DMI are void of such dramatic changes in correlations (**Figures 45** and **46**). Apart from episodes of negative or positive correlations lasting about 10 years, which are worth further investigation in the future, no systematic change in Indian Ocean Dipole variability on Indonesian rainfall variability can be indentified that could explain the rainfall decline over the last two decades. Hence, IPO influences appear to play a secondary role in Indonesian rainfall variability. The last part of this thesis deals which the interesting question whether the conclusion by Haylock & McBride (2001) that wet season rainfall in the Indonesian is inherently unpredictable still holds for the last decades. To answer this question, we calculated sliding-window correlations between JJA (or SON) and seasonal rainfall anomalies over the following seasons.

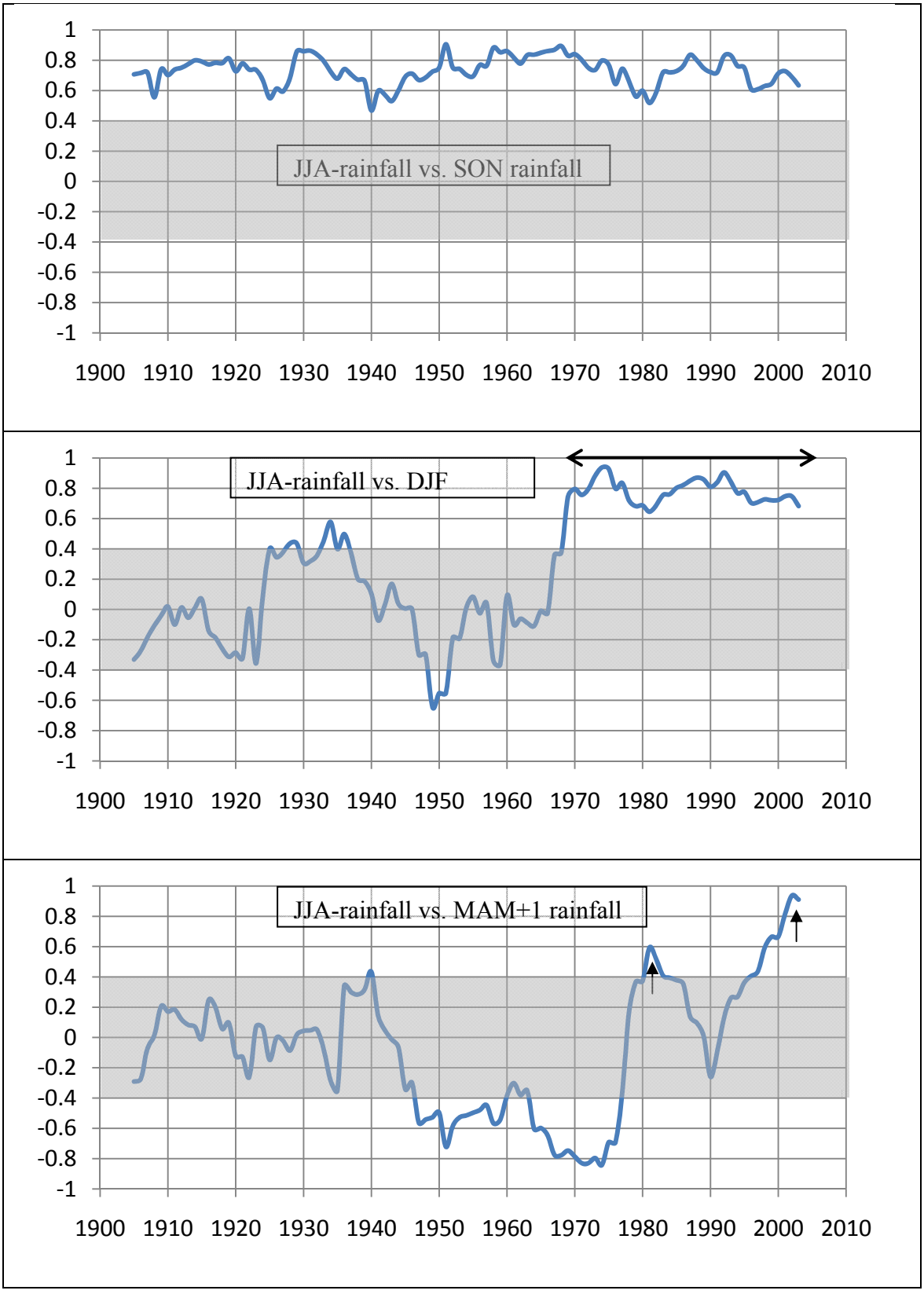

Figure 47. 11-year sliding-window correlations between JJA rainfall anomalies and rainfall anomalies in the following seasons with visibility assistance in grey area.

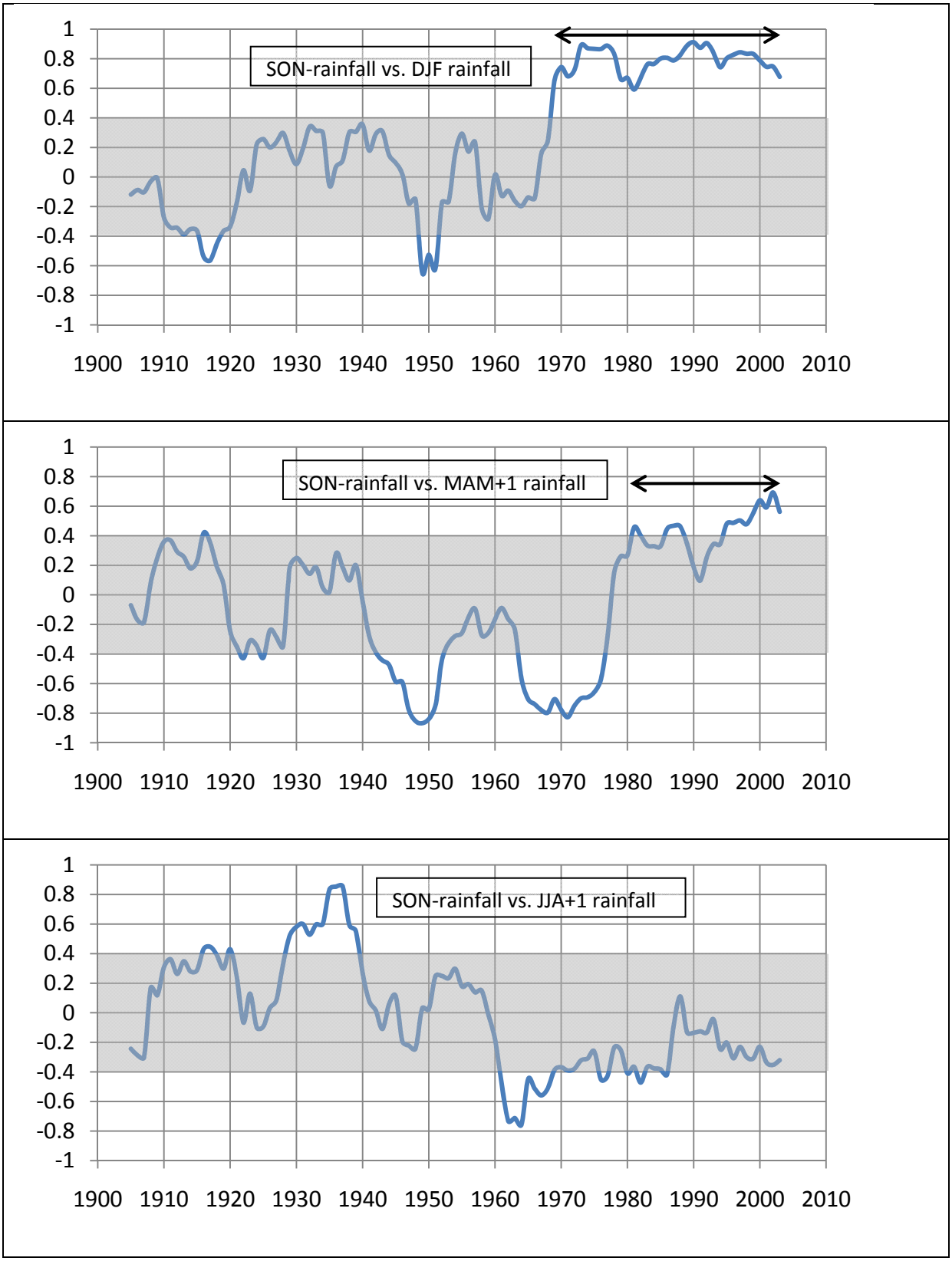

Figure 48. 11-year sliding-window correlations between SON rainfall anomalies and rainfall anomalies in the following seasons with visibility assistance in grey area.

For example, it is not a surprise that JJA rainfall anomalies show a high positive correlation with rainfall anomalies in the following SON, given that ENSO influences are dominant during these seasons. It is much more surprising that, from the early 1970s onwards, rainfall anomalies occurring in JJA or SON became strongly positively correlated with DJF rainfall anomalies (**Figure 47 and 48**). A direct correlation between JJA with DJF rainfall anomalies, for the 1969-2008 period gives a high correlation value in a range between 0.70 and 0.91 at 95% confidence level (using Fisher's transformation). In stark contrast to this, the previous 40 years (1945-1977) had almost non-existent correlations in a range between -0.358 and 0.264 at 95% confidence level. Hence, the unpredictability of Indonesian's rainfall during the wet season indicated in past investigations by Haylock & McBride (2001) and Hendon (2003) has abruptly changed to a fairly predictable state over the last 40 years. In addition to this are episodes in the 1980s and from the 1990s onwards during which strong positive correlations even extend into the MAM period of the following year. The episodes clearly correspond to episodes of prolonged ENSO influences (see **Fig. 43 and 44**).

.

CHAPTER 5: Summary and Conclusion

This study explored rainfall variability and trends in the Indonesian region for the period 1900–2008 using a number of standard statistical methods. This study identified a significant decline in annual-mean rainfall in the entire region of more than 20% commencing in the late 1980s. Before this change occured, annual-mean rainfall anomalies were mainly controlled by seasonally ENSO-induced rainfall variations occuring in the dry season (June-November). From the early 1970s onwards, however, ENSO events started to control rainfall patterns in other seasons of the year as well, which explained the spatial coherence of rainfall changes in the entire Indonesian region. Hence, the observed rainfall decline in the last decades could be attributed to two factors: 1) intra-annually prolonged ENSO influences spreading over most of the year, and 2) relatively long El-Niño dominated episodes from the 1990s onwards. In contrast to the past, Indonesian winter and summer rainfall anomalies started to become strongly intercorrelated from the early 1970s onwards. This remarkable feature indicates a sudden and robust climatic shift of rainfall patterns and its climate driver (the ENSO) in the Indonesian region. This shift indicates the likelihood that dry periods in the Indonesian region continue to be more pronounced than during the first 90 years of the last century which can have severe and detrimental socio-economic and environmental impacts. While the indicated shift of ENSO-related rainfall dynamics coincides with the onset of accelerated global warming (see **Appendix** C), their connection remains uncertain. Indian Ocean influences (i.e. the Indian Ocean Dipole) appeared to play only a secondary role in the process.

Empirical orthogonal function (EOF) analysis was employed in order to obtain - insight into dominant rainfall variability in this region based on annual rainfall data. We identified two dominant modes that significantly occurred in this region. The first EOF accounts for about 38% of variance with the dominant mode occurring in the centre of the region. This first mode presumably represents ENSO influences that are spatially coherent in the Indonesian region and this mode, like the original rainfall data, shows a significant decline from the early 1990s onwards. A smaller variance of about 9% appeared in the second EOF mode with the negative spatial loading concentrated in the southern part of the region. Interestingly, this mode also picked up a sudden change in temporal rainfall variability from the early 1990s onwards.

This study also explored the relationships between rainfall and SST anomalies at selected locations. Many details of the relationships between rainfall anomalies and regional temperature anomalies remained unclear and remain for future investigations. Overall, it appears that, with few exceptions, SSTs in the Indonesian region are unsuitable for use as indicator of rainfall variability. However, there are interesting results arising from Molucca Sea and Banda Sea, which experienced a high positive correlation between SST and rainfall anomalies at zero lag for the period June – August. This is likely due to its proximity of this region to the warm water pool in the western Pacific.

While this study has shed significant light into rainfall variability and trends in the Indonesian region, there are a number of questions that could not be addressed. For instance, it would be interesting to explore whether regional climate forecasting models captured and reproduced the shift in the atmospheric dynamics and rainfall anomalies associated with the observed prolonged ENSO influences. It would also be worthwhile to analyse atmospheric properties (e.g. pressure and humidity distributions) in the Indonesian region over the past 50 years to identify and describe changes in the atmospheric dynamics that accompanied the observed rainfall decline. These and other questions remain for future studies.

APPENDIX A: Miscellaneous Statistical Results

Normal-probability analysis

A normal-probability analysis is employed for the assessment of whether or not the rainfall data set is normally distributed compared with the bell-shaped Gaussian distribution (Wilks, 2006). The rainfall data were plotted against this theoretical normal distribution as shown in **Figure A1**. The points form an approximate straight line. thus the data set indicate departure from normality. Departures from this straight line, indicating departures from normality, appear to be relatively small.

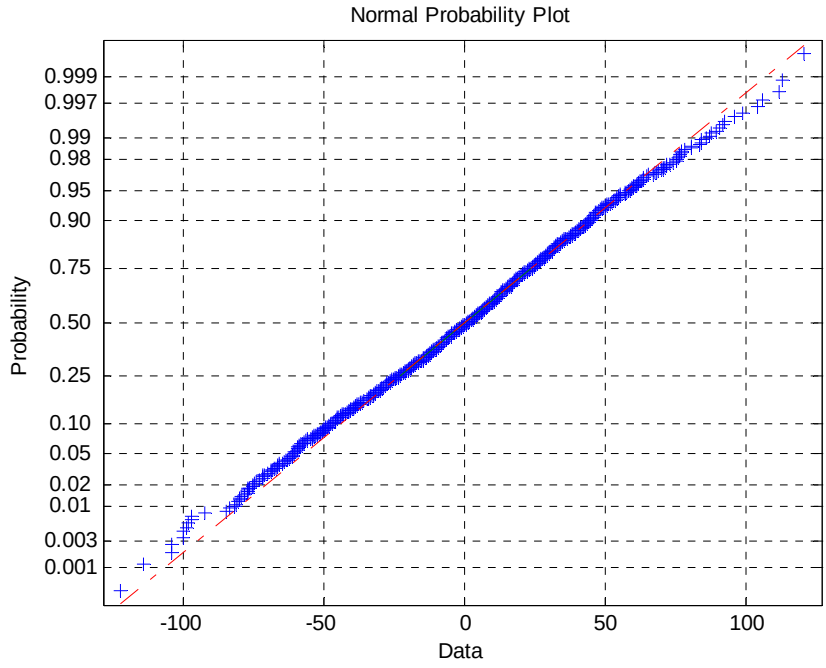

Figure A1. Normal-probability plot of the rainfall distribution (1900 – 2008) for the Indonesian region.

EOF Analysis

The eigenvalues for the first twenty four modes of combined spatial and temporal variance EOFs are graphically shown in **Figure A2** as the percentage of total variance. The first mode is dominant, representing 38% of the total variance, followed by second mode of 9% of the total variance. Only the first two modes are significant according to the criteria by North *et al.* (1982) and thus form the basis of discussion in this thesis.

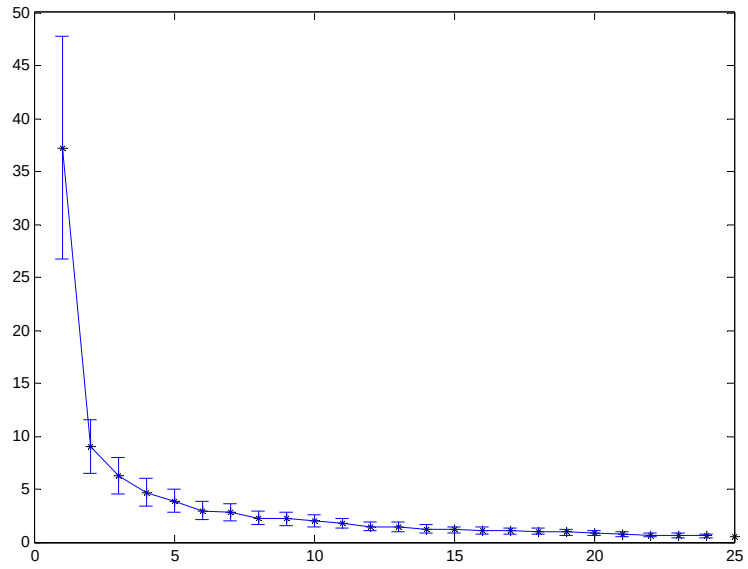

Figure A2.The first 24 EOF modes including variance explained.

Appendix B: Wavelet Analysis of Climate Drivers

Wavelet analysis was also performed for monthly mean rainfall anomalies in the entire Indonesian region and monthly values of several climate indices (Nino 3.4, DMI and IPO). **Figures B1 – B5** display the results of this analysis.

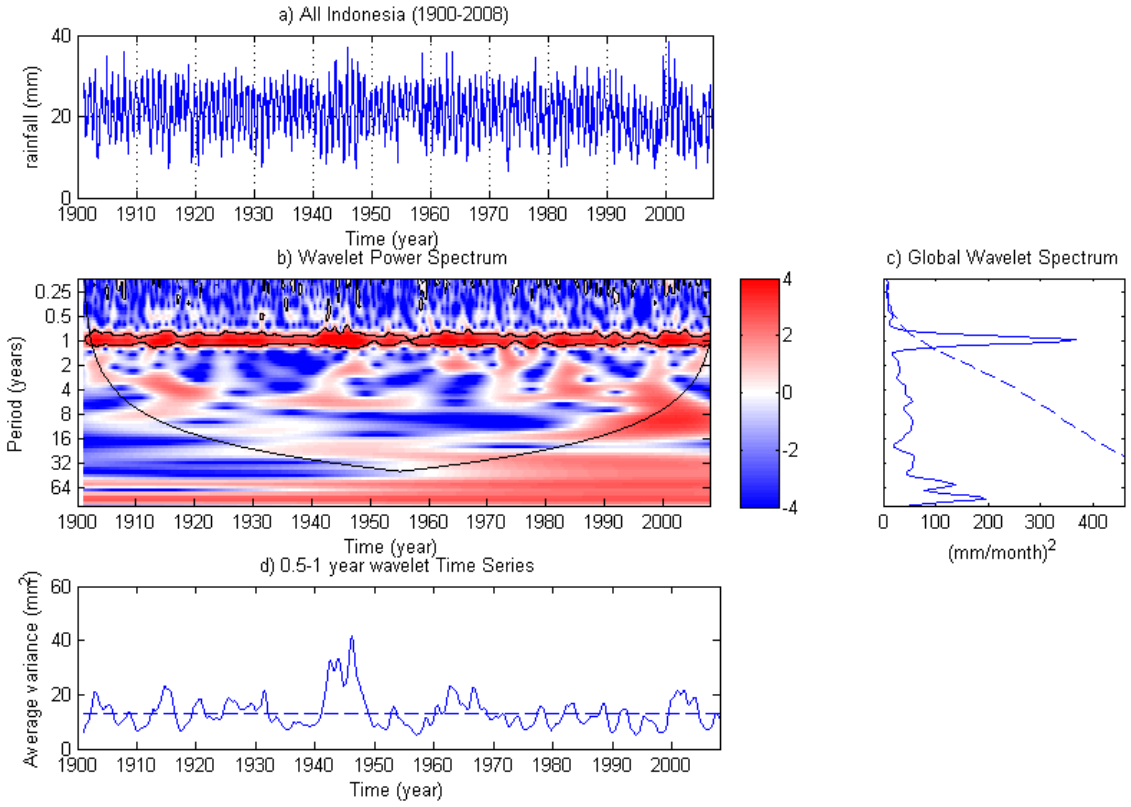

Figure B1. Wavelet analysis for monthly mean Indonesian rainfall anomalies for the period 1900-2008.

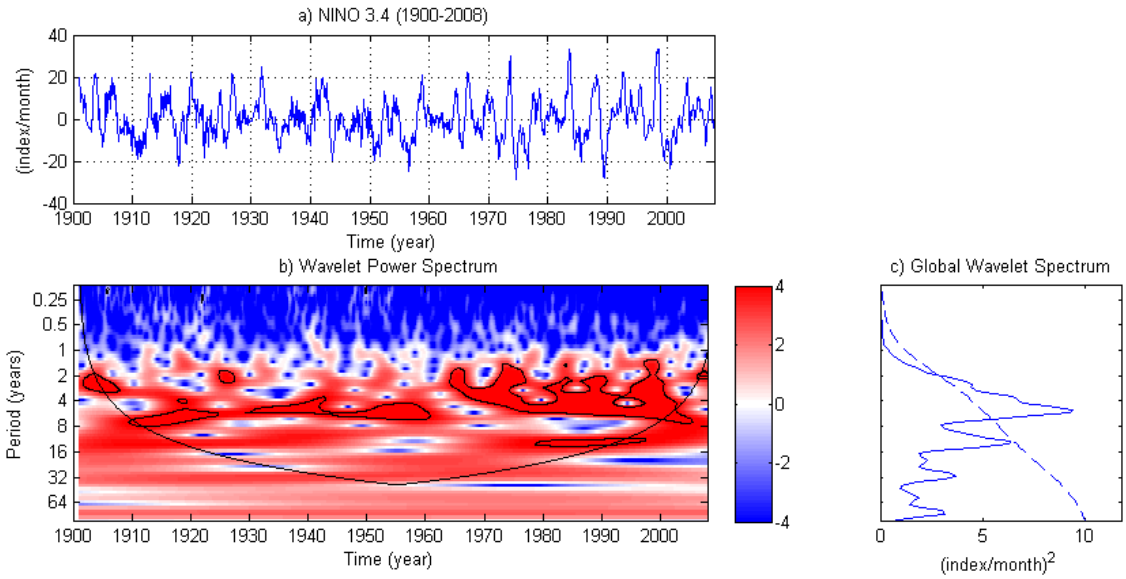

Figure B2. Wavelet analysis for monthly mean values of Nino 3.4 for the period 1900-2008.

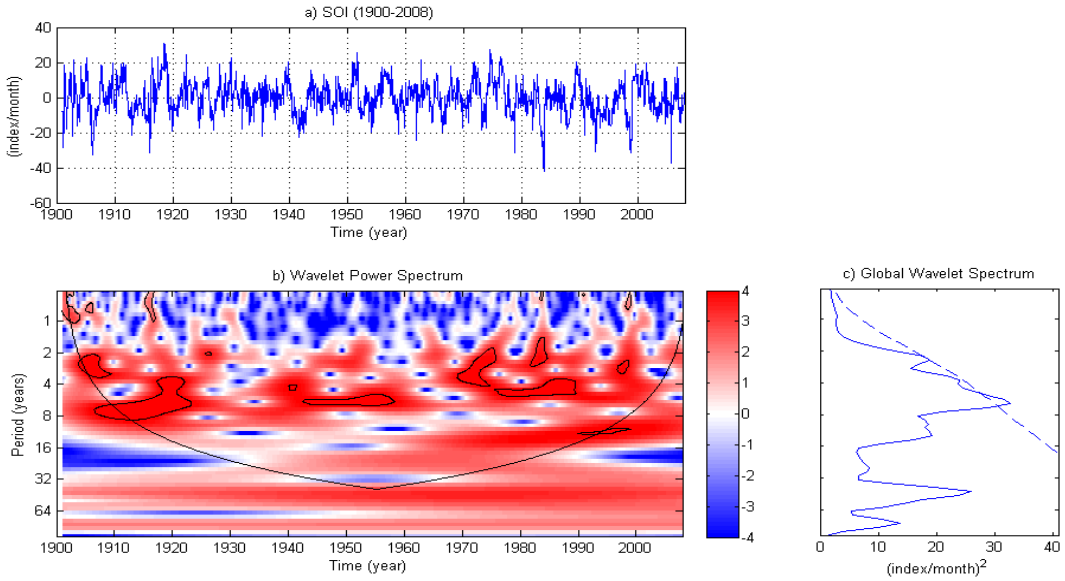

Figure B3. Wavelet analysis for monthly mean values of SOI for the period 1900-2008.

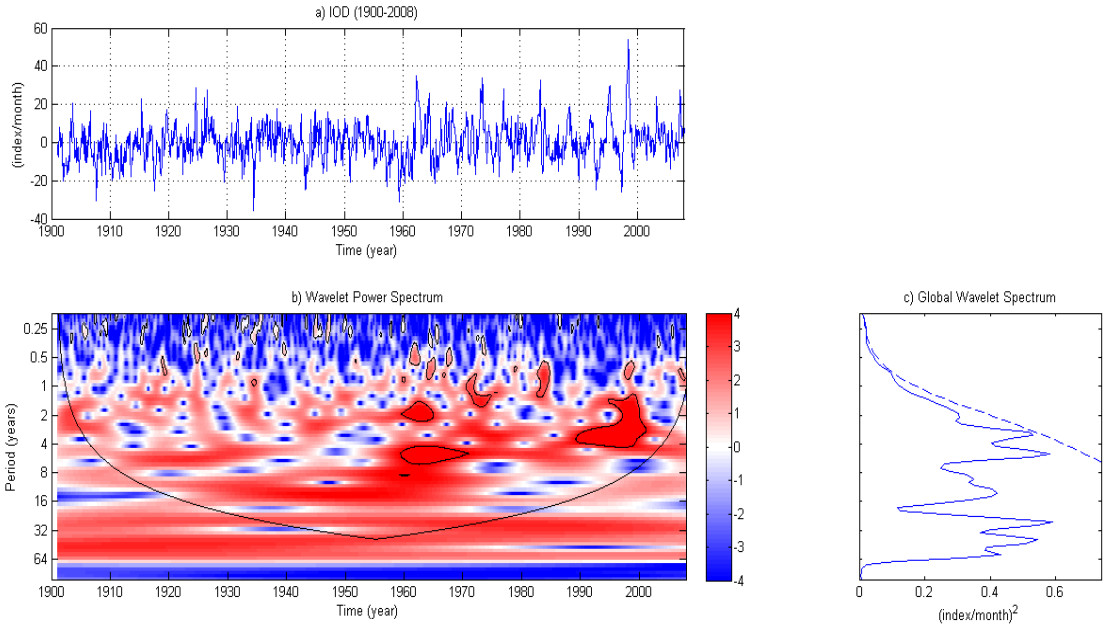

Figure B4. Wavelet analysis for monthly mean values of IOD for the period 1900-2008.

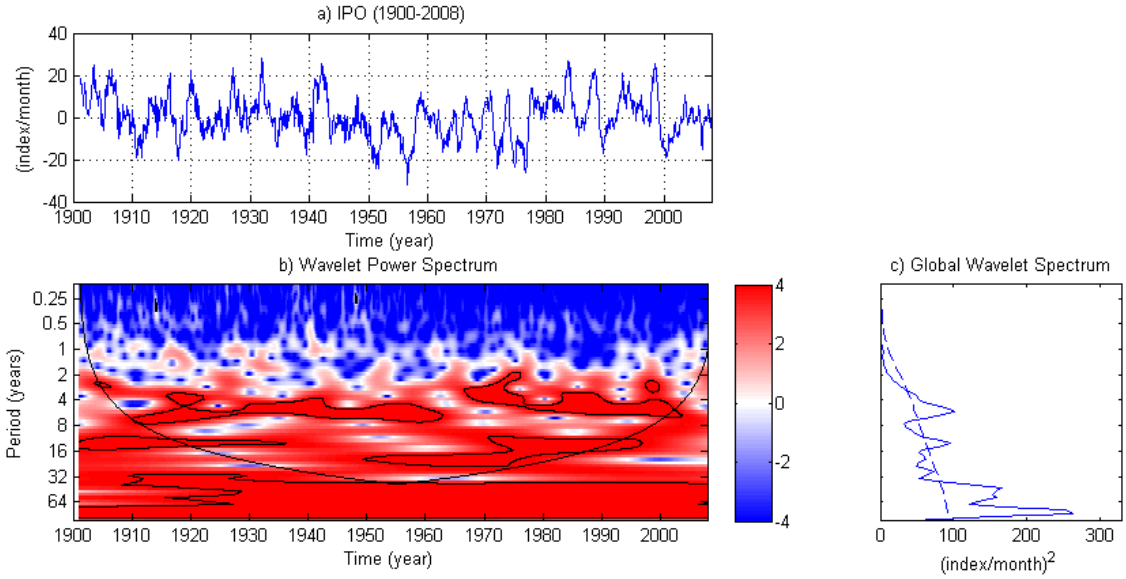

Figure B5. Wavelet analysis for monthly mean values of IPO for the period 1900-2008.

Appendix C: SST Trends in the Indonesian Region

For completeness, long-term trends of annual-mean SST anomalies in regions A*, B* nand C* are shown in comparison with the global trend of SST anomalies (**Figure C1)**. It can be seen that these anomalies largely follow the global trend but, in contrast to the latter, display an amplified intra-decadal variability. Interestingly, regions A* and B* display a variability of ~0.5°C in amplitude which often exceeds that seen in region C*. Exploration of this feature is beyond the scope of this work and remains for future studies.

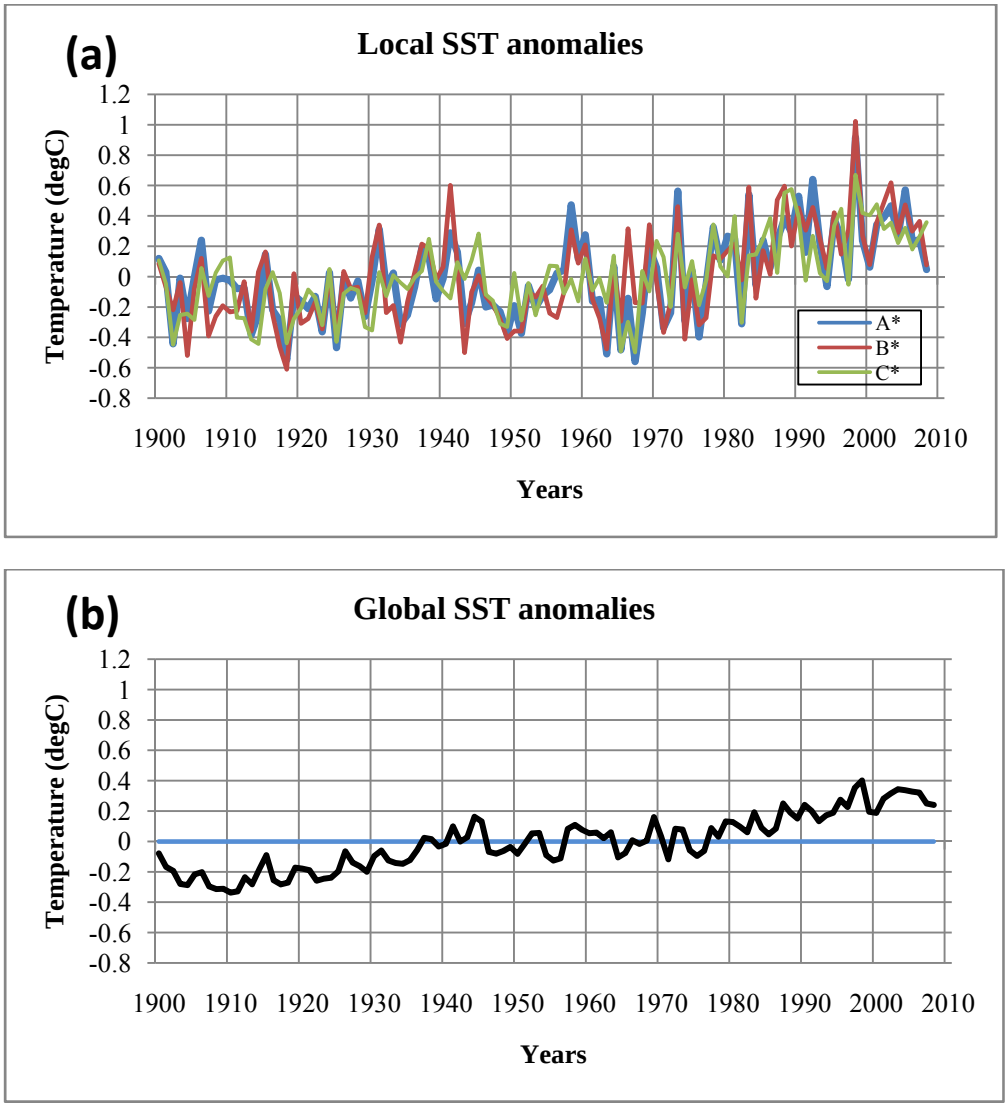

Figure C1. Time series of SST anomalies in a) region A*, B*, and C*. b) Global SST for the period from 1900 to 2008. Based on HadISST1 data.

References

Abram, N. J., Gagan, M. K., Cole, J. E., Hantoro, W. S., & Mudelsee, M. (2008). Recent intensification of tropical climate variability in the Indian Ocean. *Nature Geoscience, 1*(12), 849-853, DOI: 10.1038/ngeo357.

Allan, R. J., & Haylock, M. R. (1993). Circulation features associated with the winter rainfall decrease in southwestern Australia. *Journal of Climate, 6*, 1356-1367.

Aldrian, E., & Susanto, R. D. (2003). Identification of three dominant rainfall regions within Indonesia and their relationship to sea surface temperature. *International Journal of Climatology, 23*(12), 1435-1452, DOI: 10.1002/joc.950.

Aldrian, E. (2007). *Indonesian rainfall with a hierarchy of climate models*. Saarbrucken, Germany: VDM Verlag Dr. Muller.

Aldrian, E., Gates, L. D., & Widodo, F. H. (2007). Seasonal variability of Indonesian rainfall in ECHAM simulations and in the reanalyses: The role of ENSO. *Theoretical and Applied Climatology, 87*, 41-59, DOI:10.1007/s00704-006-0218-8.

Aldrian, E., & Djamil, Y. S. (2008). Spatio-temporal climatic change of rainfall in east Java Indonesia. *International Journal of Climatology, 28*(4), 435-448, DOI: DOI: 10.1002/joc.1543.

Allan, R., Chambers, D., Drosdowsky, W., Hendon, H., Latif, M., Nicholls, N., Smith I., Stone R., Tourre Y.(2001). Is there an Indian Ocean Dipole and is it independent of the El Nino-Southern Oscillation? *CLIVAR Exchanges, 6*(3).

Annamalai, H., Liu P., Xie S-P. (2005). Soutwest Indian ocean SST variability: its local effect and remote influence on Asian monsoons. *Journal of Climate.* 18, 4150-4167.

Ashok, K., Behera, S. K., Rao, S. A., Weng, H. Y., & Yamagata, T. (2007). El Nino Modoki and its possible teleconnection. *Journal of Geophysical Research-Oceans, 112*(C11), DOI: C11007 10.1029/2006jc003798

Ashok, K., Guan, Z. Y., & Yamagata, T. (2001). Impact of the Indian Ocean Dipole on the relationship between the Indian monsoon rainfall and ENSO. *Geophysical Research Letters, 28*(23), 4499-4502.

Ashok, K., Guan, Z. Y., & Yamagata, T. (2003). A look at the relationship between the ENSO and the Indian Ocean Dipole. *Journal of the Meteorological Society of Japan, 81*(1), 41-56, DOI: 1821 10.1029/2003gl017926.

Barnston, A. G., Chelliah, M., & Goldenberg, S. B. (1997). Documentation of highly ENSO-related SST region in the equatorial Pacific. *Atmosphere-Ocean, 35*(3), 367-383.

Barnston, A. N., Glantz, M. H., & He, Y. (1999). Predictive skill of statistical and dynamical climate models in SST forecast during the 1997-98 El-Niño episode and the 1998 La Nina onset. *Bulletin of the American Meteorological Society, 80*(2), 217-243.

Behera, S. K., Salvekar, P. S., & Yamagata, T. (2000). Simulation of interannual SST variability in the tropical Indian Ocean. *Journal of Climate, 13*(19), 3487-3499.

Boer, R., Sutardi, & Hilman, D. (2007). *Climate variability and climate changes, and their implication*. Ministry of Environment, Indonesia. Jakarta.

Boer, R., & Wahab, I. (2007). Use of sea surface temperature for predicting optimum planting window for potato at Pangalengan West Java, Indonesia. In M. V. K. Sivakumar & J. Hansen (Eds.), *Climate Prediction and Agriculture : Advances and Challanges* (pp. 135-141). Berlin: Springer

BoM (2002), Climate Glossary: Southern Oscillation Index. Retrieved 15/10 2009 from: http://www.bom.gov.au/climate/glossary/soi.shtml.

Braak, C. (1929). On the climate of and meteorological research in the Netherlands Indies. *Science in the Netherlands East Indies*, 50-64.

Chang, C.-P., Wang, Z., Lu, J., & Li, T. (2004). On the relationship between western Maritime continent monsoon rainfall and ENSO during northern winter. *Journal of Climate, 17*, 665 - 672.

Chang, C. P., Wang, Z., McBride, J., & Liu, C. H. (2005). Annual cycle of southeast Asia-maritime continent rainfall and asymmetric monsoon transition. *Journal of Climate, 18*, 287 - 301.

D'Arrigo, R., & Smerdon, J. E. (2008). Tropical climate influences on drought variability over Java, Indonesia. *Geophysical Research Letters, 35*(5), DOI: L05707 10.1029/2007gl032589

Dayem, K. E., Noone, D. C., & Molnar, P. (2007). Tropical western Pacific warm pool and maritime continent precipitation rates and their contrasting relationships with the Walker Circulation. *Journal of Geophysical Research-Atmospheres, 112*(D6), DOI: D06101 10.1029/2006jd007870

Deser, C. & Wallace, M. (1987). El Nino events and their relation to the southern oscillation : 1925 – 1986. Journal of Geophysical Research. 92, 14,189-14,196

Drosdowsky, W., & Williams, M. (1991). The southern oscillation in the Australian region. Part I : Anomalies at the extremes of the oscillation. *Journal of Climate, 4*, 619-638.

Emery, W. J., & Thomson, R. E. (1997). *Data analysis methods in physical oceanography*. New York: Pergamon: pp. 319-343.

England, M. H., Susanto, A., Phipps, S. J., & Ummenhofer, C. C. (2010). Role of the Indonesian throughflow in controlling regional mean climate and rainfall variability. *Manuscript Submitted for publication in Journal of Climate, 15 April 2009.*

Folland, C. K. (2002). Relative influences of the interdecadal Pacific oscillation and ENSO on the South Pacific Convergence Zone. *Geophysical Research Letters, 29*(13), 1643.

Folland, C. K., Parker, D. E., Colman, A. W., & Washington, R. (1999). Large scale modes of ocean surface temperature since the late nineteenth century. In A. Navarra (Ed.), *Beyond El Nino: decadal and interdecadal climate variability* (pp. 73 - 102). The Netherlands: Springer.

Giannini, A., Robertson, A. W., & Qian, J. H. (2007). A role for tropical tropospheric temperature adjustment to El Nino-Southern Oscillation in the seasonality of monsoonal Indonesia precipitation predictability. *Journal of Geophysical Research-Atmospheres, 112*(D16), DOI: D16110 10.1029/2007jd008519.

Gordon, A. L. (2005). Oceanography of the Indonesian seas and their throughflow. *Oceanography, 18*(4), 14-27.

Gordon, A. L., Giulivi, C. F., & Ilahude, A. G. (2003). Deep topographic barriers within the Indonesian seas. *Deep-Sea Research Part II, 50*, 2205-2228.

Gordon, A. L., & Susanto, R. D. (2001). Banda sea surface layer divergence. *Ocean Dynamics, 52*, 2-10.

Gordon, A. L. (1995). When is "appearance" reality? Indonesian Troughflow is primarily derived from north Pacific water masses. *Journal of Physical Oceanography, 25*(6), 1560-1567.

Hamada, J. I., Yamanaka, M. D., Matsumoto, J., Fukao, S., Winarso, P. A., & Sribimawati, T. (2002). Spatial and temporal variations of the rainy season over Indonesia and their link to ENSO. *Journal of the Meteorological Society of Japan, 80*, 285 - 310.

Hanley, D. E., Bourassa, M. A., O'Brien, J. J., Smith, S. R., & Spade, E. R. (2003). A quantitative evolution of ENSO indices. *Journal of Climate 16*, 1249-1258.

Hannachi, A., Jolliffe, I. T., & Stephenson, D. B. (2007). Empirical orthogonal functions and related techniques in atmospheric science: a review. *International Journal of Climatology, 27*, 1119-1152.

Hara, M., Yoshikane, T., Takahashi, H. G., Kimura, F., Noda, A., & Tokioka, T. (2009). Assessment of the Diurnal Cycle of Precipitation over the Maritime Continent Simulated by a 20 km Mesh GCM Using TRMM PR Data. *Journal of the Meteorological Society of Japan, 87*, 413-424.

Haylock, M., & McBride, J. (2001). Spatial coherence and predictability of Indonesian wet season rainfall. *Journal of Climate, 14*, 3882-3887.

Hendon, H. H. (2003). Indonesian rainfall variability: Impacts of ENSO and local air-sea interaction. *Journal of Climate, 16*(11), 1775-1790.

Hidayat, R., & Kizu, S. (2009). Influence of the Madden-Julien Oscillation on Indonesian rainfall variability in austral summer. *International Journal of Climatology, DOI:* 10.1002/joc.

Holton, J. R. (2004). *An introduction to dynamical meteorology fourth edition*. London, UK: Elsevier Academic Press.

Iskandar, I. (2010). Seasonal and interannual patterns of sea surface temperature in Banda Sea as revealed by self-organizing map. *Continental Shelf Research, 30*, 1136-1148, DOI: doi:10.1016/j.csr.2010.03.003.

Kirono, D. G. C., & Tapper, N. J. (1999). ENSO rainfall variability and impacts on crop production in Indonesia. *Physical Geography, 20*(6), 508-519.

Kirono, D. G. C., Tapper, N. J., & McBride, J. L. (1999). Documenting Indonesian rainfall in the 1997/1998 El Nino event. *Physical Geography, 20*(5), 422-435.

Legates, D. R., & Willmott, C. J. (1990). Mean seasonal and spatial variability in gauge corrected, global precipitation. *International Journal of Climatology, 10*, 111-127.

Lorenz, E.N., (1956). Empirical orthogonal functions and statistical weather prediction. Science Report 1. Statistical Forecasting Project. Department of Meteorology. MIT (NTIS AD 110268), 49 pp.

Manton, M. J., Della-Marta, P. M., Haylock, M. R., Hennessy, K. J., Nicholls, N., Chambers, L. E., D.A. Collins, G. Daw, A. Finet, D. Gunawan, K.Inape, H. Isobe, T.S. Kestin, P. Lefale, C.H. Leyu, T.Lwin, L. Maitrepierre, N. Ouprasitwong, C.M. Page, J.Pahalad, N. Plummer, M.J. Saligner, R.Suppiah, V.L. Tran, B.Trewin, I.Tibig, D.Yee (2001). Trends in extreme daily rainfall and temperature in Southeast Asia and the South Pacific: 1961 - 1998. *International Journal of Climatology, 21*, 269-284.

Marshall, J., & Plumb, R. A. (2008). *Atmosphere, ocean, and climate dynamics: an introductory text.* (Vol. 93). London, UK: Elsevier.

Matsuura, K., & Willmott, C. J. (2009). Terrestrial precipitation: 1900-2008 gridded monthly time series (Version 2.01). Retrieved 10/03, 2010, from: http://climate.geog.udel.edu/~climate/html_pages/Global2_Ts_2009/README.global_p_ts_2009.html

McBride, J. L., Haylock, M. R., & Nichols, N. (2003). Relationships between the maritime continent heat source and the El Nino-Southern Oscillation phenomenon. *Journal of Climate, 16*(17), 2905-2914.

McCowan, D. D. (2007). Spectral estimation with wavelets. *Honors Thesis, Ohio University, Unpublished*, 98.

Meinke, H., deVoil, P., Hammer, G. L., Power, S., Allan, R., Stone, R. C., Folland, C. Potgieter, A. (2005). Rainfall variability at decadal and longer time scales: Signal or noise? *Journal of Climate, 18*(1), 89-96.

Meyers, G., McIntosh, P., Pigot, L., & Pook, M. (2007). The years of El Nino, La Nina, and interactions with the tropical Indian ocean. *Journal of Climate, 20*(13), 2872-2880, DOI: 10.1175/jcli4152.1.

Ministry for the Environment (2008). *Climate Change Effects and Impacts Assessment: A Guidance Manual for Local Government in New Zealand.* 2nd Edition. Mullan B; Wratt D; Dean S; Hollis M; Allan S; Williams T, Kenny G and MfE. Ministry for the Environment, Wellington. xviii + 149 p. www.mfe.govt.nz.

Moron, V., Robertson, A. W., & Boer, R. (2009). Spatial Coherence and Seasonal Predictability of Monsoon Onset over Indonesia. *Journal of Climate, 22*(3), 840-850, DOI: 10.1175/2008jcli2435.1.

Neale, R., & Slingo, J. (2003). The maritime continent and its role in the global climate: A GCM study. *Journal of Climate, 16*(5), 834-848.

Nicholls, N. (1984). The southern oscillation and Indonesian sea surface temperature. *Monthly Weather Review, 112*, 424-432.

Nicholls, N. (1989). Sea surface temperatures and Australian winter rainfall. *Journal of Climate, 2*, 965-973.

North, G. R., Bell, T. L., Cahalan, R. F., & Moenig, F. J. (1982). Sampling errors in the estimation of empirical orthogonal function. *Monthly Weather Review, 110*, 669-706.

Parker, D., Folland, C., Scaife, A., Knight, J., Colman, A., Baines, P., Dong, B.W.. (2007). Decadal to multidecadal variability and the climate change background. *Journal of Geophysical Research-Atmospheres, 112*(D18).

Philander, S. G. H., & Fedorov, A. (2003). Is El Nino sporadic or cyclic? *Annual Review of Earth Planet Science, 31*, 579-594.

Philander, S. G. H. (1983). El Nino southern oscillation phenomena. *Nature, 302*, 295-301.

Philander, S. G. H. (1985). El-Niño and La-Niña. *Journal of Atmospheric Science, 42*, 652-662.

Plata, S. (2006). A note on Fisher's correlation coefficient. *Applied Mathematics Letters*. 19(6) 499-502, DOI: 10.1016/j.aml.2005.02.036

Power, S., Haylock, M., Colman, R., & Wang, X. D. (2006). The predictability of interdecadal changes in ENSO activity and ENSO teleconnections. *Journal of Climate, 19*(19), 4755-4771.

Power, S., Tseitkin, F., Mehta, V., Lavery, B., Torok, S., & Holbrook, N. (1999). Decadal climate variability in Australia during the twentieth century. *International Journal of Climatology, 19(2), 169-184.*

Qian, J. H. (2008). Why precipitation is mostly concentrated over islands in the Maritime Continent. *Journal of the Atmospheric Sciences, 65*(4), 1428-1441, DOI: 10.1175/2007jas2422.1.

Qu, T., Du, Y., Strachan, J., Meyers, G., & Slingo, J. (2005). Sea surface temperature and its variability in the Indonesian region. *Oceanography, 18*(4).

Ramage, C. S. (1968). Role of a tropical 'Maritime Continent' in the atmospheric circulation. *Monthly Weather Review, 96*(6), 365-370.

Rayner, N. A., Parker, D. E., Horton, E. B., Folland, C. K., Alexander, L. V., Rowell, D. P., Kent, E. C., Kaplan, A. (2003). Global analyses of sea surface temperature, sea ice, and night marine air temperature since the late nineteenth century. *Journal of Geophysical Research-Atmospheres, 108*(D14).

Ropelewski, C. F., & Halpert, M. S. (1987). Global and regional scale precipitation and temperature patterns associated with El Nino/Southern Oscillation. *Monthly Weather Review, 115*, 1606-1626.

Ropelewski, C. F., & Halpert, M. S. (1996). Quantifying southern oscillation precipitation relationships. *Journal of Climate, 9*, 1043-1059.

Saji, N. H., Goswami, B. N., Vinayachandran, P. N., & Yamagata, T. (1999). A dipole mode in the tropical Indian Ocean. *Nature, 401*(6751), 360-363.

Saji, N. H., & Yamagata, T. (2003). Structure of SST and surface wind variability during Indian Ocean Dipole mode events: COADS observations. *Journal of Climate*.

Salinger, M. J. (1995). Southwest Pacific temperatures: trends in maximum and minimum temperatures. *Atmospheric Research, 37*, 87-99.

Salinger, M. J., Renwick, J. A., & Mullan, A. B. (2001). Interdecadal Pacific Oscillation and south Pacific climate. *Internatinal Journal of Climatology, 21*, 1705-1721.

Schneider, N. (1997). The Indonesian throughflow and the global climate system. *Journal of Climate, 11*, 676-689.

Smith T.M., R.W. Reynolds, R.E. Livezey, D.C. Stokes., (1996). Reconstruction of historical sea surface temperatures using empirical orthogonal function. *Journal of Climate*. 9. 1403-1420.

Speer, M. S., Leslie, L. M., & Fierro, A. O. (2009). Australian east coast rainfall decline related to large scale climate drivers. *Climate Dynamics*, doi. 10.1007/s00382-00009-00726-00381.

Susanto, R. D., & Marra, J. (2005). Chlorophyl a variability along the southern coasts of Java and Sumatra. *Oceanography, 18*(4).

Susanto, R. D., Moore, T. S., & Marra, J. (2006). Ocean color variability in the Indonesian Seas during the SeaWiFS era. *Geochemistry Geophysics Geosystems, 7*(5).

Tapper, N. (2002). Climate, climatic variability and atmospheric circulation patterns in the Maritime Continent region. In P. Kershaw, B. David, N. Tapper, D. Penny & J. Brown (Eds.), *Bridging Wallace's Line: the environmental and cultural history and dynamics of the SE-Asian-Australian region* (pp. 5-28). Reinskirchen, Germany: Catena Verlag.

Torrence, C., & Compo, G. P. (1998). A practical guide to wavelet analysis. *Bulletin of the American Meteorological Society, 79*(1), 61-78.

Tomczak, M. & Godfrey, J.S. (2003). Regional oceanography: an introduction 2nd edition. Daya Publishing House.

Trenberth, K. E. (1997). The definition of El Nino. *Bulletin of the American Meteorological Society, 78*(12), 2771-2772.

Trenberth, K. (1991). General characteristics of El-Niño-Southern Oscillation. In M. Glantz, R. Katz & N. Nicholls (Eds.), *Teleconnections linking worldwide climate anomalies* (pp. 13-41). Cambridge: Cambridge University Press.

Trenberth, K. E., Jones, P. D., Ambenje, P., Bojariu, R., D.Easterling, Tank, A. K., D. Parker, F. Rahimzadeh, J.A. Renwick, M. Rusticucci, B. Soden, P. Zhai. (2007). Observation:

Atmospheric surface and climate change. In S. Solomon, D. Qin, M. Manning, Z. Chen, M. Marquis, K. B. Averyt, M. Tignor & H. L. Miller (Eds.), *Climate Change 2007: The Physical Sciecne Basis. Contribution of Working Group I to the Fourth Assessment Report of the Intergovernmental Panel on Climate Change*. Cambridge, United Kingdom and New York, USA: Cambridge University Press.

Troup, A. J. (1965). The southern oscillation. *Quarterly Journal of the Royal Meteorological Society, 91*, 490-506.

Verdon, D. C., Wyatt, A. M., Kiem, A. S., & Franks, S. W. (2004). Multidecadal variability of rainfall and streamflow: Eastern Australia. *Water Resource Resesarch, 40*, W10201.

Vimont, D. J., David S, B., & Naylor, R. L. (2010). Downscaling Indonesian precipitation using large-scale meteorological field. *International Journal of Climatology, DOI:10.1002/joc.2010*.

Vincent, D. G. (1994). The South Pacific Convergence Zone (SPCZ): a review. *Monthly Weather Review, 122*(9), 1949-1970.

Wilks, D. S. (2006). *Statistical Methods in the Atmospheric Sciences*, Elsevier.

Wheeler, M. C., & McBride, J. L. (2005). Australian-Indonesian monsoon. In W. K. M. Lau & D. E. Waliser (Eds.), *Intraseasonal variability iin the atmosphere-ocean climate system* (pp. 125-173). Berlin; Chichester, UK: Springer.

Yamagata, T., Behera, S. K., Rao, S. A., Guan, Z. Y., Ashok, K., & Saji, H. N. (2003). Comments on "Dipoles, temperature gradients, and tropical climate anomalies". *Bulletin of the American Meteorological Society, 84*(10), 1418-1422.